

**A Study of HVDC Transmission Line Audible Noise and Corona  
Loss in an Indoor Corona Cage**

By

**Mokwape Johannah Lekganyane**

Submitted in partial fulfilment of the requirements for the degree

Master of Science in Engineering (Electrical)  
University of KwaZulu-Natal

Supervisor: Professor N M Ijumba  
Co-supervisor: Adjunct Professor A C Britten

July 2007

## **Declaration**

I, the undersigned declare that the material presented in this dissertation is my own work, except where specific acknowledgement is made in the form of a reference.

---

M J Lekganyane

## **Acknowledgements**

This dissertation is dedicated to the loving memory of my mother Tsiana Rebecca Rampedi.

I would like to thank Eskom Transmission Services and Student Development for the opportunity and their continuous support.

My sincere gratitude goes to my supervisors, Professor N. M. Ijumba and Professor A. C. Britten for their immense support and guidance throughout this study.

My gratitude is extended to Professor A. D. Broadhurst for the guidance he provided in the audible noise study.

The continuous assistance from the HVDC laboratory technician, Mr A. Naidoo and the entire HVDC Centre staff is highly appreciated.

## Abstract

The main objective of this research was to study DC conductor corona loss (CL) and audible noise (AN) in the context of local climatic conditions, through corona cage measurements, and do a comparative analysis of the measured data with results available in literature and EPRI TLW software simulation results. The ultimate aim was to assess the applicability of the software to our local conditions and hence determine, if necessary, appropriate correction factors for application in HVDC transmission line designs.

For this study, short term measurements of corona AN and currents were carried out in an indoor meshed cylindrical corona cage, under DC and AC voltages. The cage was later converted into a short test line and some of the measurements repeated. The DC supply was obtained from a two stage  $\pm 500$  kV Walton-Cockroft generator. The AC voltages were obtained from a 2x100 kV, 50 Hz, AC test transformer set. The tests were performed using single solid and stranded aluminium conductors with three different diameters (1.6 cm, 2.8 cm, and 3.5 cm). All the measurements were carried out at low altitude.

A CoroCAM I camera was used to determine the corona inception gradients and to observe the corona activity at different surface gradients and under different voltages and polarities. AN measurements at different conductor surface gradients were done using the Rohde&Schwarz and the Bruël&Kjaër sound level meters. To obtain the frequency spectra, a Bruël&Kjaër octave-band filter set attached to the sound level meter was used. The measured data was corrected for both height and length effects, and then compared with simulations from the EPRI-TLW software through curve fitting.

A digital micro-ammeter connected to the centre of the cage through a 560  $\Omega$  measuring resistor was used to measure the corona current. Current pulses were viewed using a digital storage oscilloscope. To verify the corona current results obtained from the cage measurements, current measurements were also done for a point-plane spark gap. The corona current data was, later on, used to evaluate the total corona power loss for DC. The results obtained from test line measurements were used to compare the CL and AN for different configurations.



The effect of the space charge under DC voltages was assessed through current measurements. The measurements were done with the cage covered with an aluminium foil to trap the charge and then repeated with the cage uncovered. On the test line, the space charge effect was investigated using a high power fan blowing along the conductor, to simulate the wind factor.

The results of this study have shown the characteristics of corona discharges under different system voltages. The results also give an understanding of how factors such as conductor surface conditions and size, polarity and system voltage affect CL and AN. Both CL and AN were found to increase with conductor size for the same conductor surface gradient and to be higher for stranded conductors. Positive polarity DC and AC noise levels were higher than the negative polarity levels. CL under positive polarity DC was lower than the negative polarity loss.

The effects of space of space charge were noted to some extent. The comparison of test line results and cage results showed that CL depends more on the gap size and the shorter the gap the higher the loss. Hence CL results were not compared with the software simulations. The comparison between the corrected AN results and the software simulations showed a very good agreement. The comparison was done for the 3.5 cm and the 2.8 cm diameter conductors under both positive and negative polarities. The trends compared through curve fitting were quite similar and the trend line equations were of the same order of magnitude. The magnitudes of the corrected noise levels were higher than the CRIEPI and BPA predictions but closer to the EPRI prediction. Generally there is a very good and encouraging agreement between the available literature, simulation results and the results obtained from the laboratory measurements.

It is proposed, as part of further studies, to extend this work to high altitude regions and use bundled conductors as well. Consideration of different and larger test configurations will provide an understanding of the effects of geometry on corona discharges. Space charge analysis will also assist in determining the effects of space charge on different configurations.

## Abbreviations

AC	: Alternating Current
AN	: Audible Noise
BPA	: Bonneville Power Administration
CL	: Corona Loss
CRIEPI	: Central Research Institute of Electric Power Industry
CSA	: Canadian Standards Association
DC	: Direct Current
DSO	: Digital Storage Oscilloscope
dvm	: Digital Voltmeter
EPRI	: Electric Power Research Institute
HVDC	: High Voltage Direct Current
HVRTC	: High Voltage Research and Testing Centre
IREQ	: Institut de Recherche d'Hydro-Québec
neg	: Negative
pos	: Positive
RI	: Radio Interference
RN	: Radio Noise
ROW	: Right of Way
SPL	: Sound Pressure Level
TLW	: Transmission Line Workstation
TVI	: Television Interference
U	: Voltage
UKZN	: University of KwaZulu-Natal

# Table of Contents

Declaration .....	ii
Acknowledgements .....	iii
Abstract .....	iv
Abbreviations .....	vi
Table of Contents .....	vii
List of Figures .....	x
List of Tables.....	xiii
Chapter 1: Introduction .....	1
1.1 Background .....	1
1.2 Problem Identification.....	4
1.3 Research Questions .....	5
1.4 Hypothesis.....	5
1.5 Objectives.....	5
1.6 Motivation .....	5
1.7 Research Design and Methodology.....	6
1.8 Structure of the Dissertation.....	7
Chapter 2: Literature Review .....	10
2.1 Introduction .....	10
2.2 Corona Generation .....	10
2.2.1 Introduction .....	10
2.2.2 Conductor geometry .....	11
2.2.3 Phase configuration .....	11
2.2.4 Phase/pole spacing.....	11
2.2.5 Conductor height above ground .....	11
2.3 Ionisation Processes .....	12
2.3.1 Collisions.....	12
2.3.2 Attachment .....	12
2.3.3 Detachment.....	13
2.3.4 Recombination.....	13
2.4 Corona Modes .....	13
2.4.1 Introduction .....	13

2.4.2 Negative DC .....	13
2.4.3 Positive DC.....	14
2.4.4 AC .....	14
2.5 Factors that Affect Conductor Corona .....	15
2.5.1 Introduction .....	15
2.5.2 Altitude effects .....	16
2.5.3 Conductor surface conditions .....	16
2.6 Corona Audible Noise (AN).....	17
2.6.1 Introduction .....	17
2.6.2 Polarity effect .....	21
2.6.3 Conductor sizes .....	21
2.6.4 Corona cage and test line measurements.....	21
2.6.5 Effects of weather conditions .....	23
2.6.6 Frequency spectra.....	23
2.6.7 Attenuation/air absorption.....	24
2.6.8 Mitigation techniques .....	25
2.7 Corona Losses (CL).....	25
2.7.1 Introduction .....	25
2.7.2 Polarity effect .....	27
2.7.3 Effect of weather conditions.....	28
2.8 Effect of Space Charge .....	28
2.9 Radio Noise (RN).....	30
2.10 Ozone.....	31
2.11 Design Considerations.....	31
Chapter 3: Methodology.....	34
3.1 Introduction .....	34
3.2 Test Equipment .....	34
3.2.1 The HVDC voltage supply .....	34
3.2.2 The corona cage.....	36
3.2.3 Conductors .....	37
3.3 DC Measurements .....	37
3.3.1 Audible noise.....	38
3.3.2 Corona current.....	38
3.3.3 Space charge effect.....	40

3.4 AC Measurements .....	41
3.5 Experimental Procedure .....	41
3.6 Analysis of AN Results .....	42
3.7 Calculation of DC Corona Loss .....	45
3.8 Conductor Surface Conditions .....	46
3.9 Test Line Measurements .....	47
Chapter 4: Results and Analysis.....	50
4.1 Visual Corona.....	50
4.2 Conductor Surface Roughness and Corona Inception.....	51
4.3 Audible Noise.....	52
4.3.1 A-weighted noise levels .....	52
4.3.2 TLW Software A-weighted noise levels .....	61
4.3.3 Octave band frequency spectra.....	66
4.4 Corona Losses .....	73
4.4.1 Effect of conductor surface conditions.....	73
4.4.2 Effect of polarity .....	74
4.4.3 Effect of conductor size.....	76
4.4.4 Corona cage and test line measurements.....	77
4.5 Point-Plane Gap Corona Current Characteristics.....	78
4.6 Space Charge Effect .....	82
4.6.1 Stranded conductors under DC voltages .....	82
4.6.2 Solid conductors under DC voltages .....	83
4.6.3 Stranded conductor under AC voltages.....	85
4.6.4 Positive DC test line measurements .....	85
4.6.5 Visual corona.....	86
Chapter 5: Conclusions .....	89
Chapter 6: Recommendations.....	92
References .....	94

## List of Figures

Figure 3.1: Circuit diagram of the high voltage DC generator.....	35
Figure 3.2: Corona cage .....	37
Figure 3.3: The measurements cage adjacent to the corona cage.....	38
Figure 3.4: Spark gap configuration.....	39
Figure 3.5: Circuit diagram for spark gap current measurements .....	40
Figure 3.6: Corona cage covered with the foil .....	41
Figure 3.7: Line configuration used for evaluation of correction factors.....	45
Figure 3.8: Test line configuration .....	48
Figure 4.1: 3.5 cmØ stranded conductor at 33.5 kV/cm positive polarity.....	50
Figure 4.2: 3.5 cmØ stranded conductor at 33.5 kV/cm negative polarity.....	51
Figure 4.3: 3.5 cmØ stranded conductor at 33.5 kV/cm AC .....	51
Figure 4.4: Conductor roughness effect on AN for positive polarity .....	53
Figure 4.5: Conductor roughness effect on AN for negative polarity .....	54
Figure 4.6: Polarity effect on AN for 3.5 cmØ stranded conductor .....	55
Figure 4.7: Polarity effect on AN for 2.8 cmØ stranded conductor .....	55
Figure 4.8: Effect of conductor size on AN (Positive polarity, stranded conductors).....	56
Figure 4.9: Effect of conductor size on AN (Negative polarity, stranded conductors).....	57
Figure 4.10: Comparison of cage and test line AN measurements (3.5 cm Ø stranded conductor, line height of 70 cm, positive polarity) .....	58
Figure 4.11: Variation of acoustic power with conductor surface gradient for a test line and corona cage for 3.5 cmØ stranded conductor, positive polarity (line height of 70 cm ).....	60
Figure 4.12: Effect of system voltage on AN for a 3.5 cmØ stranded conductor .....	61
Figure 4.13: Comparison of TLW software prediction methods with UKZN results (3.5 cmØ stranded conductor, positive polarity) .....	62
Figure 4.14: Comparison of trends for UKZN with EPRI results by curve fitting (3.5 cm Ø stranded conductor, positive polarity).....	62
Figure 4.15: Comparison of TLW software prediction methods with UKZN results (3.5 cmØ stranded conductor, negative polarity) .....	63
Figure 4.16: Comparison of trends for UKZN with EPRI results by curve fitting (3.5 cmØ stranded conductor, positive polarity).....	64

Figure 4.17: Comparison of TLW software prediction methods with UKZN results ( 2.8 cmØ stranded conductor, positive polarity) .....	65
Figure 4.18: Comparison of TLW software prediction methods with UKZN results ( 2.8 cmØ stranded conductor, negative polarity) .....	65
Figure 4.19: Comparison of trends for UKZN with EPRI and BPI results by curve fitting (3.5 cm Ø stranded conductor, AC).....	66
Figure 4.20: Positive polarity frequency spectrum for a 2.8 cmØ stranded conductor .....	67
Figure 4.21: Effect of conductor size on positive polarity frequency spectrum at 33.5 kV/cm .....	68
Figure 4.22: Effect of conductor surface gradient on positive polarity frequency spectrum for 2.8 cmØ stranded conductor.....	68
Figure 4.23: Negative polarity frequency spectrum for 2.8 cmØ stranded conductor .....	69
Figure 4.24: Effect of conductor size on negative polarity frequency spectrum at 24.3 kV/cm .....	70
Figure 4.25: Effect of conductor surface gradient on negative polarity frequency spectrum for 2.8 cmØ stranded conductor.....	70
Figure 4.26: AC frequency spectrum for 2.8 cm Ø stranded conductor.....	71
Figure 4.27: Effect of conductor size on AC frequency spectrum at 28.9 kV/cm.....	72
Figure 4.28: Effect of conductor surface gradient on AC frequency spectrum for 3.5 cmØ stranded conductor .....	72
Figure 4.29: Effect of conductor surface condition on corona losses for positive polarity .....	73
Figure 4.30: Effect of conductor surface condition on corona losses for negative polarity .....	74
Figure 4.31: Effect of voltage polarity on corona losses for a 3.5 cmØ stranded conductor .....	75
Figure 4.32: Effect of voltage polarity on corona losses for a 2.8 cmØ stranded conductor .....	75
Figure 4.33: Effect of conductor size on corona losses under positive polarity for stranded conductors .....	76
Figure 4.34: Effect of conductor size on corona losses under negative polarity for stranded conductors .....	77
Figure 4.35: Comparison of corona losses in a corona cage and test line for a 3.5 cmØ stranded conductor (Line1: H = 70 cm, Line2: H = 37.5 cm).....	78
Figure 4.36: Polarity effect on corona current in a point-plane gap (gap spacing = 8.6 cm) .....	79
Figure 4.37: Corona current pulses under positive polarity (U = 40 kV).....	80
Figure 4.38: Corona current pulses under positive polarity (U = 40 kV).....	80
Figure 4.39: Corona current pulses under negative polarity (U = 40 kV).....	81
Figure 4.40: Corona current pulses under negative polarity (U = 40 kV).....	81

Figure 4.41: Effect of space charge on corona current under positive polarity for a 3.5 cmØ stranded conductor .....	82
Figure 4.42: Effect of space charge on corona current under positive polarity for a 3.5 cmØ stranded conductor .....	83
Figure 4.43: Effect of space charge on corona current under positive polarity for a 3.5 cmØ solid conductor .....	84
Figure 4.44: Effect of space charge on corona current under negative polarity for a 3.5 cmØ solid conductor .....	84
Figure 4.45: Effect of space charge on corona current under AC for a 3.5 cmØ stranded conductor .....	85
Figure 4.46: Effect of space charge on corona current of a test line (H = 37.5 cm): positive polarity and 3.5 cmØ stranded conductor .....	86
Figure 4.47: Positive polarity 220 kV (a) cage not covered with foil (b) cage covered with foil ....	87
Figure 4.48: Negative polarity 220 kV (a) cage not covered with foil (b) cage covered with foil...	87
Figure 4.49: AC 220 kV (a) cage not covered with foil (b) cage covered with foil.....	87



## List of Tables

Table 2.1: Corona Modes .....	15
Table 3.1: Specifications of the high voltage DC generator.....	36
Table 3.2: Circuit parameters of the dc generator .....	36
Table 3.3: Values of the line parameters used for the EPRI TLW Software simulations for DC (Equivalent monopolar line) .....	44
Table 3.4: Values of the line parameters used for the EPRI TLW Software simulations for AC (Equivalent single phase line).....	44
Table 4.1: Calculated conductor roughness factors.....	52

## Chapter 1: Introduction

### 1.1 Background

The first electric power company was introduced in the year 1882, by Thomas A. Edison [1]. The first transmission line was of DC type with a length of 59 km operating at 2.4 kV. Subsequently electricity demand and transmission distances increased making it impracticable for DC transmission.

Few years later, the introduction of AC machines (transformers, induction and synchronous motors and generators) made AC transmission more attractive for transmitting large amounts of power over long distances with the use of high voltage transformers [2]. For many years AC transmission remained the best available method of power transmission over long distances. However, as time went, technological advances and unavoidable economical factors emerged and DC systems became more comparable to AC systems and DC transmission was re-introduced in the 1950s [3].

The benefits reaped from the use of DC transmission as compared to AC include the fact that an overhead DC line can be designed to be much cheaper per unit length and have a lower visual profile compared to an equivalent AC transmission line. DC transmission is highly preferred for long distance (>50 km) transmission of power under water, as AC cables make it less economically viable due to the capacitive charging current. To interconnect two AC systems require very reliable synchronization methods. The employment of DC systems eliminates this problem completely. The ability of DC systems to provide rapid power flow control in both directions has also been used to stabilise AC interconnected networks [4]. This is also useful in energy trading in a de-regulated market.

Large generation plants were built to take advantages of economies of scale, and transmission lines with increasingly high AC and DC voltages were constructed to allow the bulk delivery of power over long distances [2]. At present long experimental transmission lines of up to 1200 kV AC carrying bulk power have been installed and DC lines of up to  $\pm 600$  kV DC are operational

## Chapter 1: Introduction

### 1.1 Background

The first electric power company was introduced in the year 1882, by Thomas A. Edison [1]. The first transmission line was of DC type with a length of 59 km operating at 2.4 kV. Subsequently electricity demand and transmission distances increased making it impracticable for DC transmission.

Few years later, the introduction of AC machines (transformers, induction and synchronous motors and generators) made AC transmission more attractive for transmitting large amounts of power over long distances with the use of high voltage transformers [2]. For many years AC transmission remained the best available method of power transmission over long distances. However, as time went, technological advances and unavoidable economical factors emerged and DC systems became more comparable to AC systems and DC transmission was re-introduced in the 1950s [3].

The benefits reaped from the use of DC transmission as compared to AC include the fact that an overhead DC line can be designed to be much cheaper per unit length and have a lower visual profile compared to an equivalent AC transmission line. DC transmission is highly preferred for long distance (>50 km) transmission of power under water, as AC cables make it less economically viable due to the capacitive charging current. To interconnect two AC systems require very reliable synchronization methods. The employment of DC systems eliminates this problem completely. The ability of DC systems to provide rapid power flow control in both directions has also been used to stabilise AC interconnected networks [4]. This is also useful in energy trading in a de-regulated market.

Large generation plants were built to take advantages of economies of scale, and transmission lines with increasingly high AC and DC voltages were constructed to allow the bulk delivery of power over long distances [2]. At present long experimental transmission lines of up to 1200 kV AC carrying bulk power have been installed and DC lines of up to  $\pm 600$  kV DC are operational

worldwide. A few examples of extra high voltage (EHV) lines are the 765 kV lines in Canada, 765 kV American Electric Power Service system (AEP) in the U.S., 765 kV lines in South Africa, 750 kV and 1150 kV lines in Russia, the  $\pm 533$  kV DC line in South Africa, the  $\pm 600$  kV Itaipu DC lines and the  $\pm 500$  kV Nelson River lines [2, 5].

There are also several high voltage transmission projects that are being considered worldwide. Examples of such projects are the 650 km, 1000 kV UHVAC transmission line pilot project and the  $\pm 800$  kV UHVDC lines being considered in China [6]. Another example is the 3500 km,  $\pm 800$  kV Westcor project in which a transmission line is being considered for bulk power delivery from the DRC to Southern Africa [7]. Although feasibility studies of these projects have been done, research on a number of technical issues needs to be finalised prior to the implementation of these projects. From the operational point of view, issues surrounding insulation coordination, corona and electromagnetic fields at such high voltages need to be clarified.

One of the design factors in high voltage transmission lines is corona activity. Conductors and fittings energised at high voltages, both AC and DC are characterised by high corona activity. It is manifested as hissing and crackling audible noise (AN), radiated and conducted TV and radio interference (RI), corona loss (CL) and ozone generation [8]. Ion generation and ground level electric fields are also significant in the case of HVDC transmission lines. Earlier studies have shown that corona activity is related directly to the high levels of conductor surface gradients produced on the small-diameter conductors that were used at the time [9].

The main challenge is to minimise the operational conductor surface gradients during the design stages of the transmission lines. The conductor surface gradient depends very much on the following factors [10]:

- System voltage
- Conductor diameter
- Clearances between the conductor and adjacent phase conductors
- Clearances between the conductor and earth

- Number of conductors per phase/pole
- Bundle geometry (diameter of bundle and position of sub-conductors)
- Conductor surface condition
- System frequency

Apart from the conductor gradients, corona also depends on weather conditions such as temperature, pressure, humidity, snow, rain, fog, dust and movement of the air [8]. The design of EHV transmission lines in South Africa is distinguished from that of elsewhere by the altitude factor [10]. It has also emerged that the 765 kV lines in South Africa are equivalent to the 1000 kV lines from the corona point of view [2]. At high altitude, compared to sea level, there is most corona activity especially in terms of AN levels.

Transmission line corona problems have been reported by people staying next to the lines passing in high altitude areas such as the 765 kV AEP lines [2]. Eskom received AN complaints related to two of the 400 kV AC lines in the period from 1979 to 2004 [10]. Transmission lines in Poland (400 kV) are also considered to be acoustically disturbing for the environment [11]. There have not been many reported corona problems with regards to the currently operating DC lines. However, with much higher voltages being considered extra care needs to be taken when selecting the parameters to be used.

Several prediction methods for generating functions of corona have been developed. These methods are mainly based on measurement data obtained from test lines and corona cages located in the respective regions. Such methods were developed by amongst others CRIEPI in Japan, BPA and EPRI in the US, and IREQ in Canada. Software packages which can be used to predict electric fields and corona effects were also developed. The predicted electrical quantities will, therefore, vary with the meteorological conditions in the regions where the measurements were taken. As a result these prediction methods could be somewhat unrealistic when used for the Southern Africa climate and high altitudes.

## 1.2 Problem Identification

Corona generated AN and radiated RI have a negative impact on the environment, while the corona power loss has a technical impact on the transmission line in terms of conductor power loss, thereby reducing the overall transmission efficiency. The radiated radio noise affects communication systems adjacent to the line. Since corona activity increases with the system voltage, it has to be given more attention in the design of modern lines because of the current shift towards higher voltages for increased transmission efficiency over long distances.

Anticipated corona problems are usually minimised in the design stage of the transmission line guided by technical considerations and legal restrictions. Different regions and utilities have different limits for the effects of conductor corona. In this case the design engineer relies on the acquired experience, available software packages and equations (mostly empirical). Consequently, it is not possible to design with certainty, a transmission line that will operate free of corona.

The presently used methods of predicting the corona effects in the design stage of transmission lines were developed based on measurements, mostly done on test lines and corona cages located in places with different climatic or atmospheric conditions. Therefore, application of these methods to transmission line designs elsewhere, must take cognisance of variations in the climatic conditions. For example, Southern Africa has a unique climate, with low altitude coastal areas and very high altitude inland areas which experience high intensity of corona activity. So in order to have reliable designs from corona point of view, in future, new methods or correction factors need to be adapted. The new methods will have to be in agreement with the Southern Africa climatic conditions.

The appropriate methods or correction factors for predicting corona effects can only be determined by conducting experiments locally. This study intends to investigate the applicability of the existing methods to the Southern Africa environment, through simulations and laboratory measurements of AN and CL.

### **1.3 Research Questions**

Are the available methods for predicting conductor corona AN applicable to the Southern Africa meteorological conditions? To what extent is conductor CL dependent on transmission line parameters?

### **1.4 Hypothesis**

Since conductor corona is dependent on meteorological conditions and transmission line parameters, transmission line corona performance under Southern Africa conditions will be design dependent and different from that elsewhere.

### **1.5 Objectives**

The objective of this research was to:

- Measure the AN and corona current generated by conductor corona under HVDC voltages and local meteorological conditions,
- Compare the measured noise levels with the predictions made by the EPRI-TLW software,
- Assess the suitability of the EPRI software prediction methods in the AN design of transmission lines under the South African atmospheric conditions and
- Determine the characteristics of HVDC conductor CL.

### **1.6 Motivation**

To produce a reliable line design, a thorough understanding of conductor corona performance at different altitudes and air densities is necessary.

This study will assist in the following ways:

- Provide an understanding of the effects of conductor surface conditions, system voltage polarity and the conductor size on conductor corona,
- Show the effects of space charge on the measured quantities,
- Provide a comparison of DC and AC corona and
- Provide an evaluation of the applicability of the available conductor corona prediction methods to the Southern Africa conditions.

This study will result in a positive impact on the environment and the transmission line and, therefore, will save the utilities money and time spent on penalties and mitigation techniques when the transmission line is in the operation phase.

## **1.7 Research Design and Methodology**

The methodology that was adopted to prove the hypothesis is summarized as follows:

- An extensive literature review on conductor corona and its generating functions was carried out for both DC and AC systems. The equations for predicting corona effects were also investigated as well as the test configurations and conditions from which they were derived.
- Simulations were carried out using the EPRI-TLW software for both DC (positive and negative) and AC voltages. The Cahora Bassa transmission line configuration data was used as the input for a single conductor.
- The available laboratory corona cage set-up was modified with suitable corona rings and insulators to facilitate AN and CL measurements.
- Visual corona was observed using CoroCAM I.
- AN and CL short term indoor measurements were carried out at a low altitude region (Durban).
- The effect of space charge on the measurements was assessed.



- The obtained laboratory results were compared with the prediction methods for EPRI, BPA and CRIEPI obtained from the EPRI-TLW software package.
- The cage was converted into a short test line and measurements repeated thereafter a comparison of the cage and the test line results was done.

## 1.8 Structure of the Dissertation

This dissertation is structured in the following manner:

- Chapter 1: Introduction

The background, research problem, objectives and motivation are described in this chapter. This chapter also outlines the approach adopted in undertaking the study.

- Chapter 2: Literature Review

This chapter covers the literature reviewed on conductor corona and its effects, modes, ionisation processes and characteristics under both AC and DC voltages. The research on conductor corona carried out elsewhere is also covered in this chapter.

- Chapter 3: Methodology

Methods, techniques and apparatus used to test the hypothesis and the ones used to analyze data and validity of the study are described in this chapter.

- Chapter 4: Results and Analysis

The results obtained through measurements and the software package are presented in this chapter. A comparison of the results and observations with the literature review is also presented in this chapter.

- Chapter 5: Conclusions

Conclusions based on the findings of the study are presented in this chapter.

- Chapter 6: Recommendations

Recommendations and proposed areas for further research are presented in this chapter.

- References

All the literature resources that have been consulted and cited in the dissertation are listed in this section.

- Appendices

Specifications of the test and measuring equipment used in the study and the papers presented at conferences are presented in this section.



## Chapter 2: Literature Review

### 2.1 Introduction

Corona is a discharge phenomenon that occurs when the air surrounding the high voltage transmission line conductors operating at high surface gradients is ionised. It generates appreciable audible noise (AN), radio noise (RN), corona loss (CL), ozone and space charge in the case of DC lines. Corona is also dependent on meteorological conditions, line configuration and conductor surface gradient. As a result it has become an important transmission line design factor. Corona tests to assess the performance of transmission lines with regard to the above factors are conducted either on test lines or corona cages. In this chapter, the different corona modes and processes are discussed as well as the findings of other researchers who have done extensive research on corona generation and its effects.

### 2.2 Corona Generation

#### 2.2.1 Introduction

Conductor corona has become a significant factor. For example, in the design of Eskom's 765 kV lines in South Africa, choice of certain parameters was influenced by corona performance, such as choosing a six-conductor bundle instead of a four-conductor bundle to limit corona generated AN [10]. Earlier studies have shown that corona generation is related to conductor surface gradients [9, 12], and it is a result of small electrical discharges which occur when the electric field intensity on the conductor surface exceeds the electrical breakdown strength of the surrounding air [13]. Reference [14] also confirms conductor surface gradient as the design factor which most influences the corona performance of transmission lines. For air, at standard pressure and temperature, the critical corona inception gradient is above 30 kV/cm peak or 21 kVrms for AC fields [10]. The conductor surface gradient on its own is influenced by the following line parameters:

### **2.2.2 Conductor geometry**

Conductor surface gradient reduces with increasing conductor diameter, however, the corona inception gradient decreases as the conductor diameter increases [10]. Effect of conductor geometry on ground level electric field is minimal, though larger conductors result in slightly higher fields at ground level, by virtue of the fact that they generate more charge than smaller conductors for the same voltage [15].

### **2.2.3 Phase configuration**

The different configurations (i.e. horizontal, delta, and vertical) applicable to a single AC circuit yield different ground level electric fields. With some configurations, lower fields are achievable at an expense of increased noise levels. Configurations which result in smaller effective diameter lead to low field levels at ground due to less charge generated. However due to the small diameters, the conductor surface gradients are increased and consequently high noise levels [15].

### **2.2.4 Phase/pole spacing**

Increasing the phase spacing reduces the conductor surface gradient and therefore the corona effects are also reduced. With increased phase spacing, the cancellation of the fields at ground level is not maximally achievable; this resulting in high field levels [15].

### **2.2.5 Conductor height above ground**

Reference [15] reports conductor height above ground to have a larger influence on the maximum field at ground compared to the field at the surface of the conductor. Generally increasing the clearances between the ground and the conductors reduces the conductor surface gradient [10]. In the corona performance study reported in [16], the electric field was found to vary almost linearly with the minimum height with a slope of about 2.6 kV/m per meter change in the minimum height.

Generation of corona is not only determined by the distribution of gradient around the surface of the conductors but also by condition of the conductor surfaces [12]. Usually nicks, scratches

and debris deposited on the surface of the conductors lead to increased conductor corona. Weather conditions have also been found to have a significant influence on the surface of the conductors affecting the corona effects differently depending on the nature of the electric field.

Corona performance results on monopolar and bipolar cage tests presented in [17] showed differences between the cage and the line data. This gives the impression that the corona generation functions are not only a function of the conductor surface gradient but also the conductor-ground geometry. Corona generation has a significant effect on the ion distribution at ground and hence the electric field distribution at ground.

## **2.3 Ionisation Processes**

Corona discharges are characterised by a series of processes involving electrons, air molecules, atoms, and ions in the vicinity of line conductors. The processes are, as discussed below, ionisation and excitation, attachment, detachment and recombination.

### **2.3.1 Collisions**

Collision ionization mainly increases the number of electrons in the air. It occurs when the kinetic energy of the free electron is at least equal to the ionization energy of the atom with which it collides [10]. Excitation provides an atom and an electron whilst ionisation provides a positive ion and two free electrons. If the electron energy is not sufficient to cause ionization or excitation, the collision will increase the kinetic energy of the atom slightly. Ionisation and excitation may also be due to absorption of photon energy by the atoms rather than collisions of atoms with electrons [9]. In this case it is known as photoionisation.

### **2.3.2 Attachment**

Attachment tends to decrease the number of electrons in the air. It is characterized by direct and dissociative attachment processes. It occurs when an electron occupies one of the free energy levels in the outermost shell and converts the atom into a negative ion [10]. The process is more prevalent in electronegative gases such as sulphur hexafluoride and oxygen.

### 2.3.3 Detachment

It occurs when a negative ion loses its extra electron to return to its neutral state. The free electron can then continue to take part in the ionisation process through collisions and excitation [10].

### 2.3.4 Recombination

Recombination occurs when an electron collides with a positive ion and assumes the place of an electron that was removed when the ion was formed. A neutral molecule will be formed and will be in an excited state until it reaches the ground state by emitting a photon [10]. Positive and negative ions may also recombine to form a neutral atom [9].

## 2.4 Corona Modes

### 2.4.1 Introduction

Conductor corona occurs in different modes, from onset to breakdown, depending on the type of applied voltage. Under DC voltages, the modes are polarity dependent. For AC voltages a combination of the positive and negative modes is usually observed due to the alternating nature of the system voltage.

### 2.4.2 Negative DC

During negative corona the free electrons are accelerated away from the negative electrode (cathode) [10]. If there is enough kinetic energy, the free electrons will result in more collisions and eventually an avalanche will occur. The electrons move faster and dominate the tip of the avalanche [9]. Beyond the ionisation region recombination processes may take place resulting in negative ions. Thus in the gap the positive and the negative ions will exist. Corona is characterised by: Trichel pulses, glow discharge and pre-breakdown streamers (see Table 2.1). Trichel pulses are characterised by comparatively fast initial rise and small amplitudes whilst a typical positive pulse has much larger amplitude, slower initial rise and a longer duration [18].

### 2.4.3 Positive DC

During positive corona, the free electrons are attracted to the positive electrode (anode). More collisions occur resulting in the formation of less mobile positive ions from the anode into the inter-electrode space. The repulsion between the anode and the positive ion space charge causes the charged cloud to move into the gap. The avalanche and ionization occur at the tip of the positive streamer. If the field is high enough to sustain secondary avalanches then breakdown will occur. Otherwise recombination will occur [10]. Positive polarity corona modes are burst corona or onset streamer, glow discharge and pre-breakdown streamer (see Table 2.1).

### 2.4.4 AC

In HVAC systems the conductor surface gradient varies continuously with time. Different corona modes i.e. positive and negative as discussed above can be observed within one cycle of the applied voltage [10]. The AC corona mode observed each cycle resembles closely its DC counterparts and their pulsative modes are always associated with the supply frequency [18] (see Table 2.1). In the study carried out at the Waltz Mill 1100 kV station as discussed in [19], the AC corona plumes were observed to be longer for larger diameter conductors as opposed to smaller conductors.

A summary of the corona modes under DC voltages is given in Table 2.1.



Table 2.1: Corona Modes [10]

POSITIVE CORONA		NEGATIVE CORONA	
Mode	Characteristic	Mode	Characteristic
Burst Corona or Onset Streamer	High radio noise (Predictable spectral shape, from a few kHz to about 30 MHz)  Crackling type audible noise	<b>Trichel pulses</b>	<b>Low intensity radio noise</b> , wide unpredictable spectrum up to 100's of MHz
Glow	No radio noise  Some hum-type (100/120 Hz) audible noise	Glow	No radio noise  Some audible noise
Pre-breakdown streamer	High radio noise	Pre-breakdown streamer	High radio noise

## 2.5 Factors that Affect Conductor Corona

### 2.5.1 Introduction

Extensive research on corona has been carried out and well documented by many researchers around the world. Empirical equations for predicting corona effects have also been developed from a series of measurements conducted by research institutions and utilities. It is very clear from corona test results reported in most papers and text books that for HVAC lines corona effects (i.e. AN, RI, CL and ozone) increase during foul weather conditions. Similar observations are reported in references [9, 10, 11, 13, 20, 21]. However, in the case of HVDC lines, only the corona loss, fields and ions, and ozone increase during foul weather conditions [9, 13, 20]. AN and RI are found to increase under fair weather conditions for HVDC lines.

### 2.5.2 Altitude effects

The relative air density at sea level is usually very close to unity whereas high altitude regions are normally characterised by low pressures and low air density. At high altitude the corona onset voltage is lower due to the reduced pressure [22]. At low pressure less energy is required by electrons to ionise and breakdown voltage also decreases with decreasing pressure. The number of atoms per cubic centimetre and the probability of ionizing collisions increase as the pressure increases [13]. Air density varies inversely proportional to the temperature and directly proportional to the air pressure due to increased free mean path. The relationship between corona inception and humidity is of a non-linear nature; generally, corona inception decreases with humidity [18]. It is also stated in [13] that halogens and water vapour have the ability to capture electrons through electron attachment; as a result, increasing the humidity in the air gap improves the gap breakdown strength and therefore high corona inception and breakdown voltages.

Reference [23] presents the Westinghouse and the Italian formulae which have been proven, through tests; to be applicable for correcting RI measurements made at sea level to higher altitudes. The Italian formula can also be applied for AN and CL altitude corrections. However its applicability for altitudes below 300 m is not certain [23], for South Africa, according to [10], line designers support the Italian altitude correction formula for up to 2500 m above sea level. The Westinghouse formula requires the knowledge of the average relative air density (RAD) which is not always readily available.

A study of the impact of RAD on corona under HVDC conditions was carried out using the Grizzly mountain database. The results from this study as presented in [24] showed that the relative air density relationship with HVDC corona performance is similar to that under AC conditions. Furthermore, under positive polarity, the electric field and the ion current density were found to increase with RAD up to RAD of 0.9, beyond which they decreased.

### 2.5.3 Conductor surface conditions

Most operating transmission lines use stranded conductors in bundled geometries. Stranding of the conductors, contamination and any form of precipitation on the surface of the conductor,

constitute surface irregularities which result in increased effective conductor surface gradients [18]. Smooth polished conductors have a roughness factor of about 1, practical stranded conductors with nicks and scratches have roughness factors in the range of 0.6 to 0.8 [25]. Wet weather conditions can reduce the conductor surface roughness factor even more, presumably in the range of 0.3 to 0.6 [26]. Airborne substances such as dead insects, dust and leaf particles stuck on the surface of the conductors, also result in an increase in the effective conductor surface gradients [13]. It was also established that the number of airborne particles stuck on the conductor surface is higher in summer which contributes more towards increased fair weather corona activity [13].

## **2.6 Corona Audible Noise (AN)**

### **2.6.1 Introduction**

As mentioned above, during corona discharges the rapid movement of electrons during ionisation result in the sudden transfer of kinetic energy to neutral air molecules through collisions. Reference [9] states that the transfer of kinetic energy is equivalent to an explosion taking place at the corona site, which gives rise to the generation of acoustic waves. In essence corona discharges are a source of acoustic pulses. Under AC voltages bursts of acoustic pulses are generated near the peak of the positive cycles. The alternating voltage results in the pure tones at frequencies corresponding to the even harmonics of the system frequency. In the case of DC systems, there is no generation of the pure tones due to the absence of any modulating influence of the voltage. Basic laws of acoustics are used to analyse the transmission line AN with some assumptions made. For the analysis it is assumed that:

- Corona is distributed uniformly along the length of the conductor and AN generation can be characterised by a uniform distribution of acoustic power per unit length.
- The microphone used is ideal and responds equally to the pressure waves irrespective of the angle of incidence.
- Sound waves do not experience any attenuation as they propagate.
- Reflection of the sound waves by the ground is negligible [9].

Considering a single conductor above ground and solving equations from acoustic theory as shown in [9], the sound pressure  $P$  sensed by the microphone can be determined as follows:

$$P = \sqrt{\frac{c\delta A}{2\pi R} \tan^{-1} \frac{l}{2R}} \quad \dots 2.1$$

Equation 2.1 is applicable to a short transmission line, for an infinitely long line 2.1 reduces to Equation 2.2.

$$P = \sqrt{\frac{c\delta A}{4R}} \quad \dots 2.2$$

Where,

$P$  = sound pressure level (Pa)

$c$  = propagation velocity of sound waves (m/s)

$\delta$  = air density ( $\text{kg/m}^3$ )

$A$  = generated acoustic power density (W/m)

$l$  = length of the conductor (m)

$R$  = distance between the noise source and the point of observation (m)

The exact value for the propagation velocity of sound waves is obtained from Equation 2.3 [28]. However, this value is taken as 331 m/s in most calculations including those in [13].

$$c = 331.4 \sqrt{1 + \frac{\theta}{273}} \quad \dots 2.3$$

Where,

$\theta$  = temperature in degrees

According to [9] the air density varies with ambient temperature and at sea level it is about  $1.22 \text{ kg/m}^3$  in summer and  $1.28 \text{ kg/m}^3$  in winter. In the [13] experimental work, a value of  $1.29 \text{ kg/m}^3$  is used for the air density.

With the sound pressure  $P$  and the generated acoustic power density  $A$  expressed in dBA at a reference of  $20 \mu\text{Pa}$  and  $1 \text{ pW/m}$  respectively, Equations 2.1 and 2.2 become,

$$P(\text{dBA}) = A(\text{dB}) - 10 \log R + 10 \log \left( \tan^{-1} \frac{l}{2R} \right) - 7.82 \quad \dots 2.4 \text{ (short line)}$$

$$P(dBA) = A(dB) - 10 \log R - 5.86 \quad \dots 2.5 \text{ (long line)}$$

The above equations are applicable to AN generated from both HVAC and HVDC transmission lines.

AN is greatly affected by the conductor surface gradient [11, 29] compared to any other factors. The parameters of the line only have an insignificant influence on AN. For example, in the design considerations discussed in [15] it is mentioned that variations in conductor height will only result in small variations with AN generated. The AC laboratory results mentioned in [21] indicated that as the surface gradient increased, audible noise increased until it reached saturation levels and the difference in noise levels between conductor arrangements decreased with increasing conductor surface gradient. Practical conductor surface gradients on operating lines seem to be in the range of 15 kV/cm to 30 kV/cm. For this reason, the BPA prediction formulae as presented by Chartier and Stearns [28] are valid for gradients between 12 and 25 kVrms/cm for AC and between 17 and 29 kV/cm for DC. Furthermore, the equations which are incorporated in the EPRI's software "ACDCLINE" are valid for gradients between 15 and 30 kV/cm for DC transmission lines. Conductor surface gradient is also dependent on system voltage. Reference [13] reports that a 10% change in the operating voltage yields a 5 dB change for HVDC corona AN and a 3.6 dB change for HVAC lines due to increased surface gradients.

A consideration of the AN, ions, and RN effects in the design stage of the line can minimize the effect of all these corona-related effects [29] thereafter in the operation phase. In order to determine the behaviour of corona AN, long term and short term AN measurements can be done. Long term measurements are more reliable because they take into consideration the effects of different weather conditions on the measurements. Measurements techniques and instruments may also affect the noise levels measured. It is also worth mentioning that measured AN depends on the distance between conductor and the microphone used to measure the noise levels [12]. Depending on the procedures employed during the measurements, data obtained may be influenced by one or more of the following factors [30]:

- Incorrect microphone orientation

Most available microphones are not ideal, i.e. they respond differently to the sound pressure waves depending on their type, size and orientation relative to the noise source. During tests,

the microphone might not be well positioned with respect to conductors such that it captures less noise compared to what is actually generated.

- Poor or incorrect calibration procedures of the measuring equipments

Calibration methods for all the equipment used need to be followed precisely in line with the manufacturers recommendations. A general check-up of the equipment on a frequent basis also helps to identify any malfunctioning or calibration errors.

- High background noise levels

Depending on the location of the test site or the operating line and the time during which the measurements are performed, the background noise can affect the measurements significantly. A better practice will be to take measurements at night time when man-made noise sources are minimal.

- Effects of the electric field on the microphone systems especially DC ions

The operation of the microphone and the recording system can be affected by the electric field if placed within the stronger field. The AC and the DC fields will have different effects on the microphone. In the case of short term measurements, the presence of the operator of the equipment can also impact on the measured noise levels.

Since the operation of high voltage lines began and corona related AN complaints received, extensive measurements have been carried out. The measurements were intended to determine the characteristics of AN in relation to, amongst other factors, the conductor surface gradient, the nature of the system voltage, conductor sizes as well as weather conditions. As part of determining the corona generation functions, about five (5) different equations developed for the prediction of AN were compared in [20]. From the comparison shown, the prediction methods are not always in good agreement. It is suspected that the differences are due to the different conditions under which the measurements were carried out. According to [20], the most widely used prediction methods are the ones developed by EPRI at the HVTRC and at BPA. The  $L_{50}$  acoustic power levels of these methods appear to be in good agreement and

apparently, this holds for most lines. The results of the study of the comparison of AN prediction methods described in [30] also show that there are deviations between AN levels predicted using different empirical formulae and between predicted and measured levels for both AC and DC measurements.

### **2.6.2 Polarity effect**

Corona generated pulses on positive polarity conductors have higher magnitude and longer decay times resulting in more generated AN [13]. On the other hand the pulses on negative corona are smaller and more frequent, generating less noise. As a result, negative pole AN is often considered negligible in the prediction of AN [9, 13, 23, 28, 31]. Results of a study carried out at IREQ in a monopolar outdoor test cage indicated that positive polarity AN levels were about 7 dB to 10 dB higher than the negative polarity AN under fair weather conditions [17]. In [13], it is reported that the previous test results from cages showed a difference of about 8 dB between the positive and the negative polarities which is in good agreement with [17].

### **2.6.3 Conductor sizes**

The electric field in the vicinity of large diameter conductors tends to support longer streamers than the electric field around small conductors corresponding to higher noise being produced from larger conductors. This was mentioned in [10] and agrees very well with the results presented in [17, 19]. In [10], it is stated that AN increases with increasing conductor diameter for the same conductor surface gradient. In a study of conductor selection for the 1100kV AC Waltz Mill substation presented in [19], it was observed that during the tests, AN increased with the conductor size for the same surface gradient and with the number of subconductors for the same gradient and the same subconductor size. Based on the monopolar and bipolar cage studies reported in [17], the general trends showed that with all other parameters remaining the same, AN increased with the conductor size and the conductor surface gradient.

### **2.6.4 Corona cage and test line measurements**

It is uncertain as to whether the cage and test line AN results are similar i.e. as to whether the cages can simulate the electrical environment around conductors of an operating transmission line. A comparison of the cage and single phase test line results reported in [12] showed that

similar results were obtained only when the line and the cage tests were run simultaneously than when tested under different conditions. According to [28] the slope of the AN or other corona phenomena versus the conductor surface gradient characteristics is smaller for conductors tested in cages and also saturation does not occur on test lines. The discussions in [17], which are based on DC measurements, clearly caution that the cage data cannot be directly used to predict the performance of a line. However, it is also mentioned that if the slopes on the corona generation functions, with respect to other parameters such as conductor surface gradient, are the same for the line and the cage data, then the empirical relationships derived from the cage may be used to predict line performance. The observed corona generation quantities for AN, RI and CL were higher than those of the test line when plotted against the maximum bundle gradient [17]. While on the issue of the reliability of the cage data, it is very logical and for the essence of this study to give details of the AN corona cage study that was carried out at CRIEPI. The study as reported in [31] argues that test cages can be used to measure and predict corona AN under DC conditions provided the space charge field effect is taken into account rather than just the static field. In the study, two corona cages, a square cage and a cylindrical cage of different sizes as well as the Shiobara HVDC test line were used. The space charge field was evaluated from the measured corona current, space charge density and the mobility of the ions.

In terms of the results obtained, there was good agreement between the measurements carried out in the two cages when the space charge surface gradient was considered compared to when only the static surface gradient was considered. The generated sound pressure level increased linearly with the maximum conductor surface gradient in the presence of space charge [31]. Different polarity arrangements on the test line yielded different AN levels. There was fair agreement between the cage and the test line AN results even when expressed in terms of space charge modified field. The test cage measurements were not of a long term; consequently, weather conditions were attributed to the discrepancies. It was then concluded that AN is directly related to the space charge field under the same weather conditions and conductor surface conditions regardless of the electrode arrangement. In the paper discussions [31], it emerged that there was a case where the current measured on the negative pole was about twice that measured on the positive pole and the discussers question was as to what effect this will have on the calculated space charge field since their calculations are based on current measurements. Unfortunately negative polarity measurements had not been considered in this



particular study. The other comment was whether the results obtained in Japan can be used to predict AN elsewhere; the response to this was that only if the weather conditions are the same then the results can be applicable.

### **2.6.5 Effects of weather conditions**

Climatic conditions affect corona differently depending on the system voltage. HVAC and HVDC line design considerations for AN are similar. However, there are some important differences as discussed in [13]. HVDC corona AN is higher under fair weather conditions, during wet weather conditions, the ionization is much higher and the amount of space charge is also higher such that the surface gradient is reduced. In physical terms the increased corona activity during foul weather suppresses the positive polarity plumes which are the primary source of the AN [29]. This also plays a role in the tolerability of HVDC noise. It is most likely to be intolerable since it occurs mostly under fair weather conditions when most people are outdoors and there is no rainfall masking the line noise [13]. Under AC conditions, however, AN tends to be higher under wet weather conditions. In Poland a short term AC noise study was carried out on operating 400 kV lines and it was found that AN increased from 35 dB under fair weather conditions to about 57 dB under heavy rain conditions, with measurements done at 15 m from the middle of the span[11]. Observations mentioned in [19] include that during heavy rain conditions, AC noise approached saturation, and corona inception was even lower than Peek's predictions. The differences between fair and foul weather conditions AN for DC and AC voltages is apparent and is also incorporated in software tools. For instance AN prediction formulae in the BPA corona performance software, for DC lines, rainy weather AN is estimated by subtracting 6 dB from the  $L_{50}$  fair weather AN. In contrast, the  $L_{50}$  fair weather AN is estimated by subtracting 25 dB from the  $L_{50}$  rainy weather for AC systems [23].

### **2.6.6 Frequency spectra**

Reference [9] mentions that the amplitude and the shape of the frequency spectrum depend on the intensity and waveform of the acoustic pulses generated as well as the frequency response characteristic of the microphone used. According to [28], at the time the research was carried out, there was insufficient data to determine whether the shape of the frequency spectra characteristics for AC and DC lines is constant, independent of the line configuration or the voltage. In [32] it is reported that AN frequency spectrum varies in level and shape depending

on the weather conditions. Although there are differences, the hum component is very common in AC noise. Reference [11] states that AC frequency spectrum consists of pure tones (supply frequency and its multiples) superimposed on broadband crackling or the hissing type noise (1 to 15 kHz). Another observation that was made in [21] is that the hum component varied considerably with lateral distance from the line, which makes it difficult to compare the hum component from different conductors under field conditions. According to [13] the pure-tone component of the HVAC AN noise modifies the nature of the noise and also contributes to the resulting annoyance. A description of a typical AC frequency spectrum is given in [28]. For AC lines, the frequency spectrum appears to be flat for frequencies above 500 Hz under rainy conditions. However, the shape seems different for other wet-weather conditions. AC noise levels for frequencies below 1 kHz are difficult to predict and are presumed to be a function of the conductor ageing. Evident to this, the AC frequency spectrum presented in [28] also shown in [2] showed a 10-14 dB difference in hum content for measurements done in the first year of operation and nine years later. For frequencies between 1 kHz and 8 kHz the noise levels remained similar. The annoying effect of the AN under DC conditions is mainly due to the high frequency crackling noise [28], as there are no hum components from the power frequency. There are slight differences in the low frequencies of the frequency spectra shown in [9]. In [13] the noise level is higher in the low frequencies and decreases up to 125 Hz. However, in [9] the noise level is lower at 31 Hz, increases up to 63 Hz from which it decreases up to 250 Hz. It is also mentioned in [13] that the best indicators of corona AN generated from HVDC lines are the octave band measurements from 500 Hz and above, due to the effect of the background noise on the low frequency noise levels. DC noise spectrum obtained during dry conditions from the Dalles DC test line with twin 46.2 mm conductors, gave a flat frequency response for frequencies from 1 kHz up to 8 kHz [28].

### 2.6.7 Attenuation/air absorption

Applying the inverse square law to a transmission line of infinite length, the sound pressure level is inversely proportional to the square of the distance. This implies that it decreases with  $10\log R$  where  $R$  is the radial distance between the microphone and the conductor. This is also reported in [2, 21]. However, AC measurements conducted at BPA, Apple Grove and Hydro-Quebec showed that the sound pressure decreases with  $10\log R$  to  $13.3\log R$  [28]. DC data from The Dalles DC test centre showed that the attenuation rates are even higher for DC.

### 2.6.8 Mitigation techniques

As mentioned above, propagation of the acoustic pulses depends on the distance away from the noise source but as for transmission lines; the corona AN attenuates relatively slowly with increasing distance. As a result, increasing right-of-way (ROW) is not an effective way of reducing AN [15].

BPA contracted Westinghouse and General Electric to consider techniques that could be used to reduce transmission line AN [33]. Several options were considered and it appears that almost each one of them had a disadvantage. Earlier considerations of AN in the design stage can assist with regards to the costs associated with applying mitigation techniques. According to [33], the following options were considered:

- The use of thin wires or sharp edges to produce less impulsive ultra corona – they produced strong 120 Hz hum, generated TVL, produce excessive losses and their durability is doubted.
- Insulating the conductors - only thick insulation was effective. Tests showed that it is susceptible to corona damage, increases wind loading on towers and reduces the load carrying capability of the lines. Also requires stronger towers to support the heavier conductors.
- The use of large thin-walled conductive tubes surrounding the conductor – seemed to be most practical and effective.
- Reconductoring the line was very effective, it reduced the AN from 64 dBA to 49 dBA on two BPA transmission lines, but it is very costly.

## 2.7 Corona Losses (CL)

### 2.7.1 Introduction

Reference [9] states that corona processes such as movement of charged particles, collisions between charged particles and neutral molecules require energy. In the case of transmission

lines the energy required is drawn from the high voltage source connected to the conductor and converted to many other forms of energy. The rate at which the energy is drawn from the source is power and may be identified as corona power loss. The creation and movement of positive and negative ions is mainly responsible for the generation of CL. According to [9], the electrons created in corona discharges have a very short lifetime and current pulses produced by their rapid movement do not contribute significantly to the CL. The theoretical analysis for both AC and DC CL is shown in [9]. However, it is also mentioned that the theoretical calculation or prediction of CL based entirely on a theoretical approach has not yet been successfully accomplished.

Physical mechanisms responsible for generation of CL under DC are different from AC because of the constant applied voltage. During corona discharges the ionic space charge having the same polarity as the conductors fills the entire inter-electrode space. The generated space charge drifts towards the ground or the opposite polarity conductor for monopolar arrangements. For bipolar arrangements the ions mix in the region between the negative and the positive poles resulting in recombination [26]. The velocity of ions is proportional to the electric field and depends on the mobility of the ions [13]. A theoretical analysis of DC corona power loss based on a number of assumptions is given in much detail in [9] for both monopolar and bipolar configurations.

Corona power losses are affected by all the factors that affect corona inception and greatly affected by atmospheric variables such as wind, humidity and aerosols under DC conditions [9]. In the study reported in [17], CL was found to increase with the conductor surface gradient and the conductor size with all the other parameters remaining the same. The evaluation of AC corona losses requires the knowledge of the electric distribution in the vicinity of conductors whereas for analysis of DC losses, the field distribution in the entire inter-electrode space has to be known [34]. Reference [13] states that DC losses are also dependent on the potential difference between the conductor and the ground. Corona current of a DC line depends on the line geometry particularly the pole spacing [13]. In the case of unipolar lines a change in conductor height has a much larger influence on CL than a corresponding change in conductor size [9]. CL depends on the position of the bundle relative to the ground and the extent to which the position influences the movement of space charge [12]. It also depends on the proximity of the grounded cage effects in cases where test cages are used [20]. According to [35], the line

height and the pole spacing in case of bipolar arrangements, influence the amount of corona current that will reach the ground and consequently the corona current that will be measured. Care should also be taken when considering the diameter of an overhead ground wire to ensure that the space charge does not cause the surface gradient of the ground wire to be higher than the corona inception. If the ground wire goes in to corona then a bipolar mode is established and a drastic increase in CL and other corona effects will be incurred [9].

CL measurements for predicting the corona performance of a transmission line under AC conditions can be carried out using test cages and test lines. However, DC test cage results cannot be used to directly predict the performance of an operating line due to the differences in space charge distributions [9]. In terms of measuring equipment, CL measurements under AC fields involve detection of small current component in phase with the voltage in the presence of a very large out-of-phase capacitive current component and, therefore, require instruments that can measure low power factors [9]. Reference [26] also mentions that AC CL measurements require detection of small power loss in the presence of large reactive components. References [22, 26] state that CL can be measured with watt meters or watt transducers, bridge circuits and a combination of bridge circuits and watt meters. According to [12] AC losses are normally measured with a self-balancing Schering bridge to avoid manual balancing at high voltages and especially in the case of long term measurements. For DC measurements, CL in test cages or on test lines are estimated by measuring the current flowing through the conductor and multiplying with the applied voltage [9].

### **2.7.2 Polarity effect**

Reference [9] reports that monopolar test line results have shown that the influence of conductor polarity on space charge field and CL is not significant whilst bipolar test and operating lines have shown that the difference between the negative and positive CL is quite small, with the negative CL being higher than positive polarity in fair weather and positive CL higher in rain conditions. However there was a case where measurements on bipolar operating transmission line clearly shown that under fair as well as foul weather conditions the current density profile at ground level was dominated by corona on the negative conductor. Bipolar DC test line study presented in [36] has shown that higher current densities were measured under the negative pole than under the positive pole. In the monopolar cage study carried out at IREQ,

the fair weather positive polarity CL were about 2 to 6 dB higher than the negative polarity CL, whereas in wet weather they were almost similar with the positive polarity increasing by about 5 to 6 dB [17].

### 2.7.3 Effect of weather conditions

DC CL is higher under foul weather conditions especially rain [36], and also, fair weather AC losses are generally negligible as the highest losses occur under heavy rain conditions [26]. Unlike AN, both average fair weather AC and DC CL are less than the wet weather losses. In the BPA software described in [23] AC and DC fair weather losses were computed by subtracting 17 dB and 5 dB from the average rainy weather losses respectively. Loaded lines operate at increased temperatures resulting from the load current. Tests carried out on fully loaded HVDC lines showed that there is a relationship between ions, electric field and the load current according to the reports made in [22]. In the Grizzly Mountain study, negative ion current density showed a linear increase with the increasing conductor temperature [24]. Windy conditions tend to have an effect on the generated CL especially under DC conditions. According to [9], DC tests on reduced-scale models, full-scale test lines and on operating lines, have clearly established the marked influence of the perpendicular component of wind on ion current distribution at the ground level. Reference [13] states that wind affects the speed and the direction of the ions as they drift in the inter-electrode space to ground or conductors of opposite polarity. In [33] which deals with the corona design considerations, it is mentioned that at higher altitudes CL is lesser when smaller conductors are used; in contrast the  $I^2R$  losses reduce when fewer but larger conductors are used [33] making it clear that the choice of the optimum conductor size needs to be approached with caution.

## 2.8 Effect of Space Charge

AC fields change polarity every half cycle and therefore recombination of negative and positive ions in the vicinity of the conductor occurs each and every cycle. For AC lines space charge generated is confined to a small volume immediately surrounding the conductors and therefore has negligible effect on the overall field distribution within the cage [20].

However, corona under DC fields results in accumulation of positive and negative ions in the vicinity of the conductor depending on the polarity, thus a positive conductor in corona acts as a source of positive ions and vice versa [35, 37]. The corona generated space charge affects the breakdown characteristics of the gap. Under positive polarity, the gap is dominated by slower positive ions, effectively leading to a lower breakdown voltage. Under negative polarity, both negative and positive ions are present in the gap setting up a space charge field which opposes the main gap field leading to higher breakdown voltage [13]. These ions give rise to corona current and are also responsible for electric induction effects produced on objects located in the vicinity of the lines. Reference [37] presents the details of how space charge can be quantified with the knowledge of the following parameters in the vicinity of the conductors:

- Electric field intensity
- Ion current density
- Space charge density
- Mobility of the ions

Some of the above parameters are vectors and require special instrumentation to measure. Measurements done by IREQ on a test line showed that the presence of space charge generally increases the electric field at ground level. From an operating  $\pm 450$  kV bipolar line, the presence of wind seemed to be partly responsible for the distribution of space charge [37]. Work carried out at the HVTRC reported in [38] also confirms that a HVDC line in corona can increase the space charge density downwind, and that the small air ions are the predominant charge carriers near the HVDC line whereas aerosols become more predominant as the distance downwind increases.

Negative and positive space charges move in opposite directions and influence the nature of the local electric field as well as the conductor surface gradients [18]. Space charge distributed far from the conductor influences not only the electric field on its surface and around it but also that surrounding the conductor bundle of another polarity [31]. Reference [13] states that if space charge is produced in high quantities, the source ceases to be in corona until the space charge is driven by the electric field away from the conductor. Space charge suppresses the field

to below the critical level and [39] also reports that space charge in monopolar coronas always tends to reduce the ionisation region field. However, [18] reports that at much higher voltages, the electric field becomes stronger to an extent that the space charge is unable to reduce the field sufficiently and pre-breakdown streamers appear.

The effect of space charge depends on the system configuration and varies between cages of different diameters, cages and test lines and different polarity arrangements [31]. In view of this, [13] states that cage measurements can be useful in cases where not much space charge is generated; however, this does not represent operational transmission line situations. In [20] cages are not deemed to be very useful for HVDC corona generation quantities due to the generated space charge that fills the entire space of the test cage and affects the electric field at the conductor surface. Though the primary aim of this study is not based on the RN and ozone generation, it was considered essential to briefly include them in the literature review so as to have a full picture of corona effects.

## **2.9 Radio Noise (RN)**

RN refers to any unwanted disturbance within the radio frequency band. Corona discharges are pulsating in nature and the frequency spectra of the pulses can cover a considerable portion of the radio frequency band [13]. More and more compact lines are built near residential areas; these lines normally operate at high field levels and generate high RI levels which interfere with the neighbouring communication systems depending on the proximity [10]. The frequency spectrum of RN is confined to the band of about a few kHz to 30 MHz and can also degrade the dependability of power line carrier (PLC) telecommunication channels [10].

Similar to AN, RI is affected by the conductor surface gradient and it is mentioned in [13] that all predictive formulae or analysing methods utilize the conductor surface gradient as the prime parameter for estimating RI level for both AC and DC transmission levels. Reference [10] states that RI increases with conductor diameter for the same conductor surface gradient. The results of the study reported in [17] have shown that RI generally decreases with an increasing number of subconductors in a bundle and increases with conductor size and the conductor surface



gradient [17]. In HVDC transmission lines, the positive pole generates more radio interference (RI) than the negative pole and it is beneficial to arrange the poles such that the negative pole is the one closer to the human habitat [9]. In cage studies, negative polarity RI was also found to be comparatively negligible [17]. RI is influenced by external factors such as ambient weather conditions and ground resistivity [9]. High levels of RI prevail during fair weather conditions for DC lines as opposed to AC lines for which RI is higher during wet weather conditions [13, 36]. In [23] it is mentioned that RI for wet weather conditions, under DC, is slightly less than fair weather RI, and heavy rain RI is computed by subtracting about 6 dB from the fair weather RI. The RI frequency spectrum of DC transmission lines is said to be similar to that of AC lines since the generated pulses are similar for both AC and DC lines [9].

## 2.10 Ozone

Major elements of the air are oxygen and nitrogen molecules. During ionisation, the oxygen molecule may be separated into two oxygen atoms making it possible for the formation of ozone [13]. Ozone production rates were found to be influenced by conductor surface gradient, mode of corona discharge and weather variables [9]. Reference [20] states that corona generated ozone concentrations are often below the natural levels and difficult to measure. According to [9], measurements made in the vicinity of transmission lines have shown that the maximum incremental contribution by corona on transmission lines to ambient ozone levels is only of the order of few parts per billion. Reference [22] also confirms that measurements of ozone levels from EHV and UHV lines were much lower than the ambient and as a result ozone generation is not regarded as a design issue.

## 2.11 Design Considerations

There are no international limits or standards that govern corona effects, power utilities set their own standards based on their experiences and/or local regulations. During the literature scan a few limits adopted by some utilities caught sight. The BPA has a design policy of AN  $L_{50}$  level of 50 dBA under AC conditions during rain at the edge of the ROW. The BPA does not have any policy for DC lines, but  $L_{50}$  of 42 dBA during fair weather is considered acceptable by BPA

[33]. It is also believed that if a transmission line is designed for acceptable AN level, it will also generate acceptable levels of RI/TVI [22, 33]. Corona loss impact economically on the system and not on the environment and therefore does not have regulatory impact. The contribution of transmission lines to ambient ozone is also negligible [32].

Canada does not have national standard specifying limitations for audible noise from transmission lines, instead existing regulations dealing with general environmental noise sources are used. Canadian Standards Association (CSA) developed a standard for interference from high voltage AC power systems in the frequency range of 0.15 MHz to 30 MHz. this standard specifies 63 dB above 1  $\mu\text{V}/\text{m}$  fair weather interference field strength measured 15m laterally from the outer most conductor [32]. In South Africa, Eskom adopted the following limits in the design of 765 kV lines at 1500 m altitude [10]:

- RI limit of 72 dB (1  $\mu\text{V}/\text{m}$ ) at 0.5 MHz at the servitude boundary in  $L_{50}$  conditions.
- AN limit of 53 dBA at 18 m above ground at the maximum line voltage at the servitude boundary

There are no specific design limits for corona losses for Eskom, but a maximum of 5% of the full load  $I^2R$  conductor losses is considered reasonable. Reference [10] also states that there are no stated limits for ozone generated by transmission lines because it is normally comparable to the background ozone levels.



## Chapter 3: Methodology

### 3.1 Introduction

Laboratory measurements were conducted at the HVDC Centre of the University of KwaZulu-Natal situated on the Westville Campus. The laboratory is in the coastal region and near zero altitude. The main equipment that was used is the  $\pm 500$  kV DC source, 2x100 kV AC test transformer set and the corona cage. Audible noise (AN) measurements and corona current measurements were done under both AC and positive and negative DC voltages. Noise level meters, a digital micro-ammeter, digital oscilloscope and a corona camera were used as measuring and monitoring equipment. The EPRI-TLW software and previously published information was used for the analysis of the obtained results.

### 3.2 Test Equipment

#### 3.2.1 The HVDC voltage supply

The DC source is a 2-stage Walton-Cockroft generator with a maximum output voltage of +500 kV and -540 kV and 7.5 mA current capability. In the tests, only voltages up to 280 kV could be applied due to clearance limitations. The generator is supplied through a 100 kV DC test transformer. The detailed ratings and the circuit diagram of the generator are as shown in Table 3.1 and Figure 3.1 respectively. Table 3.2 shows the values of the parameters in Figure 3.1. The specifications of the AC test transformer are shown in Appendix A.

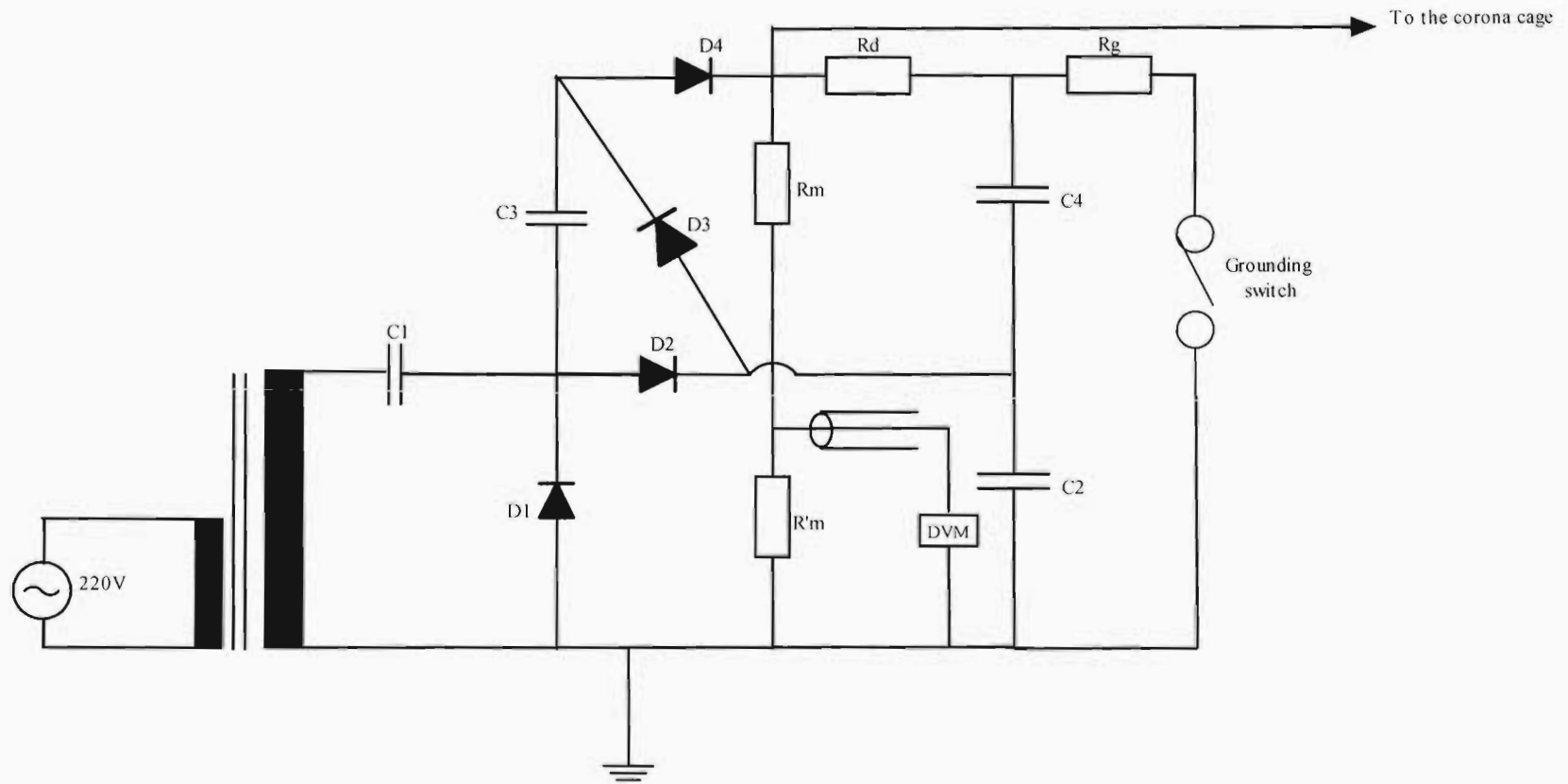


Figure 3.1: Circuit diagram of the high voltage DC generator

Table 3.1: Specifications of the high voltage DC generator

No load rated output (positive polarity):	+500kV
No load rated output (negative polarity):	-540kV
Rated continuous current:	7.5mA
Ripple voltage:	$\leq 3\%$ at rated current and voltage

Table 3.2: Circuit parameters of the DC generator

<i>Parameter</i>	Value
C1	150 kV, 100 nF
C2	300 kV, 50 nF
C3	300 kV, 50 nF
C4	300 kV, 50 nF
D1	300 kV, 20 mA
D2	300 kV, 20 mA
D3	300 kV, 20 mA
D4	300 kV, 20 mA
$R_m$	300 kV, 2 x 600 M $\Omega$
$R'_m$	560 $\Omega$
$R_d$	10 k $\Omega$
$R_g$	20 k $\Omega$
dvm	digital volt meter

### 3.2.2 The corona cage

A small indoor corona cage with a length of 2 m and diameter of 1.5 m was used. It is cylindrical and consists of three sections. The two outer rings are 1 m long each and are solidly grounded. The centre ring is normally floating to allow voltage and current measurements to be done from the centre as shown on the detailed schematic diagram in Figure 3.2. The outer rings are connected to the centre ring only mechanically and electrically insulated from it through vesconite insulators.

### 3.2.3 Conductors

Only single conductors were considered due to clearance limitations. Solid and stranded aluminium conductors with diameters 1.6 cm, 2.8 cm and 3.5 cm were tested. Solid conductors were thoroughly polished before being tested to achieve fairly good surface conditions. The conductor under test was suspended with the polymeric tension 66 kV, 460 BIL insulators obtained from Hardware Assemblies. Two corona rings each with a diameter of 50 cm were attached at each conductor end-fitting in order to reduce the electric stress around the end fittings and ensure that corona occurred only on the conductor surface.

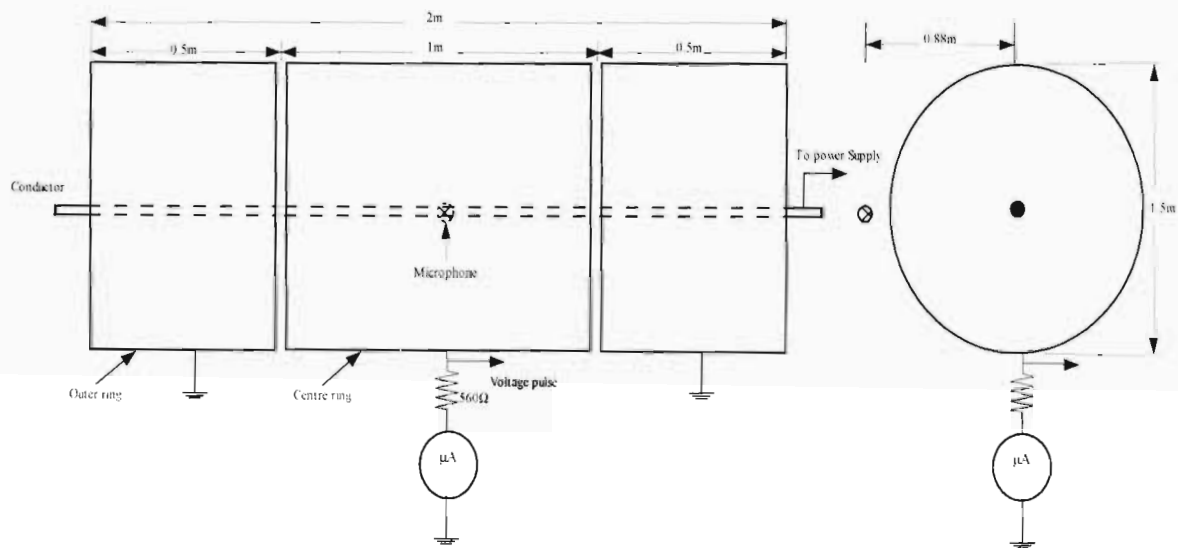


Figure 3.2: Corona cage

### 3.3 DC Measurements

Temperature, pressure and humidity were recorded at the beginning of every session of measurements and also verified at the end of the sessions. Variations of weather parameters were not significant as all the tests were performed indoors under similar conditions. The effect of wet weather was not explored. The measurements were mainly performed in the evening when traffic and all other noise sources were minimal. Repeatability of the results was verified several times and on different days.

### 3.3.1 Audible noise

The A-weighted audible noise measurements were done using the noise level meter ELT 3 from Rhode&Schwarz. It is equipped with a capacitor microphone and has non-directional properties. To obtain the octave-band frequency spectra, audible noise measurements were done using the Bruel&Kjaer noise level meter Type 2218 attached to an octave filter set, Type 1613. These measurements were done for 3.5 cm $\varnothing$  and 2.8 cm $\varnothing$  conductors. Technical specifications of both meters are included in Appendix A. The meters were positioned in a Faraday's measurements cage adjacent to the corona cage shown in Figure 3.3. The microphone was placed centrally to the corona cage and orthogonally to the conductor under test. The radial distance between the microphone and the conductor was about 0.88 m.

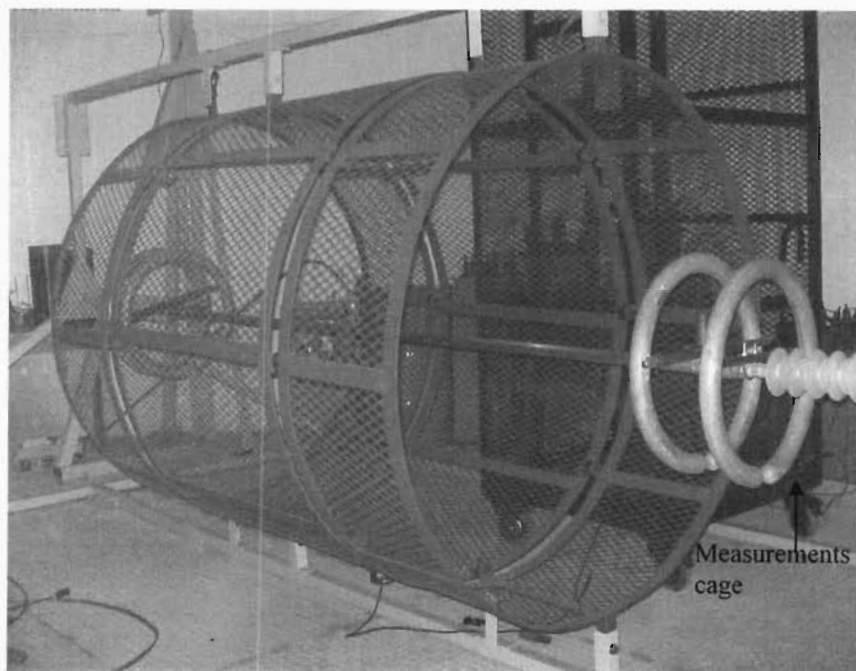


Figure 3.3: The measurements cage adjacent to the corona cage

### 3.3.2 Corona current

A digital micro-ammeter Fluke Model 187 was used to measure the corona current. It was connected in series with a 560  $\Omega$  resistor connected from the central section of the corona cage, specifications given in Appendix A. The ammeter was also placed in the measurements cage during tests.



A point-plane spark gap was used to verify some of the current measurements results. The diameters of the plane and the rod were 15 cm and 1.5 cm respectively. The length of the rod was 5 cm of which 1 cm was the 60° tip. A gap spacing of 8.6 cm was chosen to obtain high breakdown voltages. Figures 3.4 and 3.5 show the gap configuration and the circuit diagram respectively. The voltage supply was obtained from a portable variable DC source. Current pulses under both negative and positive polarities were observed using a digital oscilloscope that was connected across the measuring resistor through a coaxial cable terminated with a 75  $\Omega$  resistor. The specifications of both the portable DC source and the oscilloscope are given in Appendix A. The gap current measurements at different voltages were also measured using Fluke 187 micro-ammeter.

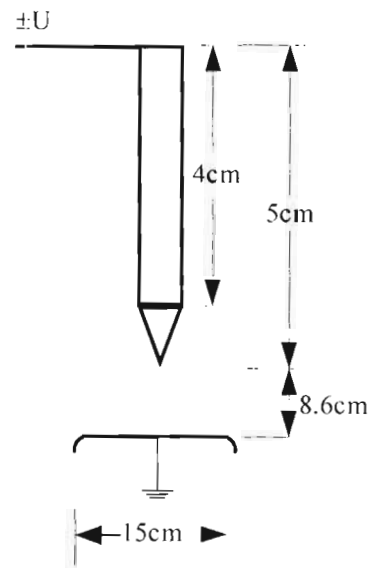


Figure 3.4: Spark gap configuration

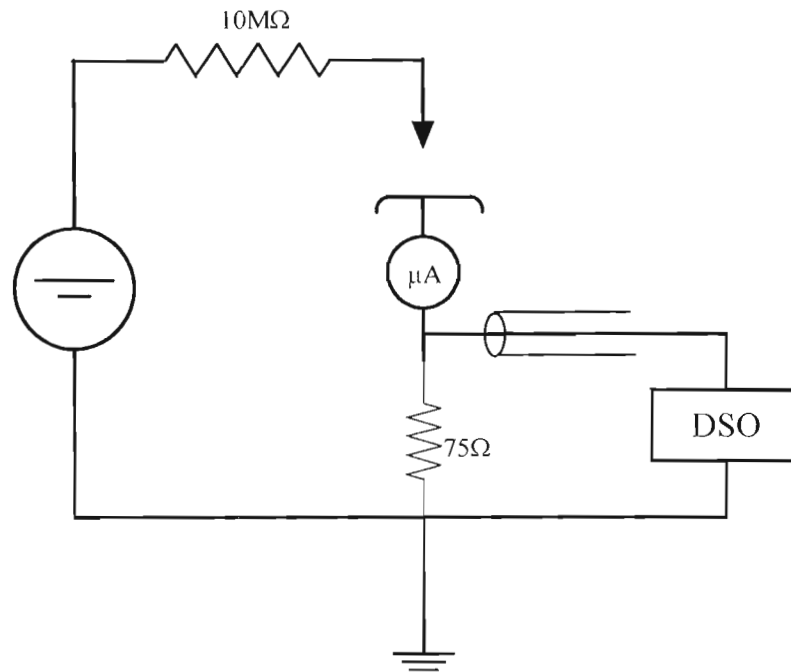


Figure 3.5: Circuit diagram for spark gap current measurements

### 3.3.3 Space charge effect

The cage was covered with aluminium foil in order to assess the effect of space charge on the gap current. Visual corona was observed for different voltages using CoroCAM I corona camera whose details are shown in Appendix A. Space charge assessment was only performed for the 3.5 cm solid and stranded conductors. Figure 3.6 shows the corona cage completely covered with the foil.

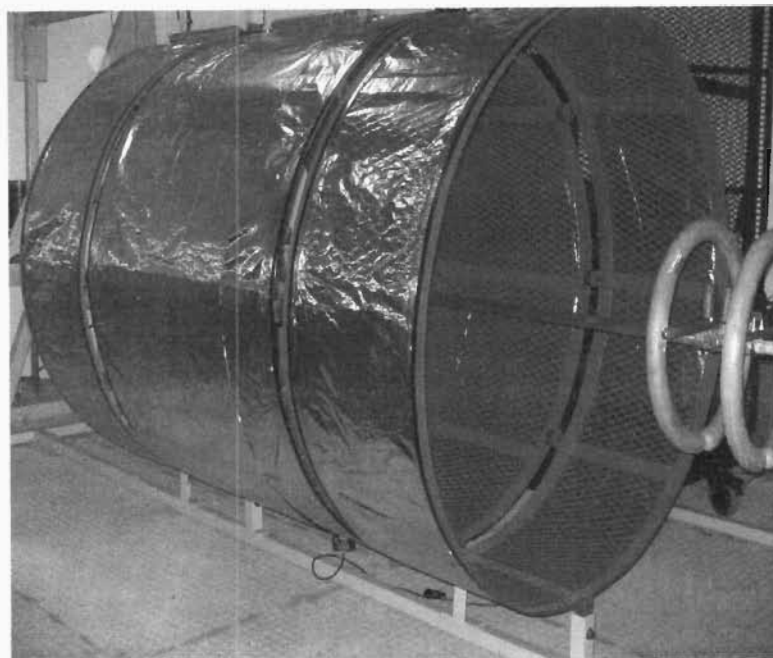


Figure 3.6: Corona cage covered with the foil

### 3.4 AC Measurements

The 2 x 100 kV AC test transformer set was used for the AC measurements. AN and corona current measurements were carried out with the same equipment and configurations as in the DC case except that the 3.5 cm stranded conductor was considered.

### 3.5 Experimental Procedure

The supply voltage was applied from the control room in steps of 10 kV. A-weighted noise levels and corona current were recorded for every 10 kV change in voltage. The static conductor surface gradient was calculated from the test configuration parameters for every voltage increment, using Equation 3.1. AC peak voltages were used for calculating conductor surface gradients. The variation of the measured quantities with the static conductor surface gradient was plotted using Matlab® for comparative analysis. Octave-band AN measurements were done for selected conductor surface gradients for frequencies from 35 Hz to 35 kHz.

$$E = \frac{U}{r \ln \frac{R}{r}} \quad \dots 3.1$$

Where,

E = static conductor surface gradient (kV/cm)

U = supply voltage (kV)

R = radius of the cage (cm)

r = radius of the conductor under test (cm)

### 3.6 Analysis of AN Results

The ACDCLINE module in the EPRI-TLW software was used to analyse the AN results obtained from the corona cage measurements. EPRI-TLW is a set of interactive software that is used for analyzing both AC and DC transmission lines electric and magnetic phenomena. It can be applied in the design of new transmission lines and refurbishment of existing lines. The program allows the user to specify the line configuration and execution options [40].

A single conductor configuration in a typical DC transmission line was assumed for the purpose of comparison. The assumed parameters of the line are shown in Table 3.3. This configuration was used throughout the simulations. The opposite polarity pole was placed 150 m away from the energized pole to minimize the field interaction between the two poles. Simulations were run for different voltage levels and the conductor surface gradients plotted against the noise levels. Only the EPRI, BPA and CRIEPI methods were considered.

AN results obtained under AC were also compared with those obtained from the software. The assumed configuration was similar to that of DC and is summarised in Table 3.4. Two phases with angles 0° and 240° separated by 150 m were considered. This was done in order to simulate a single phase scenario similar to the laboratory set-up. Only the EPRI and the BPA prediction methods supported this configuration, as a result, the CRIEPI method was not considered.

The radial distance between the microphone and the conductor for both assumed configurations and for the cage configuration are quite different. To bring the configurations to a comparable level, the correction factors were applied to the cage results. Since the intensity of noise changes with the proximity to the source producing it. With transmission lines, the noise level changes by approximately 3 dB for every doubling of the distance from the line. This implies that the sound pressure level, P is inversely proportional to  $\sqrt{r}$  where r is the radial distance between the transmission line and the microphone. The correction factor for the height effect was, therefore, obtained from Equation 3.2.

$$\Delta P_h = 10 \log \frac{r}{R} \quad \dots 3.2$$

Where,

$\Delta P_h$  = the change of the measured sound pressure level due to the height correction (dB)

r = radial distance between the microphone and the conductor in the cage

R = radial distance between the microphone and the pole conductor in the assumed configuration

The value of R was evaluated from Figure 3.7. The height correction factors for the measured DC and AC AN levels are therefore, -14.76 dB and -14.56 dB respectively.

To correct the cage results to an infinitely long line, the correction factor that was adopted is shown here as Equation 3.3.

$$\Delta P_l = 10 \log \left( \frac{\pi}{2} \tan^{-1} \left( \frac{l}{2r} \right) \right) \quad \dots 3.3$$

Where,

$\Delta P_l$  = the change of the measured sound pressure level due to the length correction (dB)

l = length of the conductor in the cage

r = radial distance between the microphone and the conductor in the cage

The length correction factor is based on the laboratory set-up only and for the dimensions given of the cage, the correction factor is -0.71 dB for both DC and AC tests. The trends of the cage and the simulations results were then compared through curve fitting.

Table 3.3: Values of the line parameters used for the EPRI-TLW Software simulations for DC (Equivalent monopolar line)

<i>Parameter</i>	<i>Value</i>
# of conductors	1
Diameter	2.8 cm or 3.5 cm
Height of the conductor	26.3 m
Sag	16 m
Altitude	0 m
Microphone height	1.6 m
Distance between the line and microphone	10 m

Table 3.4: Values of the line parameters used for the EPRI-TLW Software simulations for AC (Equivalent single phase line)

<i>Parameter</i>	<i>Value</i>
# of conductors	1
Diameter	3.5 cm
Height of the conductor	25 m
Sag	0 m
Altitude	0 m
Microphone height	1.6 m
Distance between the line and microphone	10 m

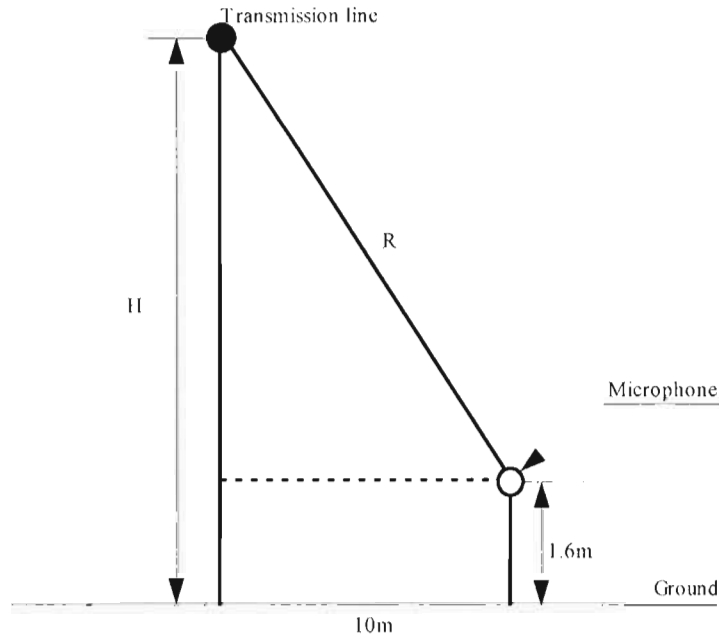


Figure 3.7: Line configuration used for evaluation of correction factors

### 3.7 Calculation of DC Corona Loss

DC corona power loss was calculated from the measured current and expressed in terms of the conductor length using Equation 3.4.

$$P_C = \frac{UI_C}{l} \quad \dots 3.4$$

Where,

- $P_C$  = corona power loss (W/m)
- $U$  = DC supply voltage (V)
- $I_c$  = measured corona current (A)
- $l$  = length of the conductor in the cage (m)

### 3.8 Conductor Surface Conditions

Surface roughness factors of the conductors were estimated by using Peek's formula for cylindrical geometry shown as Equation 3.5 [9]. The static inception gradients for different conductors were estimated after observing the corona activity using the CoroCAM I.

$$E_C = mE_o\delta \left( 1 + \frac{k}{\sqrt{\delta r_c}} \right) \quad ..3.5$$

Where,

$E_C$  = conductor corona inception gradient (kV/cm)

$m$  = conductor roughness factor

$E_o$  and  $k$  are empirical constants

$E_o$  = 31.0 kV/cm for AC

= 31.0 kV/cm for negative polarity DC

= 33.7 kV/cm for positive polarity DC

$k$  = 0.308 for AC

= 0.308 for negative polarity DC

= 0.24 for positive polarity DC

$r_c$  = radius of the conductor under test

$\delta$  = relative air density =  $\frac{(273 + t_0)P}{(273 + t)P_0}$

where,  $t$  = ambient temperature

$t_0$  = 25°C

$P$  = ambient pressure

$P_0$  = 760 torr



### 3.9 Test Line Measurements

The corona cage was later converted into a conductor-plane arrangement to represent a monopolar test line referred to hereinafter as test line. This was done by removing the cylindrical mesh around the conductor. Corona current and AN measurements were done for a 3.5 cm stranded conductor under positive polarity only. A copper plate was used to facilitate measurements of the corona current at ground level. The supporting structure was placed on the wooden blocks to isolate it from the metallic floor. The thickness of the copper plate was 2.1 cm, its length and width were 205 cm and 50 cm respectively. It was connected to ground through a 560  $\Omega$  measuring resistor in series with the Fluke 187 digital micro-ammeter. Current measurements were done with the conductor at a height of 70 cm and 37.5 cm with respect to the copper plate (ground). AN meter was positioned at the same position as with the corona cage. The conductor surface gradient was calculated using Equation 3.6. It can be noted that for the height of 37.5 cm, the term  $2H$  equals the radius of the corona cage  $R = 75$  cm, as a result Equations 3.1 and 3.6 were equivalent for this particular configuration and for the height of 70 cm the air gaps in the cage and the line were almost the same. Current measurements at the height of 37.5 cm were repeated with a high power fan directed at the conductor in order to assess the effect of the space charge. Details of the fan are included in Appendix A.

$$E = \frac{U}{r \ln \frac{2H}{r}} \quad \dots 3.6$$

Where,

- E = static conductor surface gradient (kV/cm)
- U = supply voltage (kV)
- r = radius of the conductor under test (cm)
- H = height of the conductor above ground (cm)

Corona losses were evaluated from Equation 3.4 similar to the corona cage. The variation of the corona power loss with the conductor surface gradient was plotted and compared with corona cage results. Comparison of the cage and the test line generated acoustic power was done. Figure 3.8 shows the test set-up for the line configuration.

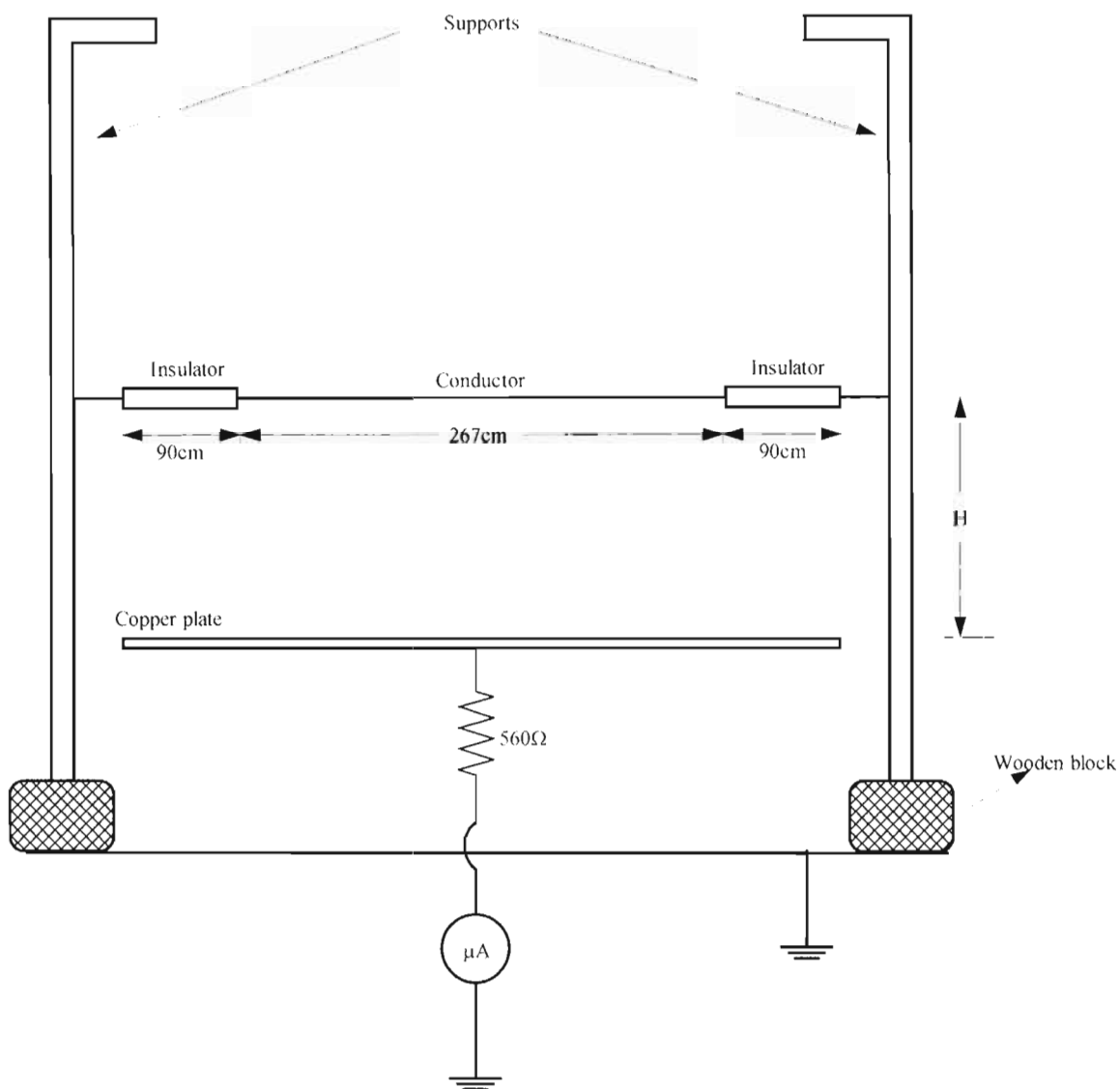


Figure 3.8: Test line configuration



## Chapter 4: Results and Analysis

### 4.1 Visual Corona

Figures 4.1 to 4.3 show visual corona observed using the CoroCAM I at 220 kV and 28.9 kV/cm, for a 3.5 cm stranded aluminium conductor. Under positive polarity the plumes are much longer, wider and very distinct (Figure 4.1). Negative polarity plumes are smaller and appear as clusters of glowing spots around the conductor (Figure 4.2). AC corona discharges in Figure 4.3 appear to resemble both positive and negative corona characteristics, with a combination of clustered glowing spots and large plumes appearing occasionally.

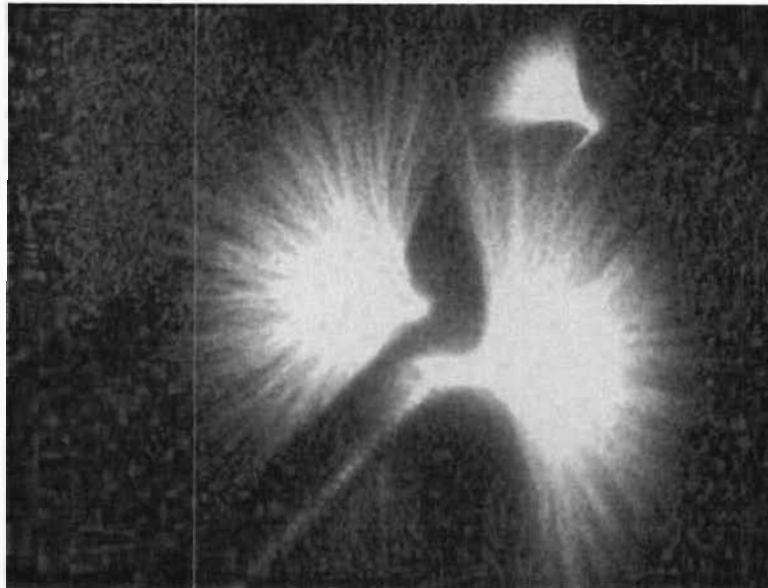


Figure 4.1: 3.5 cm $\varnothing$  stranded conductor at 33.5 kV/cm positive polarity

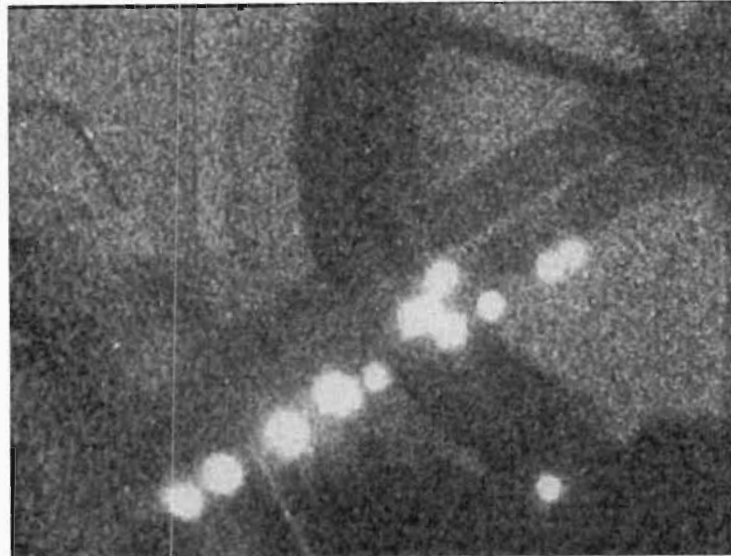


Figure 4.2: 3.5 cm $\varnothing$  stranded conductor at 33.5 kV/cm negative polarity

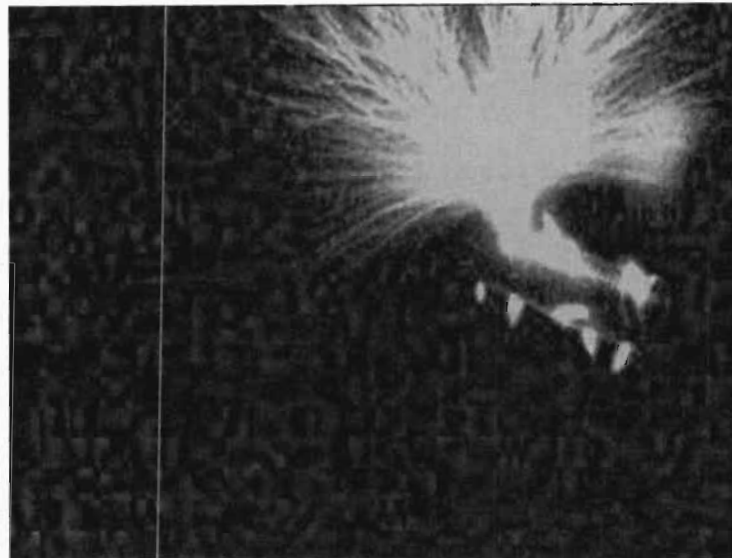


Figure 4.3: 3.5 cm $\varnothing$  stranded conductor at 33.5 kV/cm AC

## 4.2 Conductor Surface Roughness and Corona Inception

As pointed out earlier, conductor surface conditions have an influence on corona characteristics. In Table 4.1 a comparison is made of the conductor roughness factors calculated from Equation 3.5. The air density factor varied within a range of 0.95 to 0.97 with the maximum difference of 0.02.

The calculated inception gradients depend on the prevailing air density at the time the tests were done. The roughness factor of 0.8 for the solid conductor suggests that it was not perfectly smooth. Under positive polarity, the roughness factor for the 3.5 cm solid conductor is higher than that of the stranded conductor, by a factor of about 0.2. According to the observed positive and negative DC as well as AC inception gradients, the 3.5 cm stranded conductor appears to have had a roughness factor of about 0.54. The 2.8 cm stranded conductor appears to have had a surface roughness factor of about 0.58 when averaging the roughness factors calculated for positive and the negative polarities. The roughness factors obtained for stranded conductors are slightly lower than typical roughness factors of 0.6 to 0.8 suggested earlier in [26].

Table 4.1: Calculated conductor roughness factors

<b>Positive DC</b>					
	<b>U (kV)</b>	<b>Ec (kV/cm)</b>	<b>r (cm)</b>	<b><math>\delta</math></b>	<b>m</b>
Stranded	140	21.3	1.75	0.96	0.556
Stranded	125	22.1	1.4	0.97	0.561
solid	198	30.1	1.75	0.97	0.778
<b>Negative DC</b>					
	<b>U (kV)</b>	<b>Ec (kV/cm)</b>	<b>r (cm)</b>	<b><math>\delta</math></b>	<b>m</b>
Stranded	125	19.0	1.75	0.95	0.544
Stranded	120	21.3	1.4	0.95	0.599
<b>AC</b>					
	<b>U (kV)</b>	<b>Ec (kV/cm)</b>	<b>r (cm)</b>	<b><math>\delta</math></b>	<b>m</b>
Stranded	86	18.5	1.75	0.97	0.519

## 4.3 Audible Noise

### 4.3.1 A-weighted noise levels

#### 4.3.1.1 Effects of conductor surface conditions

Figures 4.4 and 4.5 show the effect of conductor surface conditions on corona discharges in terms of inception gradients and the noise levels generated. These differences are more apparent under positive polarity in Figure 4.4. The background noise is about 35 dBA and the corona noise inception gradients seem to be at 20 kV/cm [closer to 18 kV/cm] for the stranded conductor and 33

kV/cm for the solid conductor. The inception gradients observed on the AN graphs indicate levels at which the corona noise first exceeds the background noise. They do not indicate the actual corona inception levels where the first burst or onset streamer is observed (i.e. the levels shown in Table 4.1). A comparison of the noise and the normal corona inception levels shows that the normal corona inception level is higher for the stranded conductor, but lower for the solid conductor (Table 4.1)-one would have expected both to be lower. It can also be observed that the stranded conductor generated much more noise than the solid conductor; about 10 dB higher at 20 kV/cm, 25 dB at 25 kV/cm and 32 dB at 30 kV/cm. Under negative polarity, the corona noise inception for the solid conductor was also delayed, however, not as much as with the positive polarity (Figure 4.5). The stranded conductor generated about 5 to 8 dB higher than the solid conductor for a wide range of conductor surface gradients. Generally the results agree with those of positive polarity, and therefore, the differences in surface conditions as discussed in Section 4.2 have a significant effect on the generation of corona AN, especially the positive polarity AN. This could be as a result of increased corona activity from the rough spots on the stranded conductor surface. The spots have relatively high gradients. A similar characteristic was observed for conductors of other diameters.

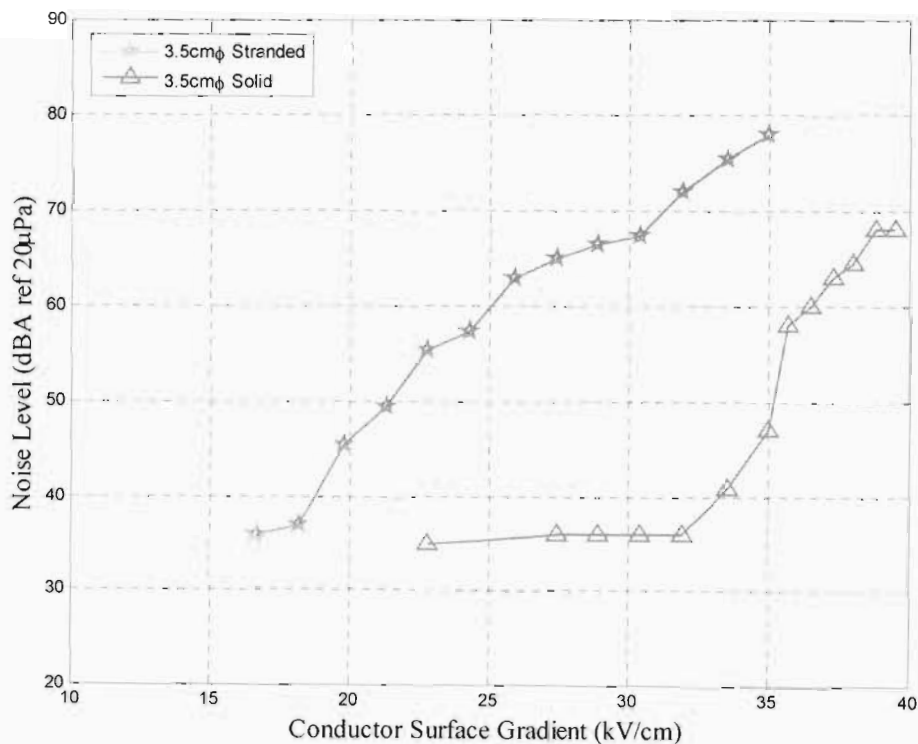


Figure 4.4: Conductor roughness effect on AN for positive polarity

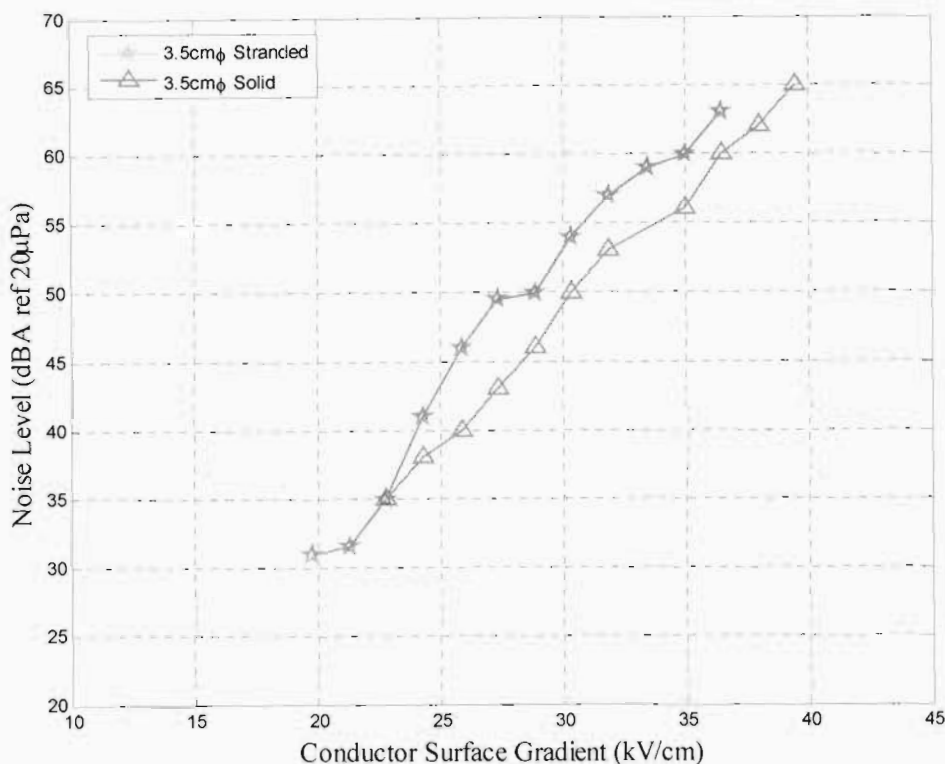


Figure 4.5: Conductor roughness effect on AN for negative polarity

#### 4.3.1.2 Effect of system polarity

The DC voltage polarity effect is shown in Figures 4.6 and 4.7 for both 3.5 cm and 2.8 cm diameter stranded conductors. The positive polarity noise is definitely higher than that of the negative polarity; about 15 dB higher for 20 kV/cm to 30 kV/cm for the 3.5 cm diameter conductor, and about 15 dB higher for 25 kV/cm to 35 kV/cm for the 2.8 cm diameter conductor. This is slightly higher than the 10 dB and 8 dB difference mentioned in [17] and [13]. Nevertheless, the results are in good agreement with the literature when it comes to the negative polarity noise being lower to an extent that it can be disregarded in the design. In terms of the observed annoyance effect, the positive polarity AN was more annoying, comprised of crackling noise. On the other hand negative polarity noise was more of a hissing sound. Generally, noise levels for both positive and negative polarities above 50 dBA were quite unbearable.



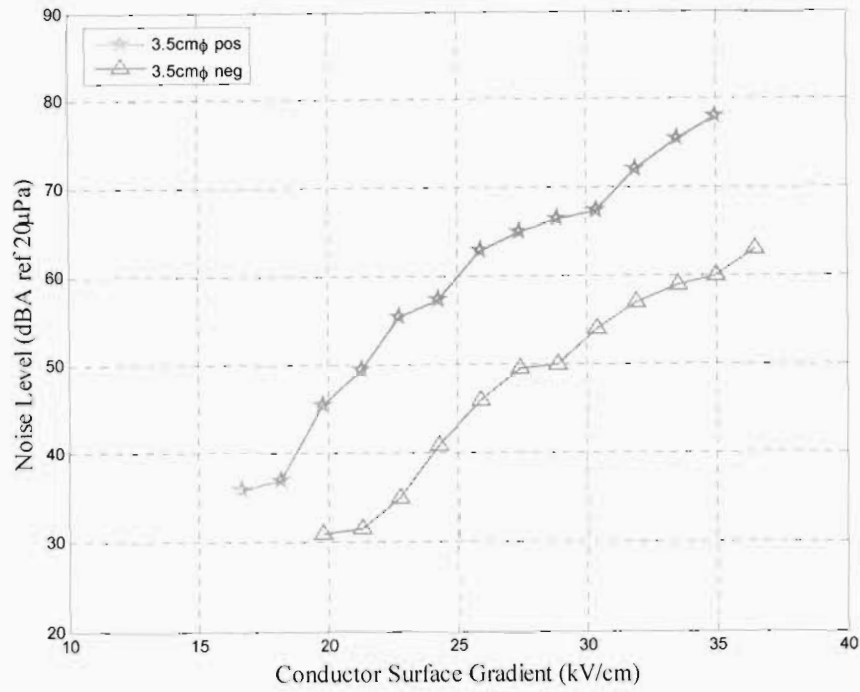


Figure 4.6: Polarity effect on AN for 3.5 cmØ stranded conductor

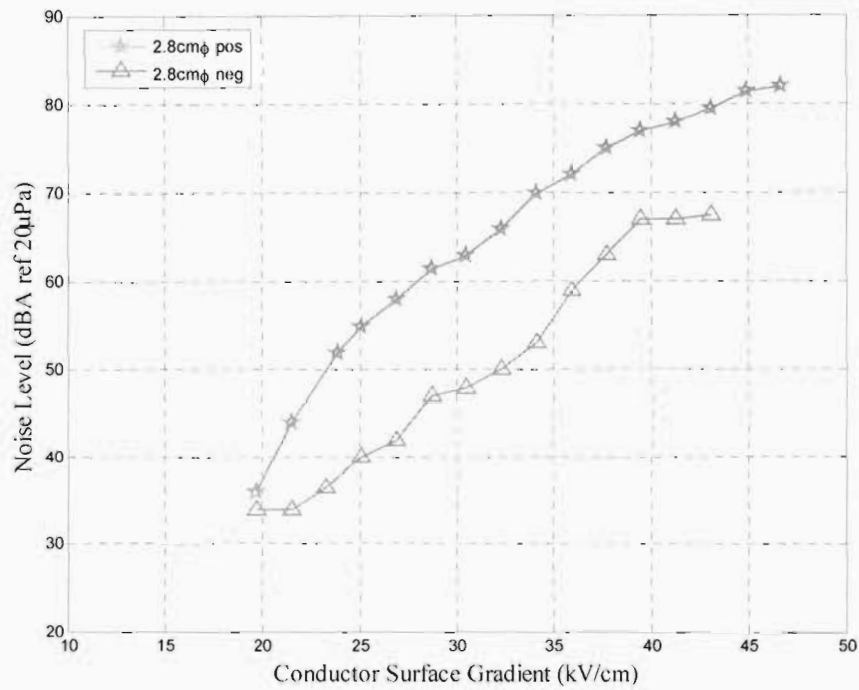


Figure 4.7: Polarity effect on AN for 2.8 cmØ stranded conductor

## 4.3.1.3 Effect of conductor size

The effect of the conductor size on the AN generation under positive polarity and negative polarity is shown in Figures 4.8 and 4.9 respectively, for stranded conductors only. Similar characteristics were observed for solid conductors as well. Larger diameter conductors produced higher noise levels than the smaller diameter conductors for the same conductor surface gradients consistently, under both negative and positive polarities. The obtained results agree very well with the results reported in [17, 19] in which the AN increased with the conductor size when all the other parameters were unchanged. In terms of conductor surface gradients, the smaller conductor result in higher operating conductor surface gradients than the larger diameter conductors for the same voltage level. The slopes of the graphs for the three conductors become steep just after the inception and then tend to flatten as the surface gradients increase above 40 kV/cm, especially for the negative polarity noise levels. This characteristic suggests that there is corona noise saturation at increased surface gradients.

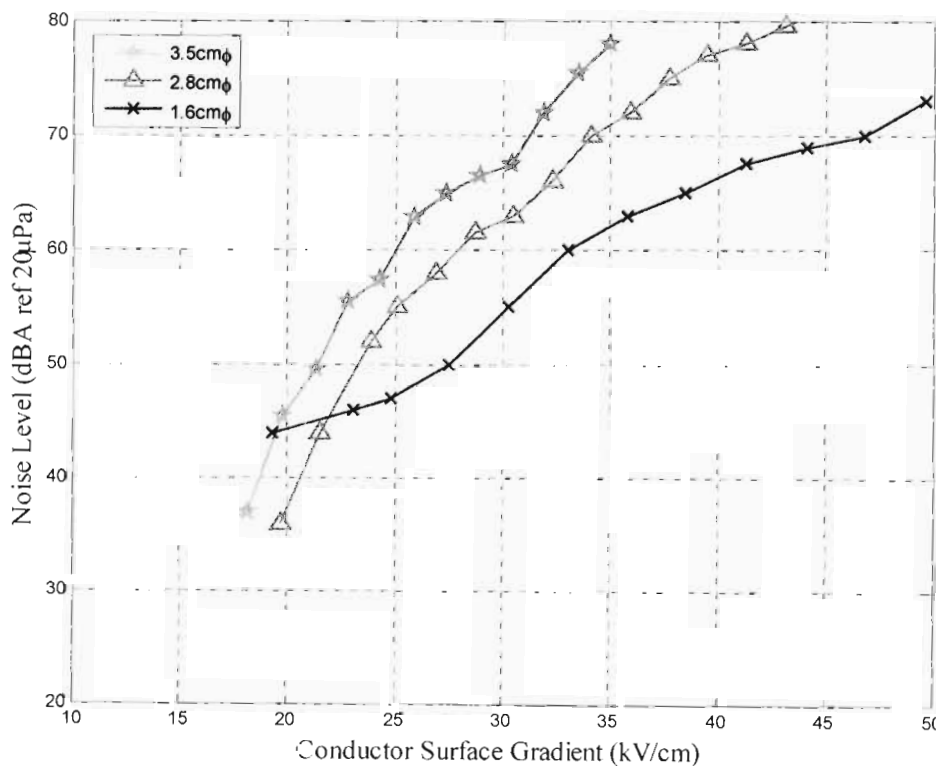


Figure 4.8: Effect of conductor size on AN (Positive polarity, stranded conductors)

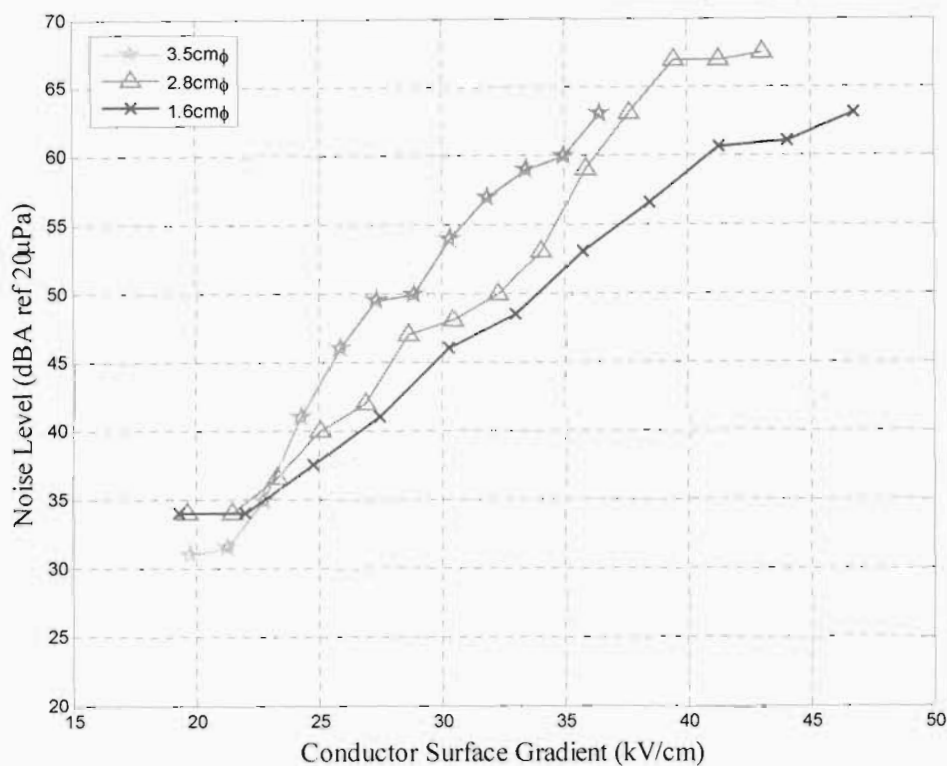


Figure 4.9: Effect of conductor size on AN (Negative polarity, stranded conductors)

#### 4.3.1.4 Corona cage and test line measurements

Comparison of the AN noise measurements obtained from the test cage and the test line under positive polarity is shown in Figure 4.10. As seen from the graphs, though the tests were not run simultaneously, there is no significant difference in the measured noise levels as one would expect. The magnitudes of the noise levels are similar for the same conductor surface gradients and the graphs also follow the same trend. It is mentioned in [17, 28] that the slopes of the cage and test line AN results are usually not similar. The observed similarities could be due to the similar test arrangements which were adopted. The results also suggest that the effect of space charge on the cage AN measurements was insignificant.

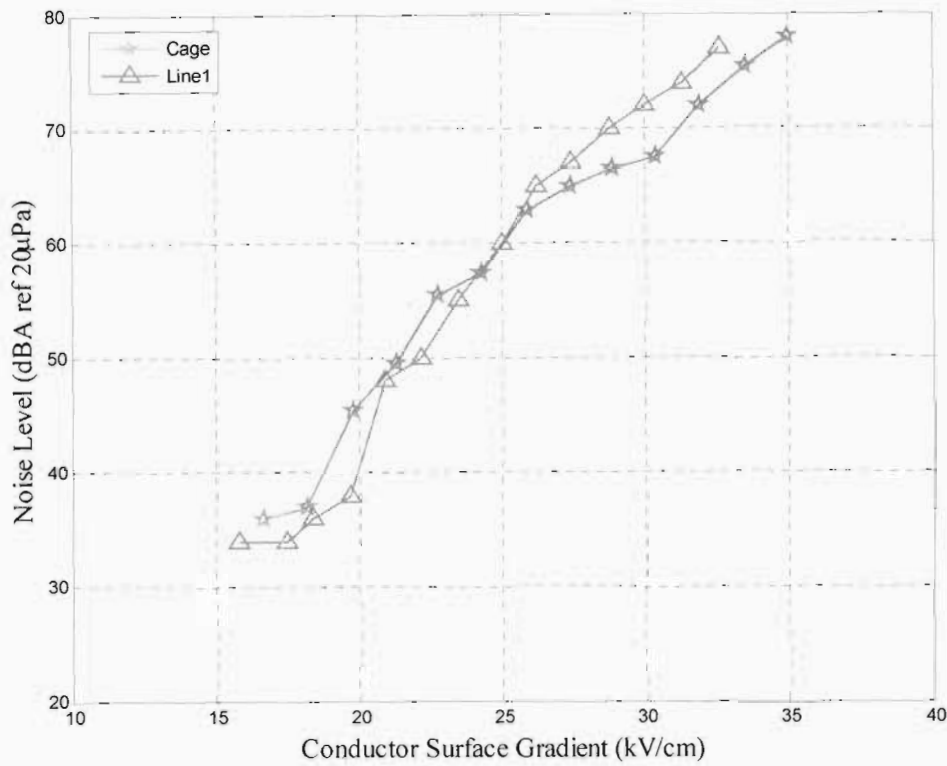


Figure 4.10: Comparison of cage and test line AN measurements (3.5 cm Ø stranded conductor, line height of 70 cm, positive polarity)

The comparison of the cage and line AN was also expressed in terms of sound power,  $A$ , at a reference of  $1 \mu\text{W}/\text{m}$ . The sound power was calculated from the measured sound pressure level by first deriving the generated sound pressure level at a distance of 1 m for an infinite length transmission line as it was done in [31]. Details of the derivation are as follows:

$$P = A(\text{dB}) - 10 \log R + 10 \log \left( \tan^{-1} \frac{l}{2R} \right) - 7.82 \quad \dots (4.1)$$

Let  $P_1$  = generated sound pressure level (dBA) standardised to the sound pressure level at a point one meter away from the conductor bundle of an infinite length:

$R_1 = 1 \text{ m}$  and  $l_1 = \infty$  then (4.1) becomes:

$$P_1 = A(\text{dB}) - 10 \log R_1 + 10 \log \left( \tan^{-1} \frac{l_1}{2R_1} \right) - 7.82 \quad \dots (4.2)$$

$$A(\text{dB}) = P_1 + 10 \log R_1 - 10 \log \left( \tan^{-1} \frac{l_1}{2R_1} \right) + 7.82$$

$$A(\text{dB}) = P_1 + 10 \log 1 - 10 \log \left( \tan^{-1} \frac{\infty}{2 \times 1} \right) + 7.82$$

$$A(\text{dB}) = P_1 + 10 \log \frac{\pi}{2} + 7.82 \quad \dots (4.3)$$

Substituting (4.3) in (4.1):

$$P = P_1 + 10 \log \frac{\pi}{2} + 7.82 - 10 \log R + 10 \log \left( \tan^{-1} \frac{l}{2R} \right) - 7.82$$

$$P_1 = P - 10 \log \frac{\pi}{2} - 7.82 + 10 \log R - 10 \log \left( \tan^{-1} \frac{l}{2R} \right) + 7.82$$

$$= P + 10 \log R + 10 \log \left( \frac{\pi}{2 \tan^{-1} \frac{l}{2R}} \right) \quad \dots (4.4)$$

If  $P = P_1$ ,  $R = 1$  m and  $l = \infty$  (4.1) becomes,

$$P_1 = A(\text{dB}) - 10 \log 1 + 10 \log \left( \tan^{-1} \frac{\infty}{2} \right) - 7.82$$

Then,

$$A(\text{dB}) = P_1 - 10 \log \frac{\pi}{2} + 7.82$$

$$A(\text{dB}) = P_1 + 5.86 \text{ (ref} = 1 \text{ pW/m)} \quad \dots (4.5)$$

To express A (dB) in terms of 1  $\mu\text{W/m}$  reference:

$$A(\text{dB}) = P_1 + 5.86 + 10 \log \left( \frac{10^{-12}}{10^{-6}} \right)$$

$$A(\text{dB}) = P_1 - 54.14 \text{ (ref} = 1 \text{ } \mu\text{W/m)} \quad \dots (4.6)$$

Figure 4.11 shows the results obtained from Equation 4.6. As expected the graphs have similar trends as those of Figure 4.10.

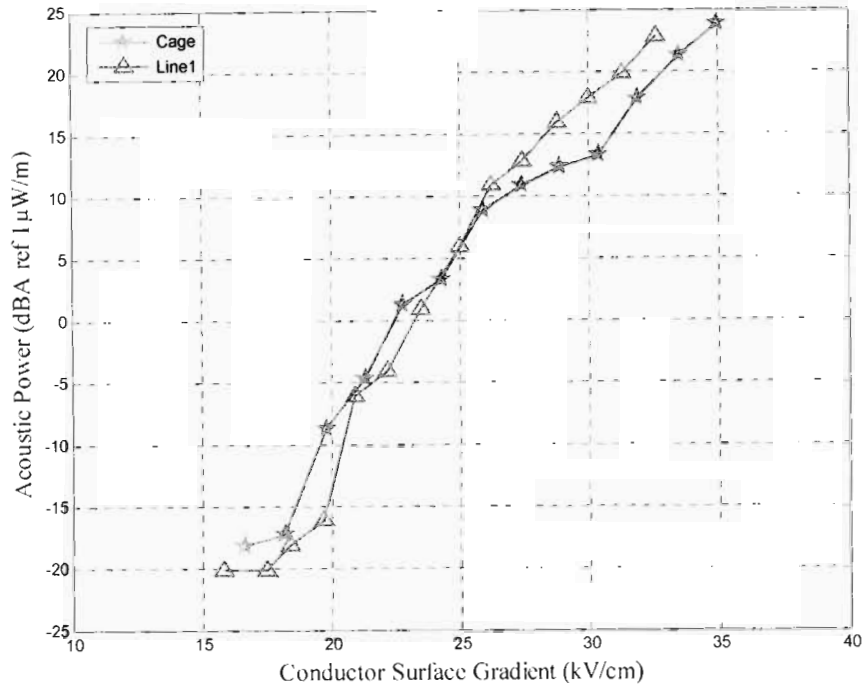


Figure 4.11: Variation of acoustic power with conductor surface gradient for a test line and corona cage for 3.5 cmØ stranded conductor, positive polarity (line height of 70 cm )

The similarity between the cage and the test line results could be due to the fact that the position of the sound level meter relative to the conductor was the same during both the test cage and the test line measurements. It is suggested in [31] that cage results will only be comparable with line results if the space charge conductor surface field is computed and used in comparison rather than the static conductor surface field. Alternatively the obtained results could mean that the effect of the space charge on the conductor surface gradient in a small cage and on a small test line with similar dimension is unnoticeable. Converting the cage into a test line only yielded a 0.67 cm increase in the active length of the conductor which, theoretically, will increase the noise level by 0.5 dB. This is a very small change to be noticed on an analogue meter.

#### 4.3.1.5 Effect of system voltage

In Figure 4.12 a comparison of the DC and AC corona noise levels is shown for a 3.5 cm diameter stranded conductor. The graphs for AC and positive DC noise are quite similar in both magnitudes and the trends. The annoyance effect of the positive DC and AC noise levels was also very similar;

however, the AC noise sounded to be more of a combination of both hissing and crackling noise. This agreed very well with the corona modes as discussed in the literature review chapter.

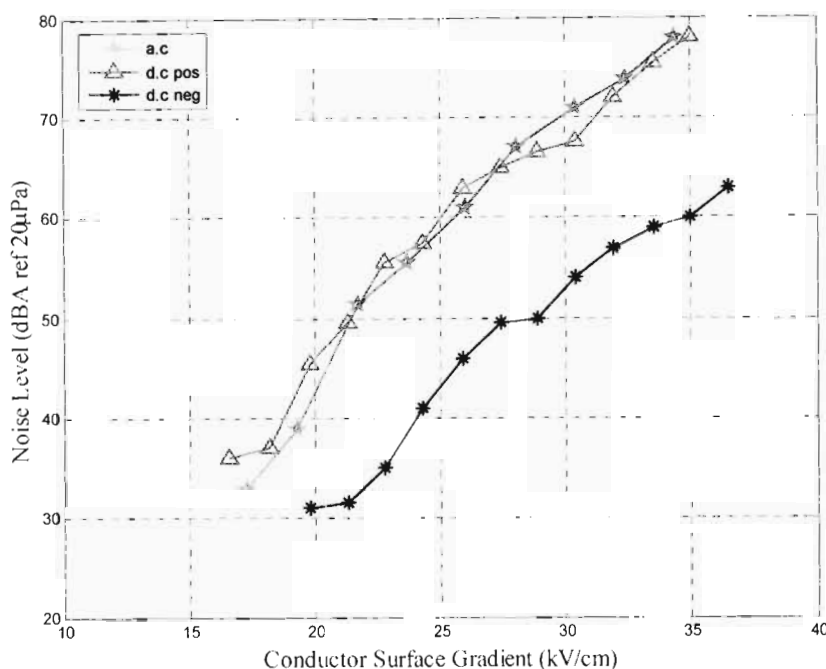


Figure 4.12: Effect of system voltage on AN for a 3.5 cmØ stranded conductor

### 4.3.2 TLW Software A-weighted noise levels

Figure 4.13 shows a comparison of the UKZN sound pressure level results (corrected for height and length as shown in Chapter 3) and the EPRI-TLW software results obtained under positive polarity with a 3.5 cm diameter stranded conductor. The BPA and the CRIEPI empirical methods predict lower noise levels compared to the EPRI method for the same configuration. The differences could be due to variations in test and atmospheric conditions. The empirical formulae used for the evaluation of AN shown in [13] are also different. There is a very good agreement between the corrected UKZN results and the EPRI prediction methods, in terms of both the trends and the magnitudes. Figure 4.14 shows the fitted trend lines for both the UKZN and the EPRI results. The graphs are both logarithmic and the equations are of the same order of magnitude.  $R^2$  is a measure of how close the trend line is to the actual graph and has a value ranging 0 to 1 where 1 is the perfect fit and 0 is the worst. Clearly the EPRI curve is perfectly logarithmic with  $R^2$  of 1 and the UKZN graph is closer with  $R^2$  equal to 0.987.

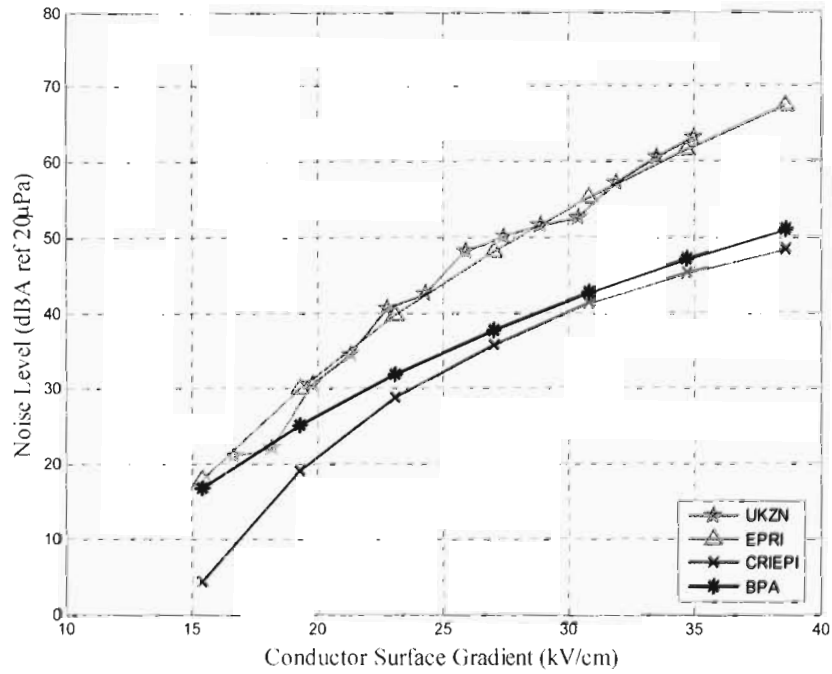


Figure 4.13: Comparison of TLW software prediction methods with UKZN results (3.5 cmØ stranded conductor, positive polarity)

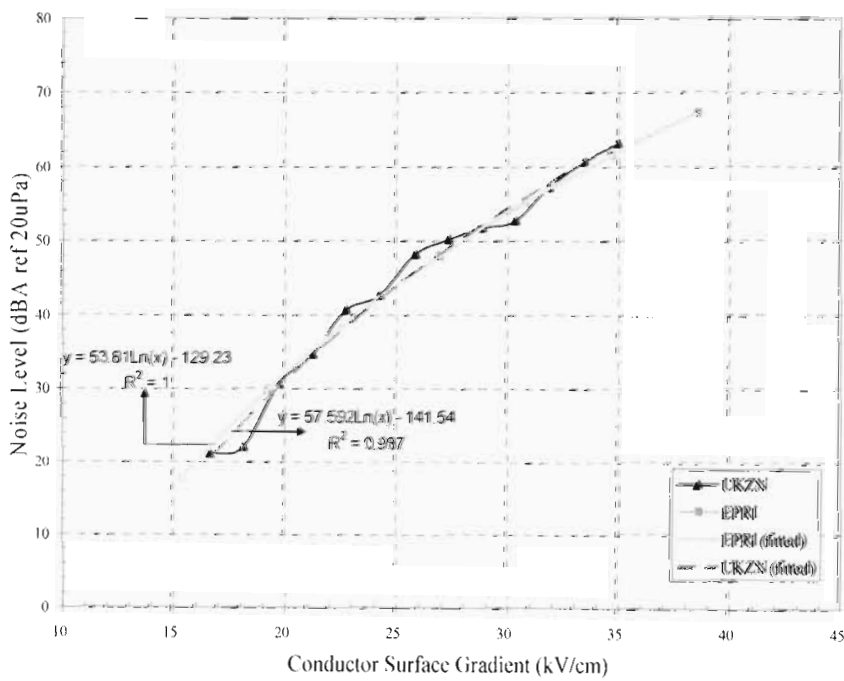


Figure 4.14: Comparison of trends for UKZN with EPRI results by curve fitting (3.5 cm Ø stranded conductor, positive polarity)



In comparing the UKZN corrected results and the TLW software results under negative polarity, similar characteristics as in the case of positive polarity were observed. As shown in Figure 4.15, The CRIEPI and the BPA predictions were lower than the EPRI. The corrected UKZN results were also in good agreement with the EPRI prediction though slightly lower in magnitudes.

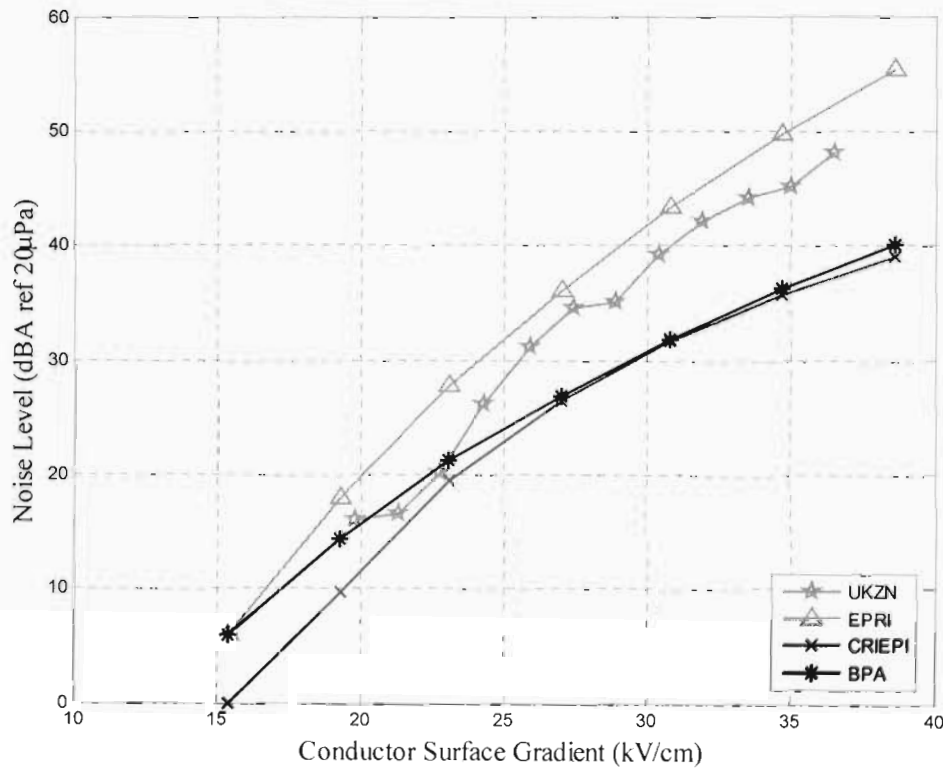


Figure 4.15: Comparison of TLW software prediction methods with UKZN results (3.5 cmØ stranded conductor, negative polarity)

The negative polarity trends for a 3.5 cm stranded conductor are compared in Figure 4.16. Both the EPRI and the UKZN graphs are logarithmic and have the same order of magnitude. The  $R^2$  value for the UKZN graph is 0.985 which is a very good agreement.

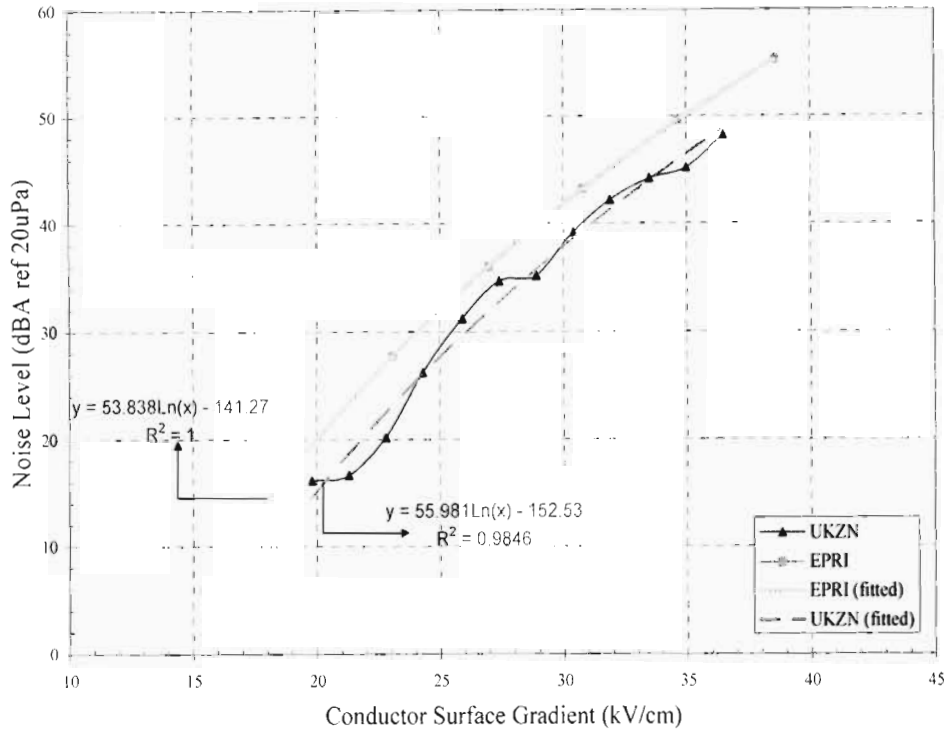


Figure 4.16: Comparison of trends for UKZN with EPRI results by curve fitting (3.5 cmØ stranded conductor, positive polarity)

The comparison of the measured results with the EPRI-TLW software results was also done for the 2.8 cm diameter conductor and the results are shown in Figures 4.17 and 4.18 for positive and negative polarity respectively. The EPRI-TLW software results are quite consistent with the BPA and the CRIEPI predictions being lower than the EPRI predictions. It can be noted that for the 2.8 cm diameter conductor the UKZN graphs are slightly lower than the EPRI prediction curve for both positive and negative polarities. Nevertheless the UKZN corrected results are in good agreement with the EPRI prediction graph for both polarities. Through a simple visual observation on the two figures, it can be noted that the trends are also in agreement similarly to the 3.5 cm diameter conductor.

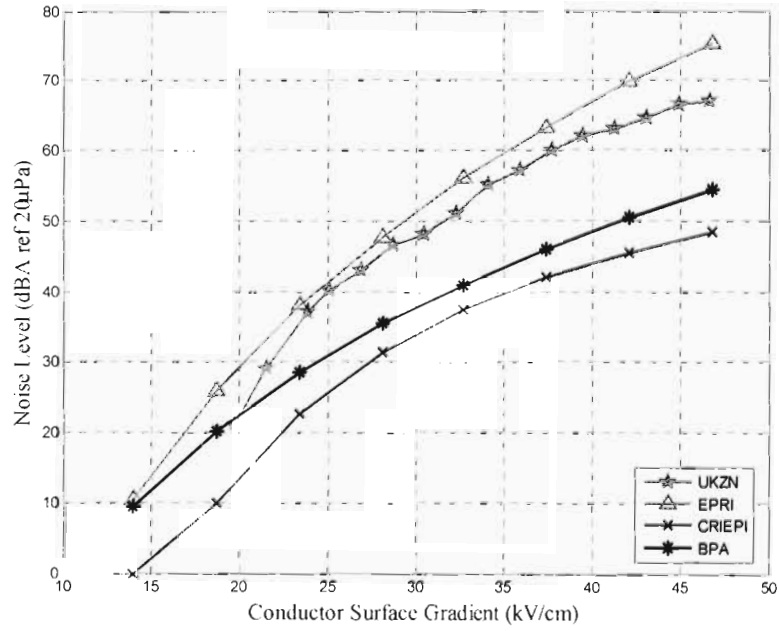


Figure 4.17: Comparison of TLW software prediction methods with UKZN results ( 2.8 cmØ stranded conductor, positive polarity)

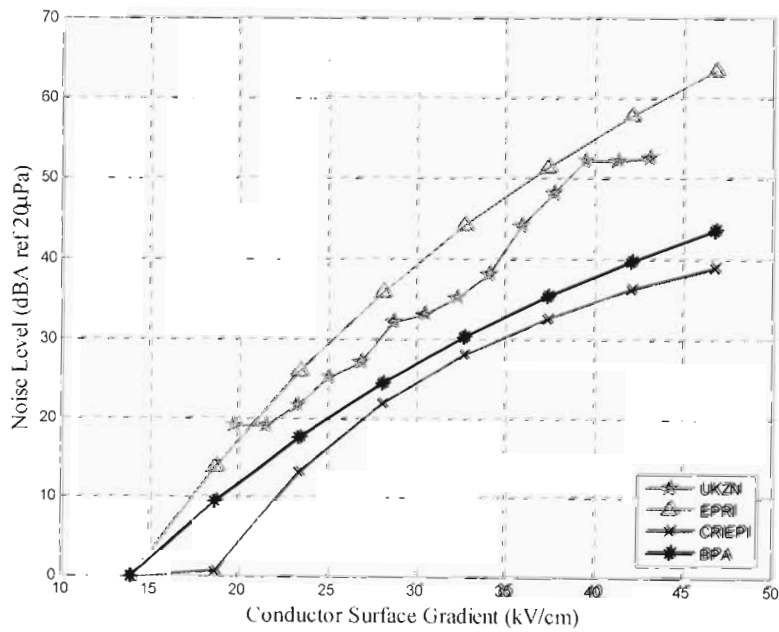


Figure 4.18: Comparison of TLW software prediction methods with UKZN results ( 2.8 cmØ stranded conductor, negative polarity)

For AC simulations, only the EPRI and the BPA prediction methods agreed with the chosen configuration. In Figure 4.19, a comparison is made of the corrected UKZN results and the TLW software results, for AC voltages. The EPRI curve is not purely logarithmic as in the case of the DC results. Compared to the DC results, the UKZN results are higher than the EPRI and the BPA predictions, but the BPA are much lower. However, the  $R^2$  values for the three fitted graphs are very close to 1 and the order of magnitude of the trend lines is quite similar.

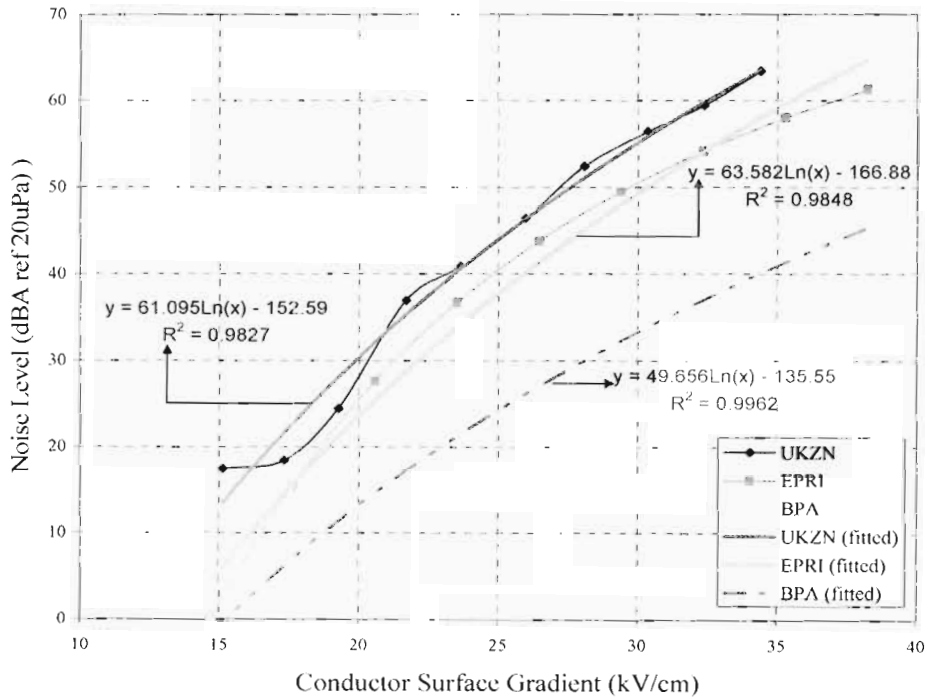


Figure 4.19: Comparison of trends for UKZN with EPRI and BPA results by curve fitting (3.5 cm Ø stranded conductor, AC)

### 4.3.3 Octave band frequency spectra

#### 4.3.3.1 Positive polarity DC

The frequency spectra results were arranged to show the effect of the static conductor surface gradient on the measured AN frequency spectra, in relation to the spectrum of the prevailing background noise for different polarities and conductor sizes. The scale of the meter that was used with the octave band filter set had 25 dB as the minimum measurable noise level. It was observed that the noise levels started to decrease beyond 8 kHz. This could be due to the effect of the 1-inch

microphone that was used. It has a flat response characteristic up to 10 kHz, beyond which it starts to decrease depending on the angle of incidence. Figure 4.20 shows the frequency spectrum of the background noise and that of the 2.8 cm diameter stranded conductor obtained at 28.9 kV/cm under positive polarity. At this surface gradient, corona AN was much higher than the background noise. It can also be noticed that the background noise was only measurable in the frequency range of up to 500 Hz which implies that it affected the measured corona AN levels in the same range. It is reported in [28] that frequencies below 1 kHz are a function of conductor ageing and in [13], it is also reported that the best indicators of HVDC corona AN are octave band measurements from 500 Hz and above. The noise was quite broadband and consisted of both mid and high frequencies because of its crackling nature, as also mentioned in [29].

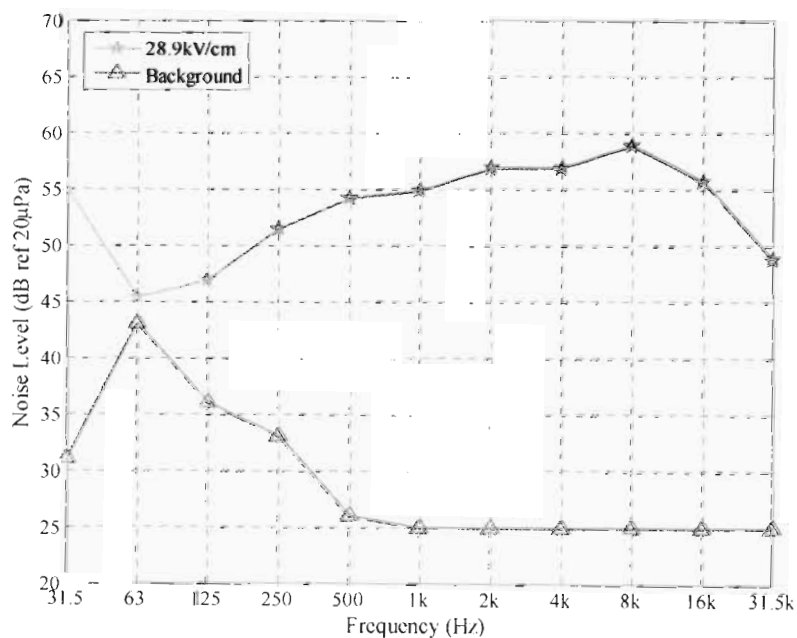


Figure 4.20: Positive polarity frequency spectrum for a 2.8 cm $\varnothing$  stranded conductor

The positive polarity spectrum in Figure 4.21 remains consistent in terms of the frequency content. There is also a consistent difference between the frequency spectra of different conductor sizes. It appears that for the same conductor surface gradient, the frequency spectra of the larger conductor is higher than that of a smaller one. This is also in agreement with the A-weighted noise levels discussed above. Figure 4.22 shows the effect of the conductor surface gradient on the frequency spectra under positive polarity. The lower frequencies show an inconclusive relationship; this can be attributed to the effect of background noise as discussed earlier. Considering frequencies higher

than 125 Hz, it appears that the higher the conductor surface gradient the higher the noise levels for the same conductor size.

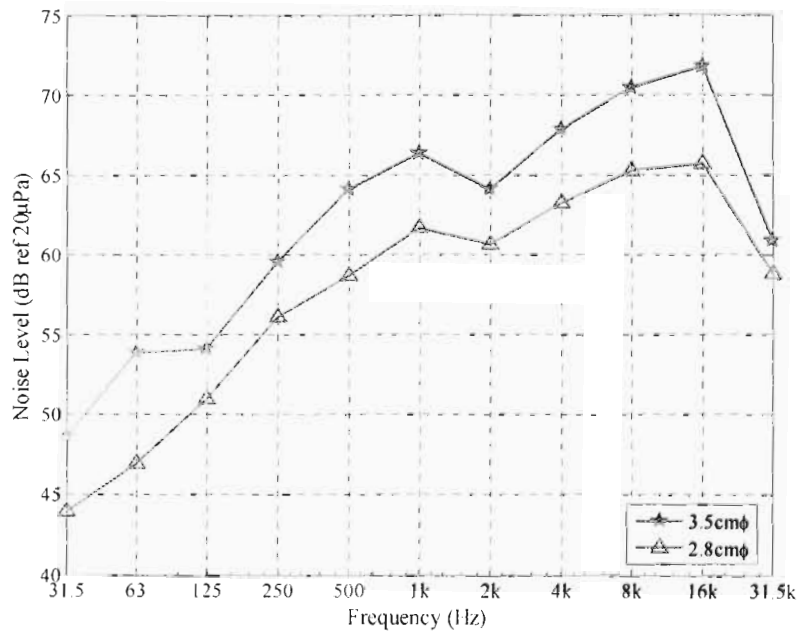


Figure 4.21: Effect of conductor size on positive polarity frequency spectrum at 33.5 kV/cm

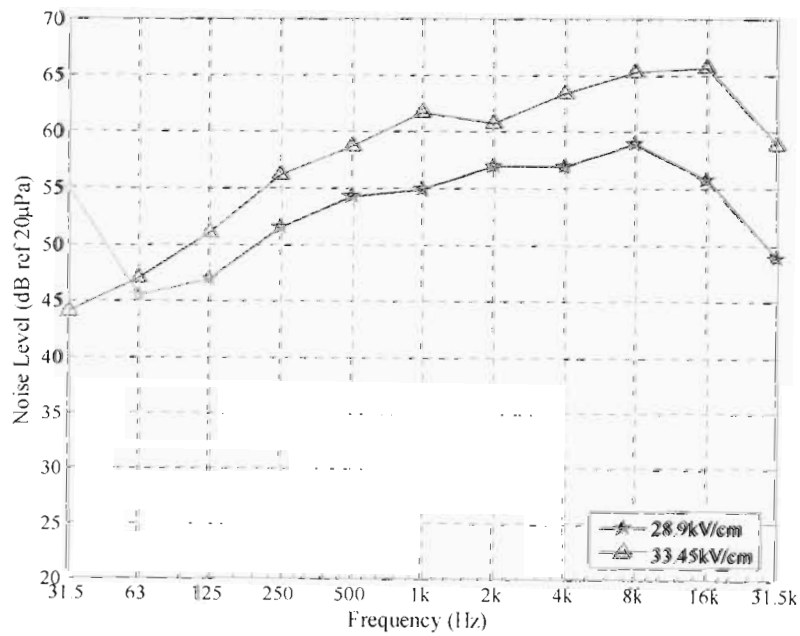


Figure 4.22: Effect of conductor surface gradient on positive polarity frequency spectrum for 2.8 cmØ stranded conductor

## 4.3.3.2 Negative polarity DC

Negative polarity frequency spectra results are shown in Figures 4.23, 4.24 and 4.25. The same effect of background noise frequencies can also be observed again here for the negative polarity measurements shown in Figure 4. 23. The negative polarity spectrum is much dominated by the higher frequencies, unlike the positive polarity noise. At lower frequencies up to 500 Hz the noise level is much more comparable to the background noise, contrary to the positive polarity case.

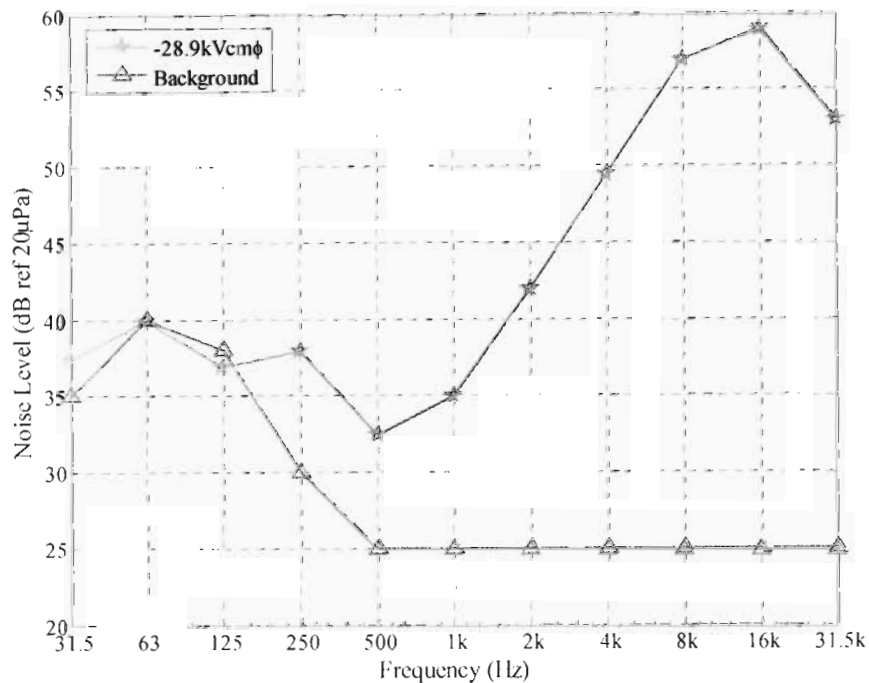


Figure 4.23: Negative polarity frequency spectrum for 2.8 cmØ stranded conductor

Figure 4.24 shows the effect of conductor size under negative polarity for 24.3 kV/cm. The high frequency content is quite clear from 2 kHz and above, the mid frequencies are very low and the low frequencies higher. Over the whole frequency spectrum the noise level of the larger conductor is higher than that of the smaller conductor, similar to positive polarity. For different conductor surface gradients in Figure 4.25, the higher conductor surface gradient resulted in higher noise levels over the whole frequency spectrum, for the same conductor size. The low frequency noise levels are again not interpretable.

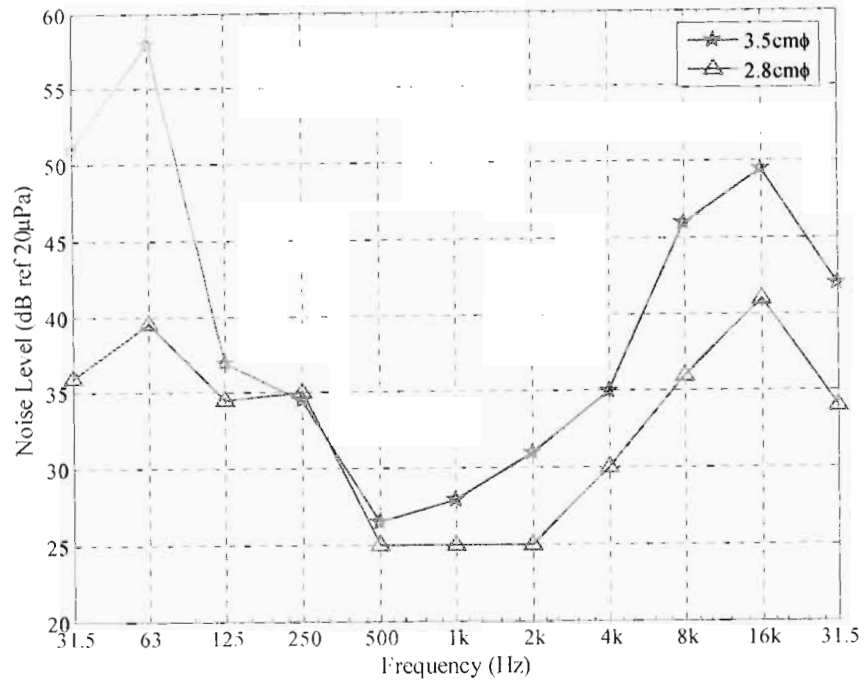


Figure 4.24: Effect of conductor size on negative polarity frequency spectrum at 24.3 kV/cm

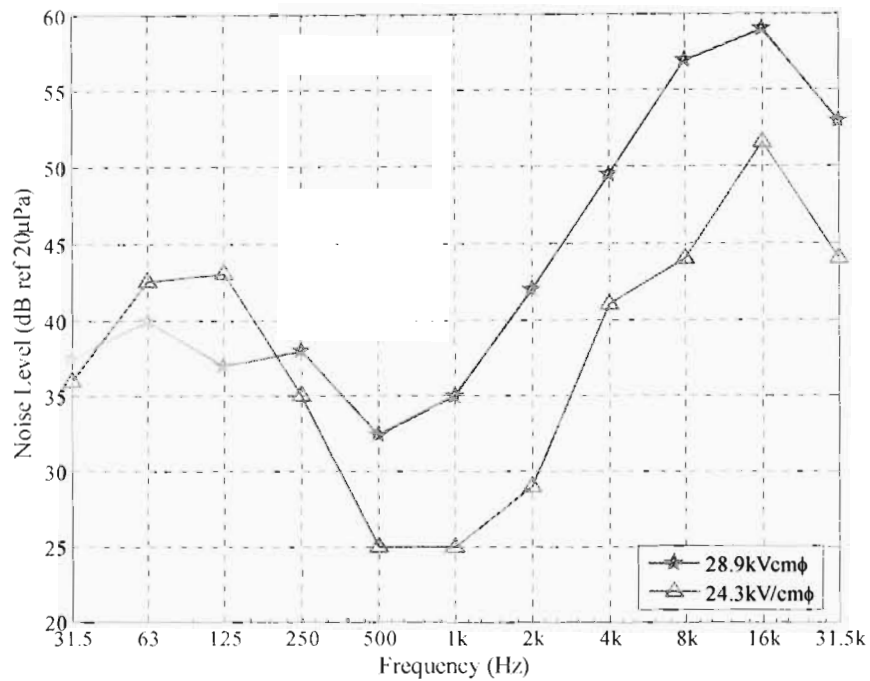


Figure 4.25: Effect of conductor surface gradient on negative polarity frequency spectrum for 2.8 cmØ stranded conductor



## 4.3.3.3 AC

AC frequency spectrum results are shown in Figures 4.26-4.28. Both low and high frequencies constitute the AC frequency spectrum. The contribution of the hum content can be noted at frequencies 63, 125 and 250 Hz. hence the background noise appears to be much lower at these frequencies. The presence of the hum component is one of the factors that distinguish AC AN from the DC noise.

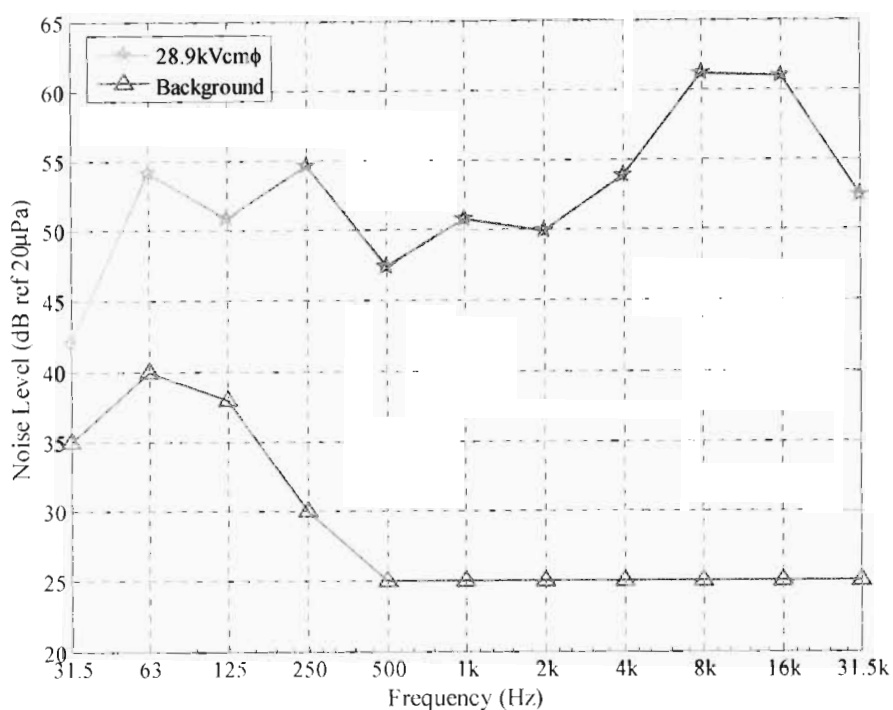


Figure 4.26: AC frequency spectrum for 2.8 cm Ø stranded conductor

In terms of conductor diameters, the AC frequency spectrum shows the same characteristics as the DC spectrum in that the larger conductor generates high noise levels (Figure 4.27). In Figure 4.28 the frequency spectra appear to be consistent in terms of trends for the different conductor surface gradients and seem to be quite similar for the higher surface gradients of 28.9 kV/cm and 33.4 kV/cm. The hum content remains notable in both figures. As also noted in [28], the noise levels for frequencies between 1 kHz and 15 kHz are quite consistent as opposed to those at the lower frequencies which are affected by both the background noise and the hum component.

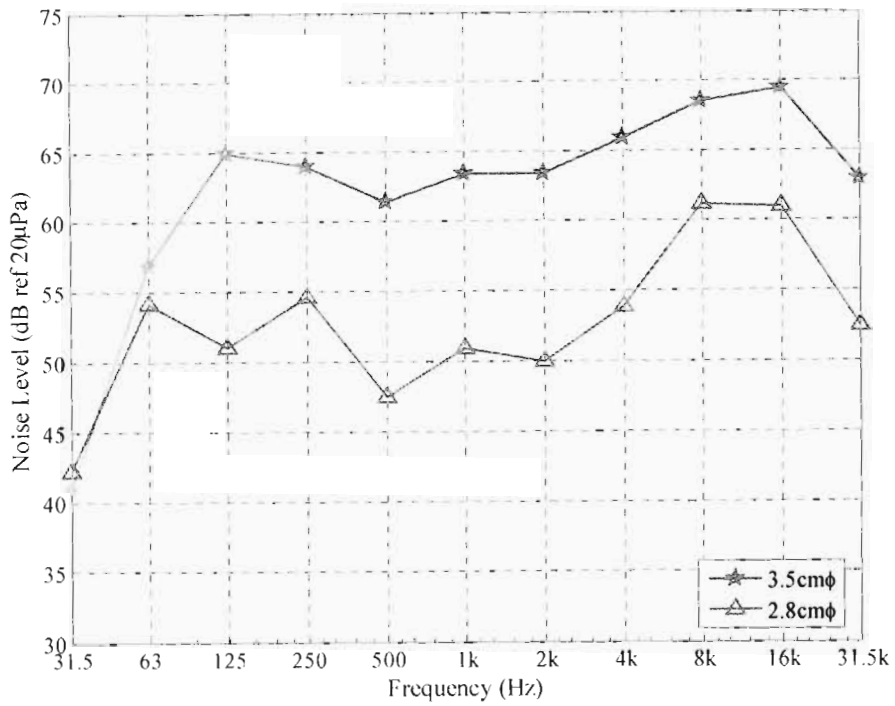


Figure 4.27: Effect of conductor size on AC frequency spectrum at 28.9 kV/cm

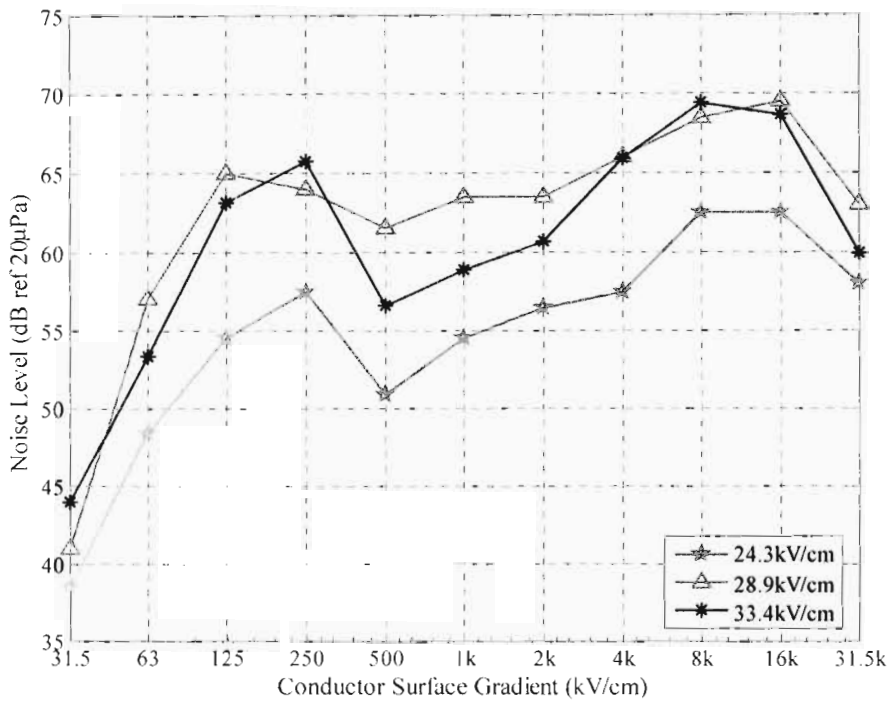


Figure 4.28: Effect of conductor surface gradient on AC frequency spectrum for 3.5 cmØ stranded conductor

## 4.4 Corona Losses

### 4.4.1 Effect of conductor surface conditions

The effect of the conductor surface conditions on the CL is demonstrated in Figures 4.29 and 4.30. It can be noted that the CL for solid smooth conductors only start increasing for conductor surface gradients above 30 kV/cm in both cases i.e. for different conductor sizes and polarities. The significant difference between these graphs demonstrates the effect conductor roughness factors reported earlier in this chapter.

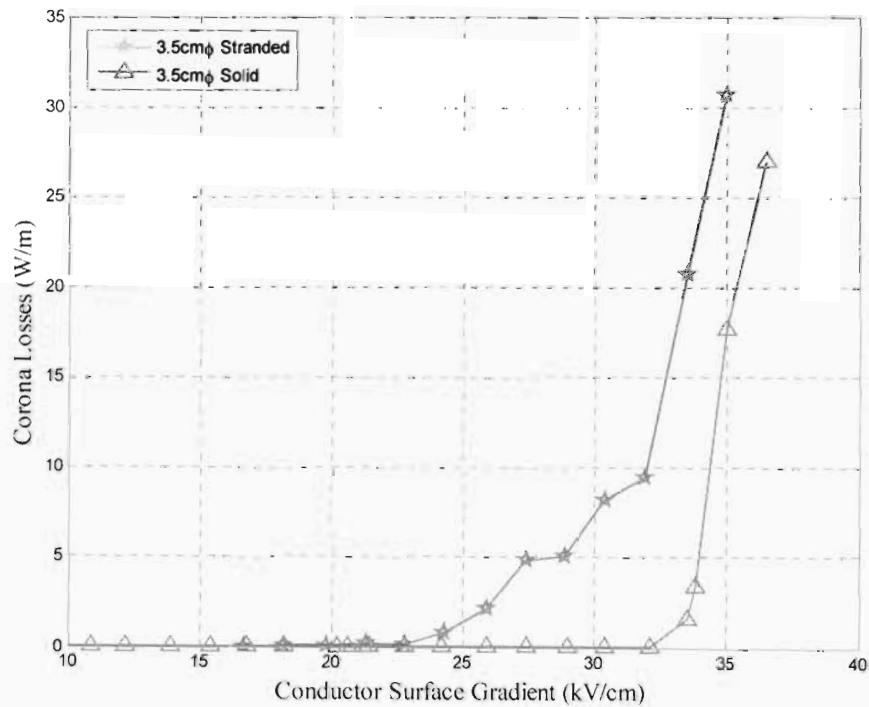


Figure 4.29: Effect of conductor surface condition on corona losses for positive polarity

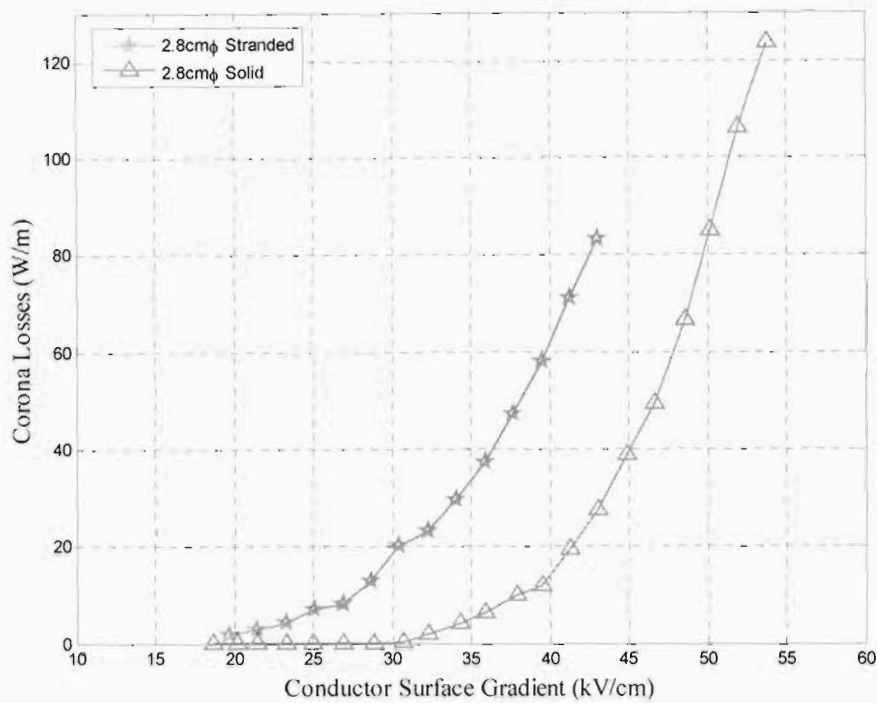


Figure 4.30: Effect of conductor surface condition on corona losses for negative polarity

#### 4.4.2 Effect of polarity

Figures 4.31 and 4.32 show the effect of polarity on DC corona power losses for 3.5 cm diameter and 2.8 cm diameter stranded conductors, respectively. For both conductors, the positive polarity loss seems to be significantly lower than the negative polarity loss, especially at higher surface gradients. For example, the difference between positive and negative CL at 35 kV/cm is about 30 W/m for both conductors. These observations are similar to what was mentioned earlier in the discussions of paper [31]. The higher CL observed under negative polarity could be due to repelled high mobility electrons and negative ions being conducted to ground rapidly.

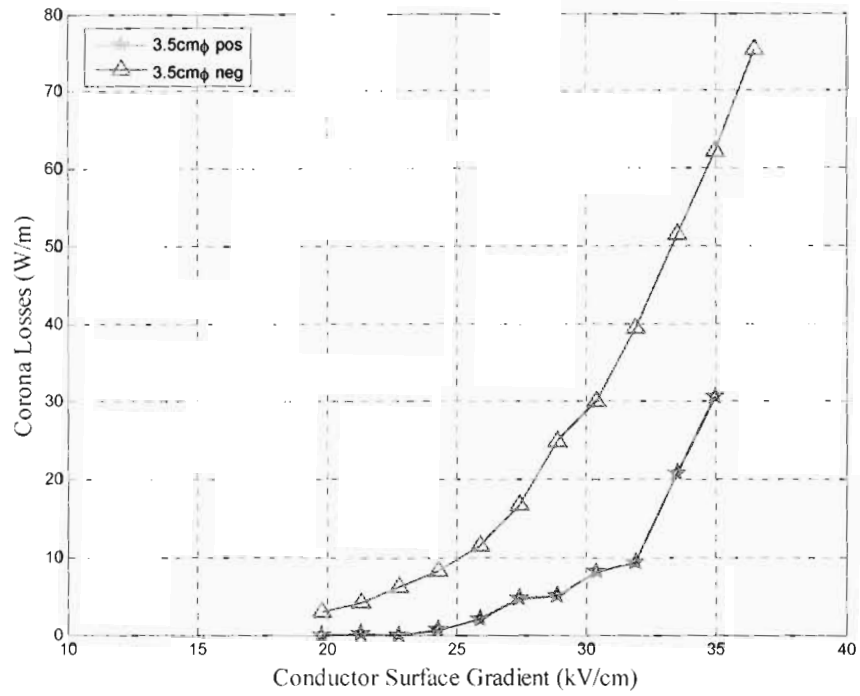


Figure 4.31: Effect of voltage polarity on corona losses for a 3.5 cmØ stranded conductor

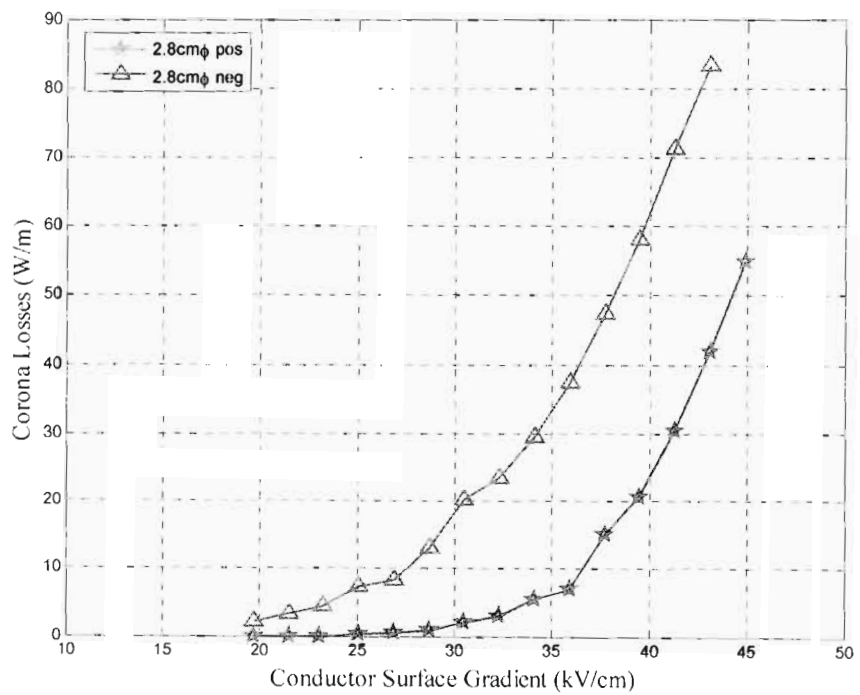


Figure 4.32: Effect of voltage polarity on corona losses for a 2.8 cmØ stranded conductor

#### 4.4.3 Effect of conductor size

In Figures 4.33 and 4.34, a comparison is made of the corona power losses incurred for different conductor sizes under both positive and negative polarities. It can be seen that the CL increases with conductor diameter for the same conductor surface gradient under both polarities. The trends of the three graphs are quite similar and their slopes show a steep increase in CL with the conductor surface gradient beyond 30 kV/cm. This could be due to the fact that large conductors tend to support longer streamers as similarly observed with the AN. Similar observations were also reported in [17]. It can be seen from both sets of curves that the polarity effect on CL is less apparent for the smallest conductor, especially in the low range of conductor surface gradients.

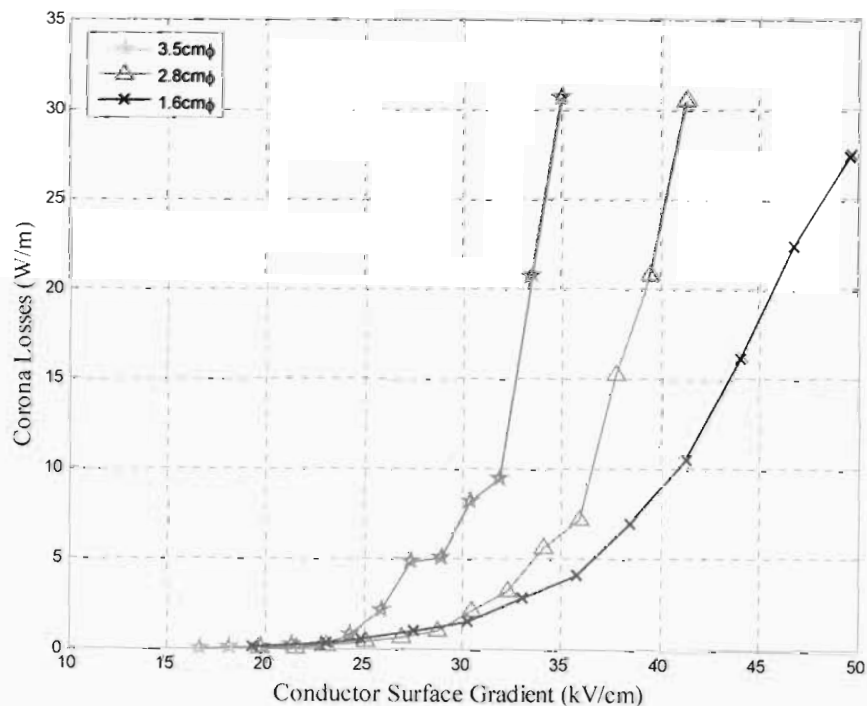


Figure 4.33: Effect of conductor size on corona losses under positive polarity for stranded conductors

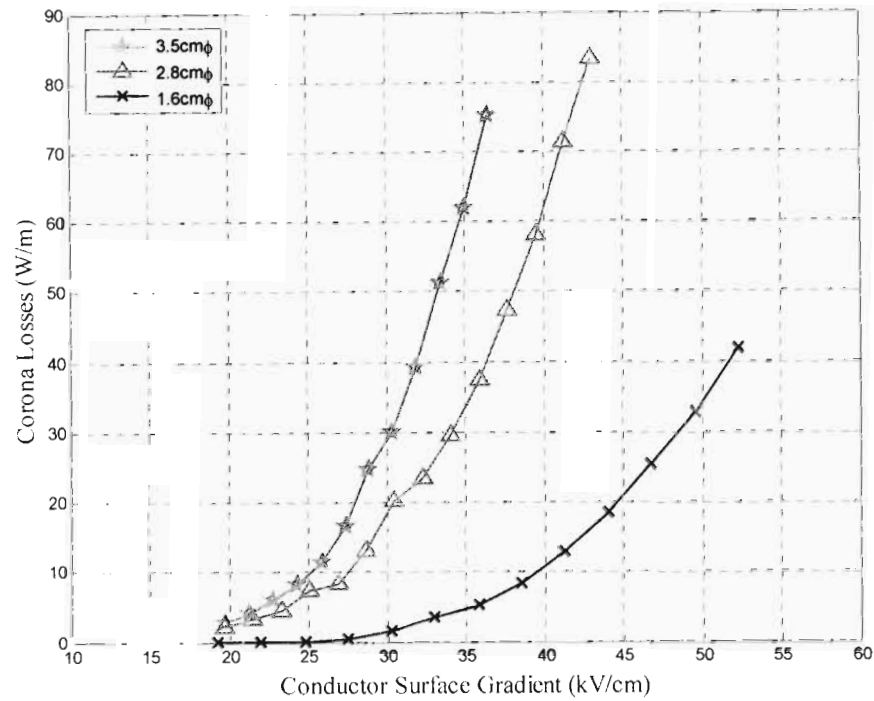


Figure 4.34: Effect of conductor size on corona losses under negative polarity for stranded conductors

#### 4.4.4 Corona cage and test line measurements

Comparison of CL for different configurations is shown in Figure 4.35. Similar corona losses were observed for the cage and the test line with a conductor height of 70 cm. However, the test line with conductor height of 37.5 cm had higher CL. The similarities between the Line1 and the cage results could be due to almost similar gap sizes in both cases. The 70 cm conductor height above ground for Line1 is almost the same as the 75 cm radius of the corona cage. The Line2 configuration gives same conductor surface gradient as that of the cage for the same applied voltage. However, Line2 losses are higher than the corona cage ones, for the same conductor surface gradient. These observations tend to suggest that the CL depends more on the resistance of the path to ground which is determined by the height of the conductor above ground or cage air gap, and not the static conductor surface gradient. This is in agreement with assertions made in [9, 13] that CL depends on the geometry of the system particularly the pole spacing and the conductor height above ground.

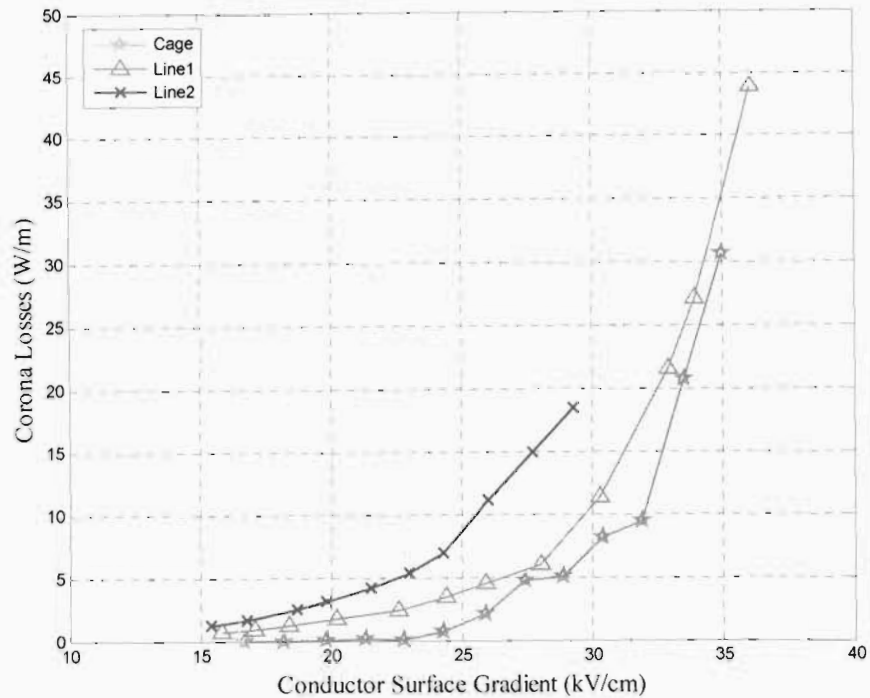


Figure 4.35: Comparison of corona losses in a corona cage and test line for a 3.5 cm $\varnothing$  stranded conductor  
(Line1: H = 70 cm, Line2: H = 37.5 cm)

CL results could not be compared with the software simulations as there are no correction factors to bring the cage and line configurations to the same level of comparison.

#### 4.5 Point-Plane Gap Corona Current Characteristics

The variation of the current with the supply voltage in a point-plane spark gap, is shown in Figure 4.37. The current increased consistently with the supply voltage. The negative polarity current is higher than the positive polarity current, the distinction becoming clearer as the voltage increases. These results agree with those obtained in the corona cage. The polarity is with respect to the point electrode. This can be attributed to the space charge effect in the gap. Under negative polarity, the negative ions and fast electrons are repelled away from the gap and quickly conducted to ground at a higher rate thereby increasing the corona current. Under positive polarity, the slower positive charges are also repelled from the gap, but are conducted to ground at a slower pace and the electrons are more involved in the discharge activity in the high field region around the anode. This



is further substantiated by the corona pulses observed at a voltage of 40 kV using a digital oscilloscope as shown in Figures 4.37 to 4.40. The positive polarity pulses had very high amplitudes compared to the negative polarity ones. The volts/division setting had to be set at 0.5 for the positive polarity to fit the screen as opposed to 0.2 for negative polarity. However, in terms of the frequency, the negative polarity pulses (Figures 4.39 and 4.40) were notably more frequent than the positive polarity pulses (Figures 4.37 and 4.38). This implies that depending on the averaging time for the ammeter, more negative pulses might be averaged within one cycle as compared to positive pulses. This could be the reason why the measured negative polarity corona current is higher than the measured positive polarity current for both the spark gap and the cage configurations.

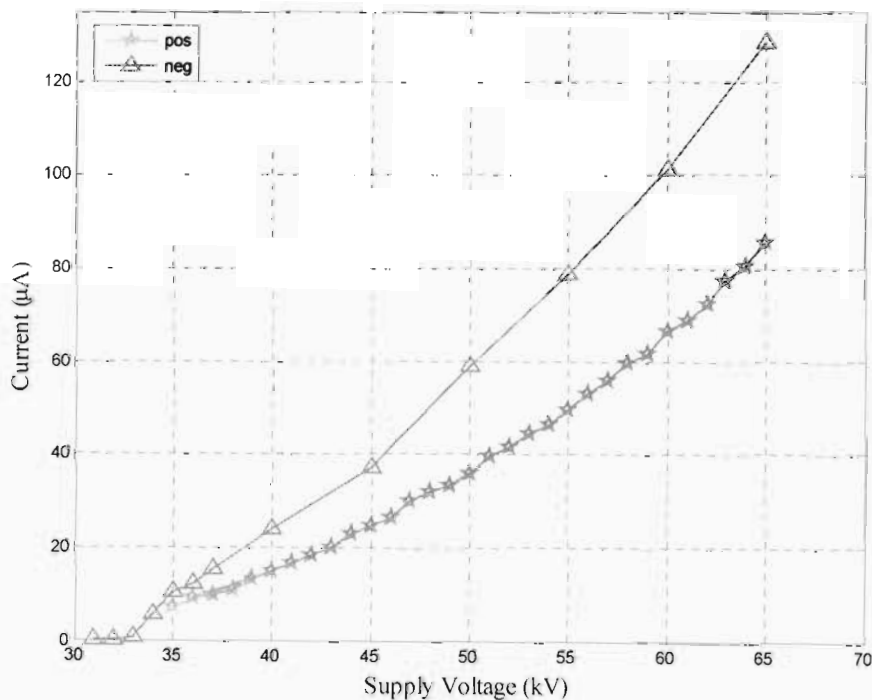


Figure 4.36: Polarity effect on corona current in a point-plane gap (gap spacing = 8.6 cm)

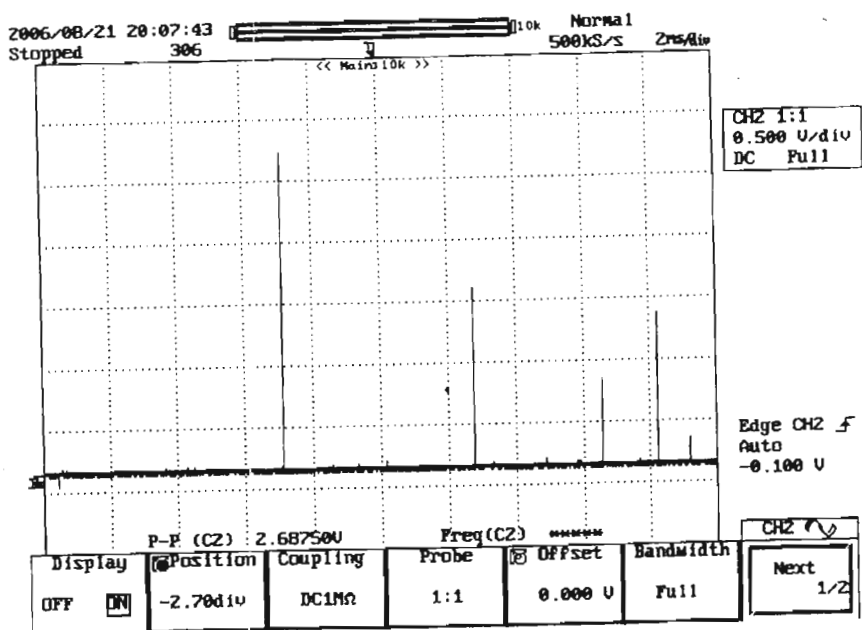


Figure 4.37: Corona current pulses under positive polarity (U = 40 kV)

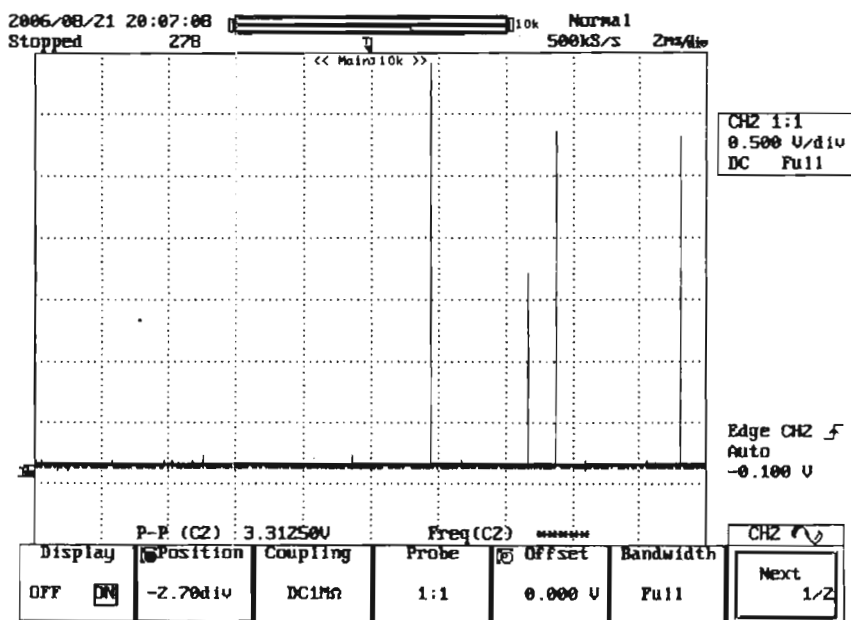


Figure 4.38: Corona current pulses under positive polarity (U = 40 kV)

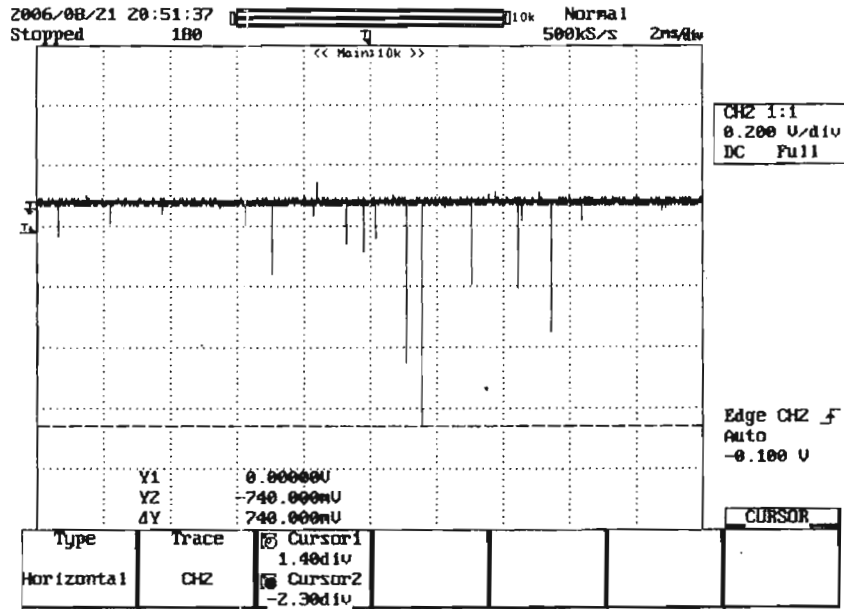


Figure 4.39: Corona current pulses under negative polarity (U = 40 kV)

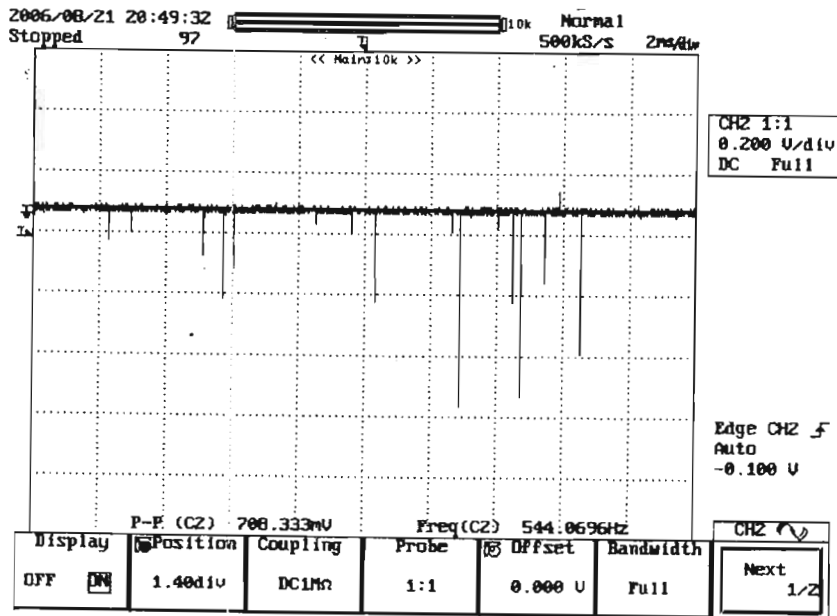


Figure 4.40: Corona current pulses under negative polarity (U = 40 kV)

## 4.6 Space Charge Effect

### 4.6.1 Stranded conductors under DC voltages

A comparison of the corona current measured for stranded conductors when the cage was covered with the foil and when it was uncovered is shown in Figures 4.41 and 4.42 for positive and negative polarities respectively. In both cases the current was slightly less when the cage was covered with foil. At higher conductor surface gradients above 35 kV/cm, the differences between the measured currents are very insignificant. This is in line with the theory that the effect of space charge becomes marginal at higher surface gradients. The results seem to suggest that the effect of space charge in the small corona cage is not significant for stranded conductors. The slight differences in the current values could be due to the current lost through the foil or slight suppression of the field by the space charge. Further work needs to be done in this area, for more clarity about what has been observed.

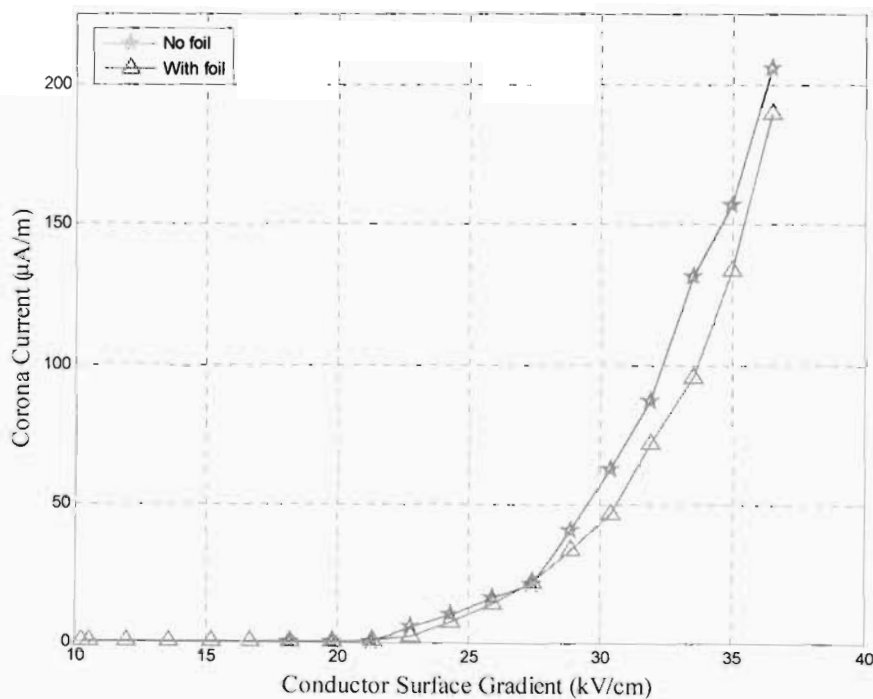


Figure 4.41: Effect of space charge on corona current under positive polarity for a 3.5 cm $\varnothing$  stranded conductor

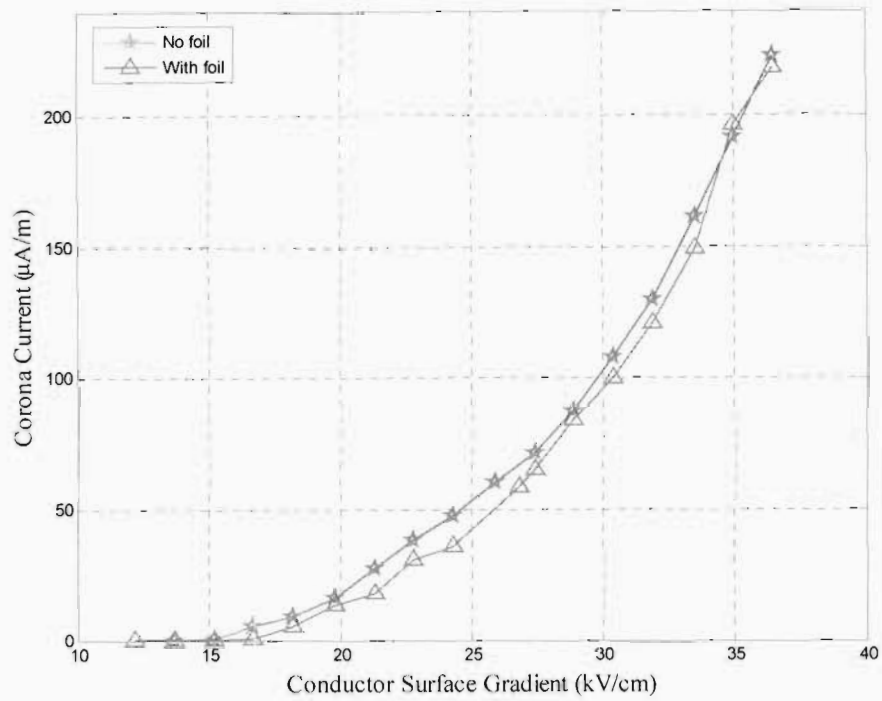


Figure 4.42: Effect of space charge on corona current under negative polarity for a 3.5 cmØ stranded conductor

#### 4.6.2 Solid conductors under DC voltages

The results obtained with solid conductors also agree with those of the stranded conductors as seen in Figures 4.43 and 4.44. In the case of solid conductors, there is a clear distinction between the results obtained when the cage was covered with a foil and when the cage was not covered even at higher surface gradients. The reduced current could either be as a result of reduced charge carriers in the gap due to conduction through the foil or suppressed field by the space charge.

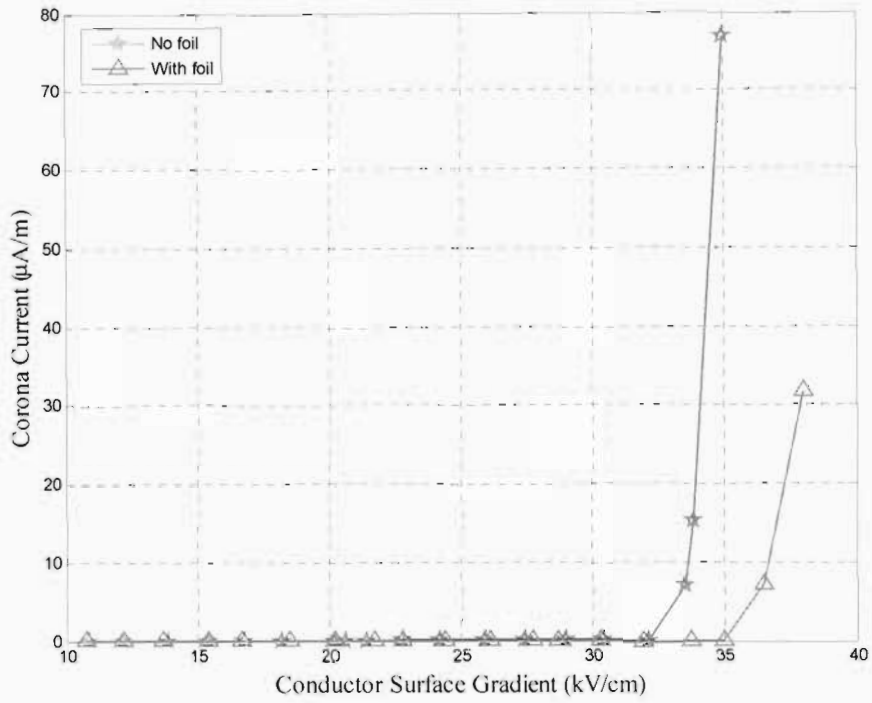


Figure 4.43: Effect of space charge on corona current under positive polarity for a 3.5 cmØ solid conductor

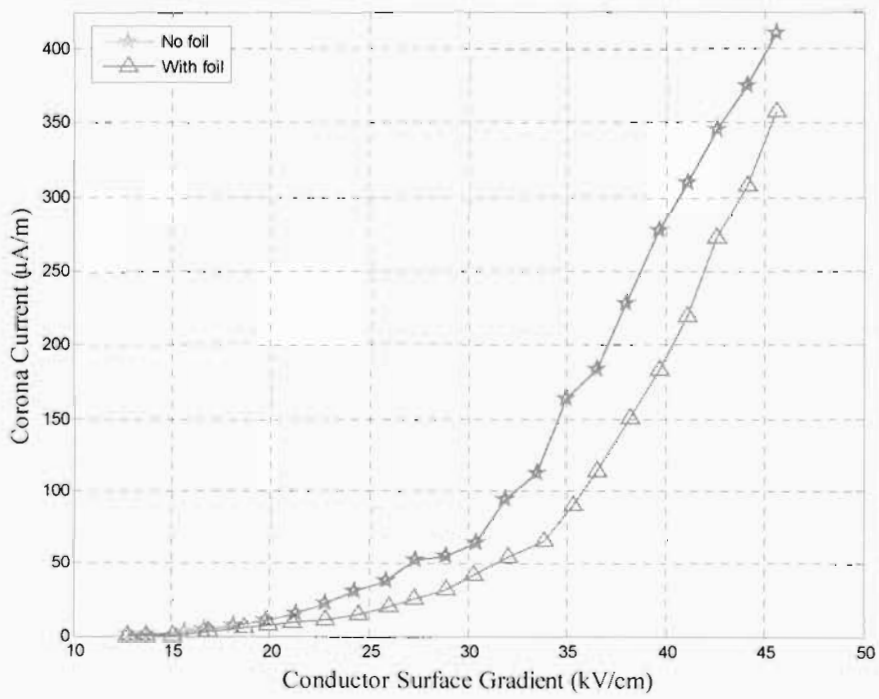


Figure 4.44: Effect of space charge on corona current under negative polarity for a 3.5 cmØ solid conductor

### 4.6.3 Stranded conductor under AC voltages

The effect of the space charge on the measured AC corona current is very insignificant especially up to 33 kV/cm beyond which there was only a slight difference in the currents measured (Figure 4.45). As mentioned in the literature review, for AC lines, space charge generated is confined to a small volume immediately surrounding the conductors and therefore, has negligible effect on the overall field distribution within the cage [20]. The differences in the higher conductor surface gradients could be that the charge carriers increased to a state where the system frequency could not allow sufficient time for the space charge to be swept away.

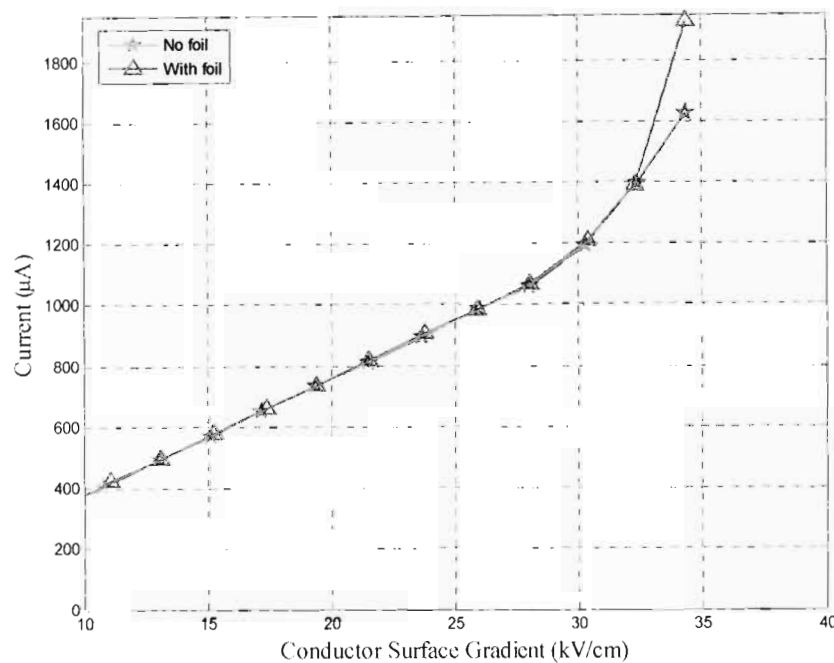


Figure 4.45: Effect of space charge on corona current under AC for a 3.5 cmØ stranded conductor

### 4.6.4 Positive DC test line measurements

In the case of the test line measurements, the current was less when the fan was blowing the air away from the conductor (Figure 4.46). The reduced current could be due the fact that there are fewer charge carriers in the conductor to ground gap due to the blowing away of the air in the vicinity of the conductor. The fan seems to have been less effective as the conductor surface gradient increased beyond 28 kV/cm. The reason could be that the charge carriers increased to such an extent that the fan was unable to adequately disperse the generated space charge similar to the case of AC above.

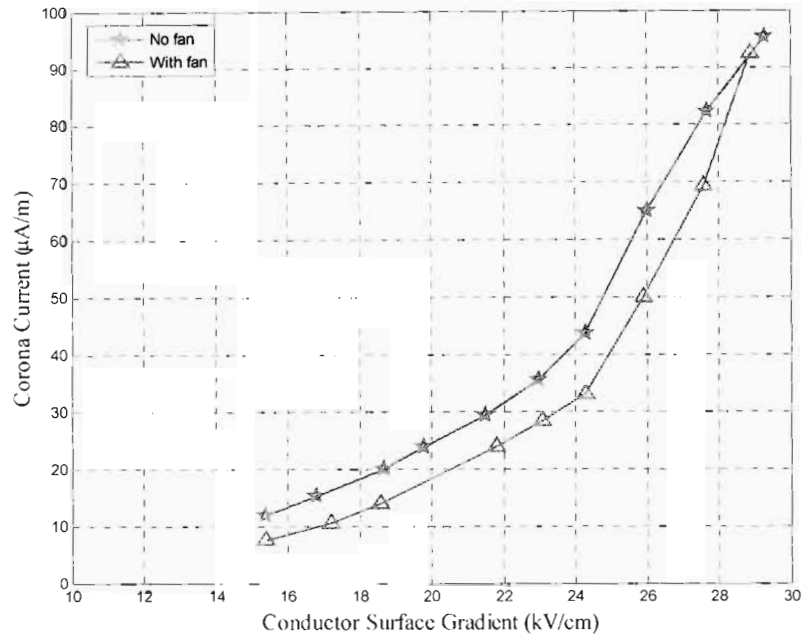


Figure 4.46: Effect of space charge on corona current of a test line ( $H = 37.5$  cm): positive polarity and 3.5 cmØ stranded conductor

#### 4.6.5 Visual corona

Visual corona for both DC polarities and AC show that the discharge was comparatively more intense when the cage was not covered with the foil. Figures 4.47 to 4.49 below show a comparison of corona visuals obtained at 220 kV when the cage was not covered and when it was covered with the foil. These correspond with the current measurements as discussed above.



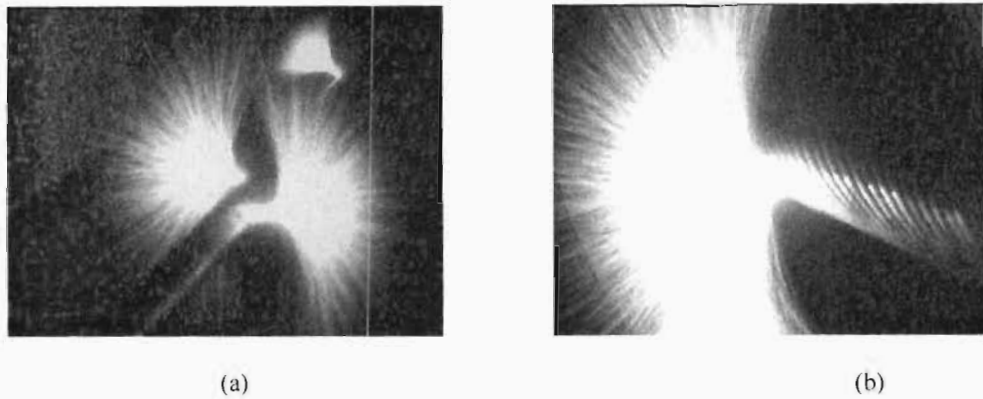


Figure 4.47: Positive polarity 220 kV (a) cage not covered with foil (b) cage covered with foil

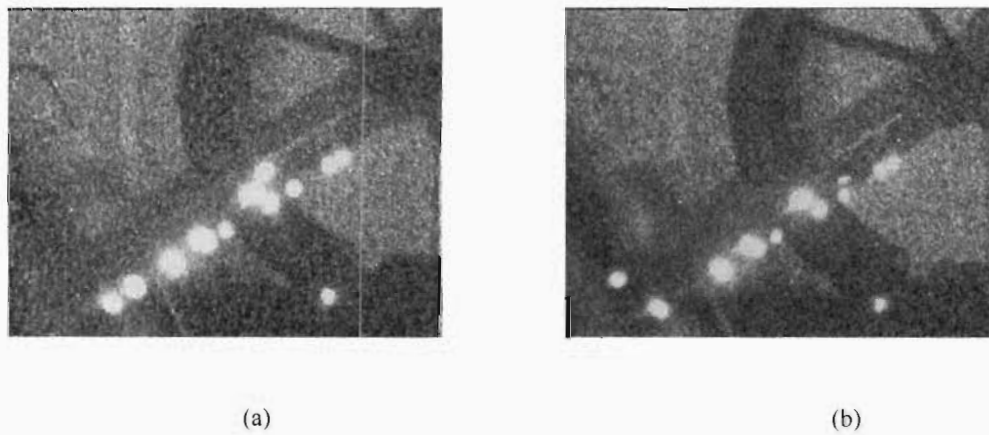


Figure 4.48: Negative polarity 220 kV (a) cage not covered with foil (b) cage covered with foil

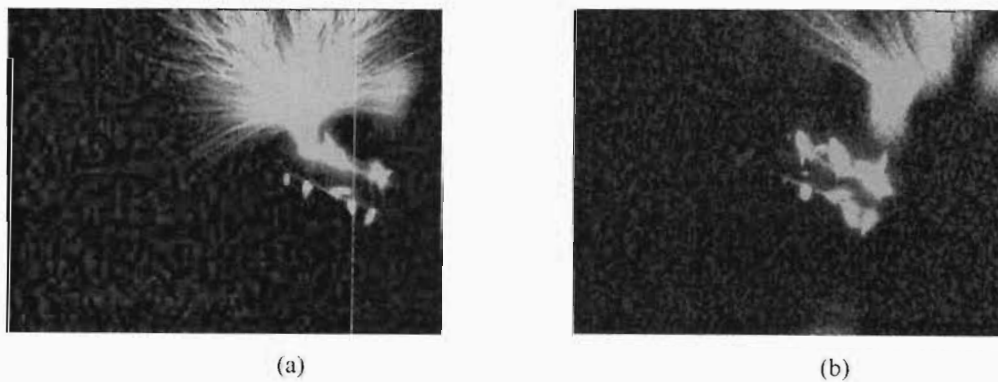


Figure 4.49: AC 220 kV (a) cage not covered with foil (b) cage covered with foil



## Chapter 5: Conclusions

The observed corona plumes showed that the positive polarity corona discharge is more intense than the negative polarity corona, whilst the AC discharge appeared to have the characteristics of both the positive and negative polarity coronas.

Corona audible noise (AN) and corona loss (CL) measurements have been carried out. The AN results demonstrated the relationship between AN and conductor surface gradient, the effect of conductor surface conditions, system polarity, system voltage and conductor size on measured A-weighted noise levels. The measurements also provided a basis for comparison of corresponding conductor-plane test configuration and corona cage AN and CL values.

AN increased as the conductor surface gradient was increased and also increased with the conductor size for the same conductor surface gradient. AN levels under positive polarity DC were much higher than the corresponding negative polarity values, but very similar to the AC noise for the same conductor surface gradient. The positive polarity and the AC noise levels were by far more annoying than the negative polarity levels. The results revealed a distinct difference between AN generated by a smooth solid conductor and that generated by a stranded conductor. Stranded conductors were comparatively noisier. A comparison of cage and test line AN results showed no significant differences between the two, most possibly due to the similarities in their geometries. The results also suggest that the space charge effects on AN are more difficult to evaluate using small corona cages and conductor-plane test arrangements.

There was very good agreement between the EPRI software and the corrected UKZN noise level results, in terms of both the trends and the levels. These results tend to suggest that the software could be used to predict noise levels in Southern Africa at least for low altitude regions since the tests were carried out at sea level only.

The frequency spectrum results showed that transmission line AN is made of different frequencies depending on the applied voltage. Under DC conditions the noise is broadband in nature whilst AC

has the hum component superimposed on the broadband component. It was also shown that the background noise influences the lower frequencies of the transmission line noise.

CL results showed that it increases with conductor surface gradient, as well as with the conductor size for a given conductor surface gradient. The CL for solid conductors is much less compared to stranded conductors. Therefore, solid conductors cannot be used to predict CL produced by stranded conductors. Monopolar negative polarity CL is higher than the positive polarity loss. Current measurements and pulses obtained from the spark gap also confirmed higher currents under negative polarity voltages. The comparison between the test line results with the corona cage results suggests that the CL depends more on the gap between the conductor and ground and the availability of the charge carriers.

Effect of space charge on the corona loss was more apparent on test line measurements. Blowing the fan in the direction of the conductor directed the charge carriers away from the conductor-ground gap and reduced the corona current. The cage measurements showed that the conduction of some of the charge through the foil reduced the current flowing to ground. With AC cage results, there were no signs of the effect of space charge on the measured current. The test line results suggest that the effect of space charge depends on the geometry of the test system and the wind conditions, and therefore, should not be generalised. Hence test cage CL results cannot be compared with software results.

The results obtained agree very well with the studies done elsewhere and provide an understanding of transmission line corona discharge in the Southern Africa context. The objectives of comparing AN results with the software simulations assessing the applicability of the software to local designs have been met. CL as well as AN characteristics have been studied in detail. Effects of space charge on DC and AC corona current have also been demonstrated.

The obtained results could be applied in the preliminary corona design of transmission lines in the Southern Africa region, for the selection of operating conductor surface gradients and transmission line parameters.



## Chapter 6: Recommendations

The measurements presented in this study were carried out at low altitudes only. Corona discharges are known to be greatly affected by climate patterns as well as the altitude. A comparison of results obtained at higher altitude and those at lower altitude will give a complete picture in terms of the effects of altitude on corona generation and the measured quantities. Therefore it will be worthwhile to extend the study to higher altitude areas.

The effect of different geometries on corona discharges can only be verified by performing tests on longer test lines or larger diameter cages and comparing the results with those of the small cage. Considering construction of a test line or a bigger corona cage will assist in validating this study even further.

Due to the dimensions of the cage, only single conductors were considered in this study. Practical transmission lines usually have bundled conductors arranged in different geometries in order to limit, amongst other factors, line losses. It is highly recommended that the applicability of the obtained results to the design of bundled conductors be explored.

Space charge is a complex factor which depends on geometries and the prevailing wind conditions. It would be interesting to make an effort to estimate the space charge conductor surface field during measurements and compare the results with those expressed in terms of static conductor surface gradient.

To obtain a comparison between AC and DC corona loss (CL), an AC self balancing bridge circuit can be designed and used to measure the low power factors associated with AC corona power loss.



## References

- [1] J. D. Glover and M. Sarma, *Power System Analysis & Design*, PWS Publishing Company, 1994.
- [2] A. C. Britten, V. L. Chartier, L. E. Zafanella, "Audible Noise", EPRI AC Transmission Line Reference Book – 200kV and Above, Third Edition, December 2005.
- [3] B. M. Weedy and B. J. Cory, *Electric Power Systems*, 4<sup>th</sup> edition, John Wiley & Sons, 1998.
- [4] F. Venter, *HVDC Systems Design and Operations*, MSc Course Notes, UKZN, 2005.
- [5] J. Arrilaga, *High Voltage Direct Current Transmission*, 2<sup>nd</sup> edition, The Institute of Electrical Engineers, 1998.
- [6] Y. Shu, "Development of ultra high voltage transmission technology in China", Proceedings of the XIV International Symposium on High Voltage Engineering, Beijing, 2005.
- [7] D. Muftic, A. Britten, C van der Merwe and R. Vajeth, "Long distance transmission: opportunities and options", Proceedings CIGRE 5<sup>th</sup> Southern Africa Regional Conference, Somerset West, 2005.
- [8] R. Arora and W. Mosch, *High Voltage Insulation Engineering*, Wiley Eastern Limited, 1995.
- [9] P. S. Maruvada, *Corona Performance of High-Voltage Transmission Lines*, Research Studies Press LTD, 2000.
- [10] T. Pillay and S. Bisnath (Editors), "Corona", *The Planning, Design and Construction of Overhead Power Lines*, Eskom Power Series Volume 1, 2005.
- [11] Z. Engel and T. Wszolek, "Audible noise of transmission lines caused by the corona effect: analysis, modeling, prediction", *ELSEVIER Applied Acoustics*, Vol. 47, No. 2, 1996, pp 149-163.
- [12] M. G. Comber and L. E Zafanella, "the use of single phase overhead test lines and test cages to evaluate the corora effects of EHV and UHV transmission lines", *IEEE Transactions on Power Apparatus and Systems*, Vol. PAS-93, Jan./Feb. 1974, pp 81-90.
- [13] G. Gela, J. J. LaForest and L. E. Zaffanella, "Corona phenomena on HVDC transmission lines", *HVDC Transmission Line Reference Book*, EPRI TR-102764, September 1993.
- [14] IEEE Corona and Field Effects Subcommittee Report, "A survey of methods for calculating transmission line conductor surface voltage gradients". *IEEE Transactions on Power Apparatus and Systems*, Vol. PAS-98, No. 6, Nov./Dec 1979, pp. 1996-2014.
- [15] "Overall design considerations", Proceedings Power Line Electromagnetic Fields and Corona Technical Seminar, paper 19d, Spokane, Washington, 1993.



- [16] R. D. Dallaire and P. Sarma Maruvada, "Corona performance of a  $\pm$  450-kV bipolar DC transmission line configuration", IEEE Transactions on Power Delivery, Vol. PWRD-2, No. 2, April 1987, pp 477-485.
- [17] R. D. Dallaire, P. S. Maruvada and N. Rivest, "HVDC monopolar and bipolar cage studies on the corona performance of conductor bundles", IEEE Transactions on Power Apparatus and System, Vol. PAS-103, No. 1, January 1984, pp. 84-91.
- [18] W. Janischewskyj, "Characteristics of RI and TVI sources", Publication 76 CH1163-5-PWR pp. 12-19.
- [19] V. L. Chartier and J. W. Bankoske, "Waltz Mill 1100kV station: conductor selection and laboratory verification", IEEE Transactions on Power Apparatus and Systems, Vol. PAS-88, June 1969, pp. 825-833.
- [20] V. L. Chartier, "Determination of corona generated functions", Proceedings Power Line Electromagnetic Fields and Corona Technical Seminar, Spokane, Washington, 1993.
- [21] D. E. Perry, "AN analysis of transmission line audible noise levels based upon field and three-phase test line measurements IEEE Transactions on Power Delivery, Vol. 91, Jan.-June 1972, pp. 857-865.
- [22] V. L. Chartier, "Measurement of corona phenomena", Proceedings Power Line Electromagnetic Fields and Corona Technical Seminar, paper 14a, Spokane, Washington, 1993.
- [23] V. L. Chartier, "Empirical Expressions for Calculating High Voltage Transmission Corona Phenomena", A paper presented at the Engineering Seminar of Bonneville Power Administration's Technical Career Program for Professional Engineers, Portland, Oregon, April 7, 1983.
- [24] Vernon L. Chartier and Richard D. Stearns, "examination of grizzly mountain data base to determine effects of relative air density and conductor temperature on HVDC corona phenomena", IEEE Transactions on Power Delivery, Vol. 5, No. 3, pp. 1575-1582, July 1990.
- [25] R. M. Morris, "Measurement of corona losses", Proceedings Power Line Electromagnetic Fields and Corona Technical Seminar, paper 13b, Washington, 1993.
- [26] P. S. Maruvada, "Methods of calculating corona losses", Proceedings Power Line Electromagnetic Fields and Corona Technical Seminar, paper 13a, Spokane, Washington, 1993.
- [27] L. L. Beranek, "Acoustics", Acoustical Society of America, Cambridge 1996.
- [28] V. L. Chartier and R. D. Stearns, "Formulas for predicting audible noise from overhead high voltage AC and DC lines", IEEE Transactions on Power Apparatus and Systems, Vol. PAS-100, No. 1, January 1981, pp 121-129.

- [29] G. B. Johnson, E. V. Larsen, D. J. Lorden, M. Smead, R. H. Lasseter and D.P. Hartmann, "External electrical and audible effects", HVDC Handbook, 1st Ed., EPRI TR-1041665, 1994.
- [30] IEEE Corona and Field Effects Subcommittee Report, "A comparison of methods of calculating audible noise of high voltage transmission lines," IEEE Transactions on Power Apparatus and Systems, Vol. PAS-101, No. 10, Oct. 1982, pp. 4090-4099.
- [31] Y. Nakano and Y. Sunaga, "Availability of Corona Cage for predicting Audible Noise generated from HVDC Transmission Line," IEEE Transactions in Power Delivery, Vol. 4, No. 2, April 1989, pp. 1422-1431.
- [32] P. S. Maruvada, "Regulations and limits", Proceedings IEEE/PES Transmission Conference and Exposition, Dallas, 1991.
- [33] V. L. Chartier, "Practical considerations in line design", Proceedings Power Line Electromagnetic Fields and Corona Technical Seminar, paper 19b, Spokane, Washington, 1993.
- [34] P. S. Maruvada and W. Janischewskyj, "Electrostatic field of a system of parallel cylindrical conductors", IEEE Transactions on Power Apparatus and Systems, Vol. PAS-88, No. 7, July 1969.
- [35] G. B. Johnson, "Degree of corona saturation for HVDC transmission lines", IEEE Transaction on Power Delivery, Vol. 5, No. 2, 1990, pp. 695-707.
- [36] P. S. Maruvada, R. D. Dallaire, P. Héroux and N. Rivest, "Long-term statistical study of the corona electric field and ion-current performance of a 900-kV bipolar HVDC transmission line configuration", IEEE Transactions on Power Apparatus and Systems, Vol. PAS-103, No. 1, January 1984, pp. 76-83.
- [37] P.S. Maruvada, "Corona-generated space charge environment in the vicinity of HVDC transmission lines", IEEE transactions on Electrical Insulation, Vol. EI-17 No. 2, April 1982, pp. 125-130.
- [38] P. J. Carter and G. B Johnson, "Space charge measurements downwind from a monopolar 500kV HVDC test line", IEEE Transactions on Power Delivery, Vol.3, No.4, October 1988, pp. 2056-2063.
- [39] E.E. Kunhardt and L. H. Luessen (Editors), Electrical breakdown and discharges in gases, Plenum Press, 1982.
- [40] EPRI Software Help Guide, TLW ACDCLINE 3.0, Copyright© 1996 EPRI.

## Appendices

### Appendix A: Specifications of Main and Auxiliary Equipment

#### Portable DC source

AC input:	4/8 kW, 3-phase: 187-228 Vrms, 48-63 Hz
DC output:	$\pm 0-125$ kV
Output current:	30 mA
Ripple:	< 0.1% of rated Urms up to 125 kV

#### AC test transformer

##### AC input

Voltage:	230 V, Single phase AC
Current:	32 A
Frequency:	50 Hz

##### AC output

Rated output voltage:	2x100 kVrms
Rated output continuous:	5 kVA
Rated output short time:	7.5 kVA
Frequency:	50 Hz
Short circuit impedance voltage:	5% approximately with respect to rated continuous kVA and rated voltage

**Walton-Cockroft generator**

No load rated output (positive polarity): +500 kV

No load rated output (negative polarity): -540 kV

Rated continuous current: 7.5 mA

Ripple voltage:  $\leq 3\%$  at rated current and voltage

**Noise level meters**Rhode&Schwarz Sound level meter (ELT3)

Measuring range: 25 to 120 dBA

Frequency range: 16 Hz to 16 kHz

Precision microphone: capacitor microphone, omnidirectional characteristic

Main direction of sound incidence: from front along longitudinal axis of set

Operating temperature range: -10 to +50°C

Bruel&Kjaer sound level meter (Type 2218)

Measuring range: 19 to 134 dBA

Octave: 14 to 134 dB

Frequency range: 10 Hz to 18 kHz

Microphone: 1" condenser microphone, omnidirectional at low frequencies, at high frequencies the sensitivity varies with the angle of incidence.

Bruel&Kjaer octave filter set (Type 1613)

Centre frequencies ( $f_0$ ): 31.5 Hz, 63 Hz, 125 Hz, 250 Hz, 500 Hz, 1 kHz, 2 kHz, 4 kHz, 8 kHz, 16 kHz, 31.5 kHz.

Cut-off frequencies: Minimum =  $f_c/\sqrt{2}$   
 Maximum =  $\sqrt{2}f_c$

### **CoroCAM I**

Field of view: 7° Horizontal 5° Vertical  
 Focus range: 0.5 m to infinity  
 Focal length: 110 mm  
 Filters: UV wide bandpass filters

### **Fluke Model 187**

DC voltage: 0 – 1000 V  
 AC voltage: 2.5 mV – 1000 V (100 kHz bandwidth)  
 DC Current: 0-10 A continuous  
 20 A for 30 seconds  
 AC current, true rms: 25  $\mu$ A – 10 A continuous  
 20 A for 30 seconds  
 Resistance: 0 – 500 M $\Omega$   
 Conductance: 0 – 500 nS  
 Capacitance: 0.001 nF – 50 mF  
 Frequency: 0.5 Hz – 1000 kHz

### **Digital oscilloscope (DL1740)**

Source voltage: 100-120 V AC / 220 to 240 V AC (switches automatically)  
 Power supply frequency: 50/60 Hz

Maximum power consumption: 200 VA

Input coupling: AC-1 M $\Omega$ , DC-1 M $\Omega$ , DC-50  $\Omega$ , GND

Input impedance: 1 M $\Omega$   $\pm$ 1.0%, 50  $\Omega$   $\pm$ 1.0%

Voltage-axis sensitivity range:

- 50  $\Omega$  input: 2 mV – 1 V/div (in 1, 2 or 5 mV increments)
- 1 M $\Omega$  input: 2 mV – 10 V/div (in 1, 2 or 5 mV increments)

Maximum input voltage:

- 1 M $\Omega$  input (at 1 kHz or less frequencies): 400 V (DC +AC peak) – 282 Vrms CAT II
- 50  $\Omega$  input: 5 V:ms max. and 10 Vpeak max

Frequency characteristics:

(-3 dB roll-off point for sine-wave input with  $\pm$ 4 div amplitude)

- 50  $\Omega$  input: 1 V – 10 mV/div over 0 (DC) to 500 MHz, or 5 mV – 2 mV/div over 0 (DC) to 400 MHz
- 1 M $\Omega$  (input defined as resistance up to the probe tip when 700988 probe is used): 10 V – 10 mV/div over 0 (DC) to 400 MHz or 5 mV – 2 mV/div over 0 (DC) to 300 MHz

A/D conversion resolution: 8bits (24LSBs/div)

Maximum sampling rate:

- real time sampling mode
  - When interleave mode is on: 1 GS/s
  - When interleave mode is off: 500 MS/s
- Equivalent-time sampling mode: 100 GS/s

**Pedestal fan (FS25)**

Speed: 1400 rpm  
Volume: 2.95 m<sup>3</sup>/s  
Noise: 56 dBA  
Power: 200 W  
Power factor: 0.83

**Appendix B: Publications Related to the Study**

- B-1 M J Lekganyane, N M Ijumba and A C Britten, “Conductor corona generated audible noise under HVDC voltages”, to be presented at the 15<sup>th</sup> International Symposium on High Voltage Engineering (ISH), Ljubljana, 27<sup>th</sup> – 31<sup>st</sup> August 2007.
- B-2 M J Lekganyane, N M Ijumba and A C Britten, “A comparative study of space charge effects on corona current using an indoor corona cage and a monopolar test line”, to be presented at the IEEE PES PowerAfrica 2007 Conference, South Africa, 16<sup>th</sup> – 20<sup>th</sup> July 2007.
- B-3 M J Lekganyane, N M Ijumba and A C Britten, “Evaluation of Prediction Methods for HVDC Corona Generated Audible Noise Using an Indoor Corona Cage”, Proceedings of the 16th Southern African Universities Power Engineering Conference (SAUPEC) 2007, University of Cape Town, Cape Town, South Africa.
- B-4 M J Lekganyane, N M Ijumba and A C Britten, “Corona Audible Noise Measurements in a Small Indoor Corona Cage under HVDC Voltages”, proceedings of the 2006 International Conference on Power System Technology (PowerCon), Paper F1012, Chongqing, China.
- B-5 M J Lekganyane, N M Ijumba and A C Britten, “The Effect of Conductor Surface Gradient on Corona Generated Audible Noise under HVDC”, proceedings of the HVDC 2006 Congress, Paper 25, UKZN, Westville Campus, Durban, South Africa.
- B-6 M J Lekganyane, N M Ijumba and A C Britten, “The dependence of corona audible noise on the conductor surface gradient”, Proceedings of the 15th Southern African Universities Power Engineering Conference (SAUPEC) 2006, pgs 22-26, UKZN, Howard College, Durban, South Africa.



## Appendix B-1

## Conductor Corona Generated Audible Noise under HVDC Voltages

M J Lekganyane<sup>1</sup>, N M Ijumba<sup>1\*</sup> and A C Britten<sup>2</sup><sup>1</sup>HVDC Centre, University of KwaZulu-Natal<sup>2</sup>Resources and Strategy, Eskom  
South Africa

\*Email: ijumba@ukzn.ac.za

**Abstract:** Corona is the ionisation of air in the vicinity of conductors, energized at high AC and DC voltages. This gives rise to acoustic waves and, hence the audible noise. In considering the transmission line designs for specific locations, the atmospheric impact on corona inception needs to be taken into account. The study was conducted to understand the relationship between corona audible noise and conductor surface gradient under local climatic conditions. Measurements of the audible noise generated by conductor corona under HVDC fields were made, and the measured noise levels compared with the predictions made by the EPRI TLW software as well as results obtained from CRIEPI and BPA. The predictions found in the EPRI TLW software were used for most of the analysis. Results obtained show that audible noise increased with conductor surface gradient. The noise levels were higher under positive polarity and for larger stranded conductors. Similar trends were observed in the variation of audible noise with conductor surface gradient for both cage measurements and the predictions. The cage results were closer to the EPRI predictions for both polarities. The outcome of the study will contribute towards the improved design of new EHVDC lines for the Southern African region.

## 1 INTRODUCTION

Corona is a discharge phenomenon that occurs when the air surrounding the high voltage transmission line conductors operating at high surface gradients is ionised. It generates unappreciable audible noise, radio noise, ozone and space charge in the case of DC lines and is also dependent on meteorological conditions, line configuration and conductor surface gradient. As a result it has become an important factor in transmission line design. In the design of Eskom's 765kV lines in South Africa, choice of certain parameters was influenced by corona performance, for example, a six conductor bundle was chosen over a four-conductor bundle to limit the corona generated audible noise (AN) [1].

Earlier studies have shown that corona generation is related to the conductor surface gradients [2], [3], and it is a result of small electrical discharges which occur when the electric field intensity on the conductor surface exceeds the electrical breakdown strength of the

surrounding air [4]. Conductor surface gradient is the design factor which most influences the corona performance of transmission lines [5]. For air at standard pressure and temperature, the critical corona inception gradient in air is 30kV/cm peak or 21kVrms for AC fields [1]. The conductor surface gradient depends on factors such as conductor geometry, transmission line phase and pole configurations as well conductor height above ground.

Generation of corona is not only determined by the distribution of gradient around the surface of the conductors, but also by the positions of the sources of corona [3]. These are normally nicks, scratches and debris deposited on the surface of the conductors. Weather conditions have also been found to have a significant influence on the surface of the conductors, thus affecting the corona effects differently, depending on the nature of the electric field. In South Africa, atmospheric conditions vary from the low altitude coastal areas to the inland high altitude ones. Consequently in considering the transmission line designs for specific locations, the atmospheric impact on corona inception needs to be taken into account.

## 2 CORONA AUDIBLE NOISE

### 2.1 Theoretical Background

During corona discharges the rapid movement of electrons during ionisation results in the sudden transfer of kinetic energy to neutral air molecules through collisions. This energy transfer is equivalent to an explosion taking place at the corona site which gives rise to the generation of acoustic waves [2]. In essence corona discharges are a source of acoustic pulses. The burst of acoustic pulses are generated near the peak of the positive cycles for AC voltages. The alternating voltage results in the pure tones at frequencies corresponding to the even harmonics of the system frequency. In the case of DC systems there is no generation of the pure tones due to the absence of any modulating influence of the voltage.

Basic laws of acoustics are used to analyse the transmission line AN on the basis of certain assumptions [2]. Considering a single conductor above ground and solving equations from acoustic theory as

shown in the sound pressure  $P$  sensed by the microphone can be determined as follows:

$$P = \sqrt{\frac{c \delta A}{2\pi R} \tan^{-1} \frac{l}{2R}} \quad (1)$$

Equation (1) is applicable to a short transmission line, for an infinitely long line (1) reduces to (2).

$$P = \sqrt{\frac{c \delta A}{4R}} \quad (2)$$

Where,

$P$  = sound pressure level (Pa)

$c$  = propagation velocity of sound waves (m/s)

$\rho$  = air density ( $\text{kg/m}^3$ )

$A$  = generated acoustic power density (W/m)

$R$  = distance between the noise source to the point of observation (m)

The exact value for the propagation velocity of sound waves is obtained from (3) [6]; however, this value is taken as 331m/s in most calculations including those in [4].

$$c = 331.4 \sqrt{1 + \frac{\theta}{273}} \quad (3)$$

Where,

$\theta$  = temperature in degrees

According to [2] the air density at sea level varies with ambient temperature and has values of about  $1.22\text{kg/m}^3$  in summer and  $1.28\text{kg/m}^3$  in winter. However, a value of  $1.29\text{kg/m}^3$  is proposed elsewhere as the air density [4].

With the sound pressure  $P$  and the generated acoustic power density  $A$  expressed in dBA at a reference of  $20\mu\text{Pa}$  and  $1\text{pW/m}$  respectively, (1) and (2) become,

$$P(\text{dBA}) = A(\text{dB}) - 10 \log R - 10 \log \left[ \tan^{-1} \frac{l}{2R} \right] - 7.82 \quad (\text{Short line}) \quad (4)$$

$$P(\text{dBA}) = A(\text{dB}) - 10 \log R - 5.86 \quad (\text{Long line}) \quad (5)$$

The above equations are applicable to AN generated from HVAC and HVDC transmission lines.

## 2.2 Field Effects

AN is greatly affected by the conductor surface gradient [7], [8] compared to any other factors. The parameters of the line often have insignificant influence on AN. For example, in the design considerations discussed in [9] it is also mentioned that variations in conductor height will only result in small variations with AN generated. The AC laboratory results mentioned in [10] indicated that as the surface gradient increased, audible noise increased until it reached saturation levels and the difference in noise levels between conductor arrangements decreased with

increasing conductor surface gradient. Practical operating conductor surface gradients seem to be in the range of  $15\text{kV/cm}$  to  $30\text{kV/cm}$ . For this reason, the BPA prediction formulae as presented by Chartier and Stearns [7] are valid for gradients between 12 and  $25\text{kVrms/cm}$  for AC and between 17 and  $29\text{kV/cm}$  DC. Furthermore, the equations which are incorporated in the EPRI's "ACDCLINE" software are valid for gradients between 15 and  $30\text{kV/cm}$  DC [4].

Early consideration of the audible noise, ions, and radio noise in the design of the line can minimize the effect of all corona-related effects [11] thereafter. To determine the behaviour of corona AN, long term and short term AN measurements can be done on either test lines or test cages. Long term measurements are more reliable as they are carried out for longer periods and reflect the influence of different weather conditions on the measurements. Measurements techniques and instruments may affect the noise levels measured. It is also worth mentioning that measured AN depends on the distance between conductor and the microphone used to measure the noise levels [3].

## 2.3 Other Effects

Due to the nature of the positive corona discharges, corona generated pulses on positive polarity conductors have higher magnitude and longer decay times resulting in more audible noise for the positive polarity [4]. The electric field in the vicinity of large diameter conductors tends to support longer streamers than the electric field around small conductors corresponding to higher noise being produced from larger conductors. This was also mentioned in [1] and agrees very well with the results presented in [12], [13].

Climatic conditions affect corona effects differently depending on the system voltage. HVDC corona AN is higher under fair weather conditions, during wet weather conditions [4]. The ionization is much higher resulting in sufficiently high space charge to suppress the surface gradient. In physical terms the increased corona activity during foul weather suppresses the positive polarity plumes which are the primary source of the AN [11].

## 3 EXPERIMENTAL PROCEDURE

DC audible noise measurements were carried out in a small indoor corona cage using a single conductor, either solid or stranded. Three different conductor diameters were considered. The cage was 2m in length with a diameter of 1.5m. The voltage source was a  $500\text{kV}$ , two-stage Walton Cockroft DC generator, for both polarities. Audible noise measurements were taken at a distance of 0.88m from the conductor using a

Robide & Schwarz sound level meter. The frequency spectra for the different conductor surface gradients were also measured using a Brüel&Kjaer filter set Type 2218 which was attached to the noise level meter. The sound level meters were placed in a measurements cage, adjacent to the corona cage, and positioned at the same height as the conductors being tested (Figure 1). Inception levels and corona activity were observed with the use of a CoroCAM I camera.

The static conductor surface gradients were calculated from the supply voltage, conductor and the cage radii. The results obtained from the cage were corrected for height and length to be able to compare them with the predictions from the EPRI TLW software. The EPRI, CRIEPI and BPA predictions found in the EPRI TLW software were used for most of the analysis.

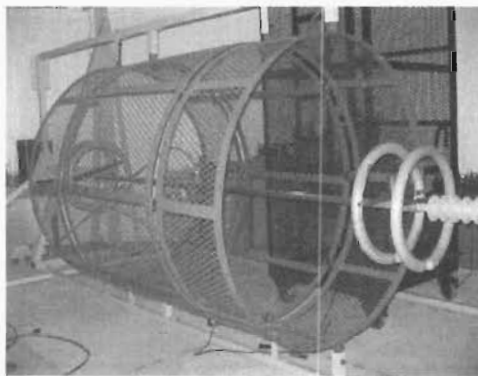


Fig. 1: Corona cage and measurements cage

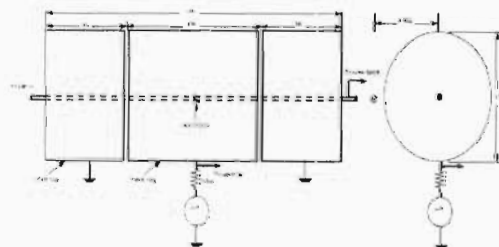


Fig. 2: schematic diagram showing the position of the noise level meter.

A single conductor configuration in a typical DC transmission line was assumed for the purpose of comparison. The opposite polarity pole was placed 150m away from the energized pole to minimize the field interaction between the two poles. The assumed parameters of the line and the configuration for evaluation of the correction factors are shown in Table 1 and Figure 3. This configuration was used throughout the simulations, which were run for different voltage

levels. The conductor surface gradients plotted against the noise levels.

The radial distance between the microphone and the conductor for the assumed configuration and for the cage configuration are quite different. To bring the two configurations to a comparable level, correction factors for height and conductor length were applied to the cage results. The intensity of noise changes with the proximity to the source producing it. With transmission lines, the noise level changes by approximately 3dB for every doubling of the distance from the line [14],[15]. This implies that the sound pressure level, P is inversely proportional to  $\sqrt{d}$ , where d is the radial distance between the transmission line and the microphone. The correction factor for the height was obtained from (6),

$$\Delta P_h = 10 \log \frac{r}{R} \quad (6)$$

where r is the distance to the noise meter from the conductor in the cage and R is the radial distance to the meter from the line conductor in the assumed configuration. Based on Figure 3, the height correction factor for the measured levels is, therefore, -14.76dB. To correction factor for the length was calculated on the basis of (7), as proposed in [2],

$$\Delta P_l = 10 \log \left( \frac{\pi}{2} \tan^{-1} \left( \frac{l}{2r} \right) \right) \quad (7)$$

Where l is the length of the cage and r is the radial distance between the conductor and microphone. Based on the cage configuration, the length correction factor is, therefore, -0.71dB. The cage and simulations results were compared through curve fitting.

Table 1: Line parameters used for the EPRI TLW software simulations.

Parameter	Value
# of conductors	1
Diameter	3.5cm
Height of the conductor	26.2m
sag	16m
Altitude	92m
Microphone height	1.6m
Distance between the line and microphone	19m

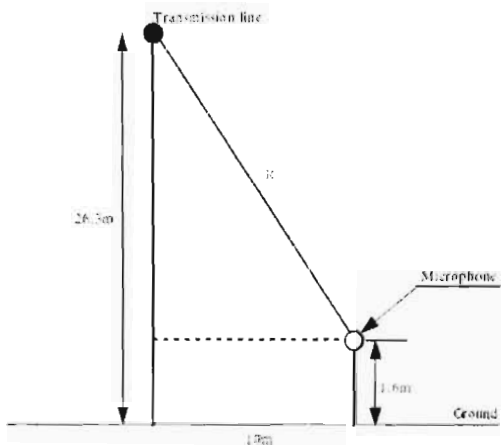


Fig. 3: Line configuration used for evaluation of correction factors.

#### 4 RESULTS AND DISCUSSION

Visual corona observations using the CoroCAM<sup>TM</sup> camera, confirmed the fundamental differences between positive and negative corona. Inception occurred at a lower voltage under negative polarity. Under positive polarity the corona was characterised by burst pulses and onset streamers, whereas under negative polarity, it was trichel pulses and glow corona (Figs 4(a) and 4(b)).

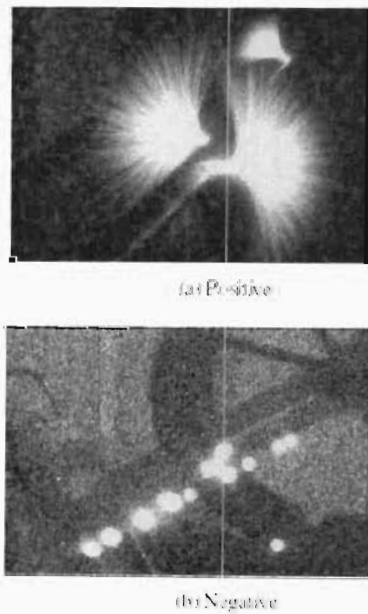


Fig. 4: Visual corona at 220kV for a 3.5cm diameter conductor

The results of the noise level measurements are shown in Figures (5) to (7). The larger conductors produced more noise for the same conductor surface gradient (Figure 5). This is similar to earlier reported findings [12], [13] and [1]. The noise levels under positive polarity are about 15dB higher compared to negative polarity for the same conductor surface gradient (Figure 6). This is in line with the observed nature of positive corona, and agrees with the results of studies carried out by EPRI [4]. This is the reason why negative polarity AN is ignored in the analysis of transmission line noise. The effect of conductor surface condition on AN is shown in Figure (7). For the 3.5 cm diameter conductor, the noise generated by the stranded conductor was about 10-30dB higher than that of the solid conductor. This is due to increased corona from additional sites of intensified electric field sites on the conductor surface. The inception gradients are 18kV/cm and 32kV/cm for the stranded and solid conductors respectively. Similar characteristics were observed under negative polarity, with regard to the effects of conductor size and surface condition.

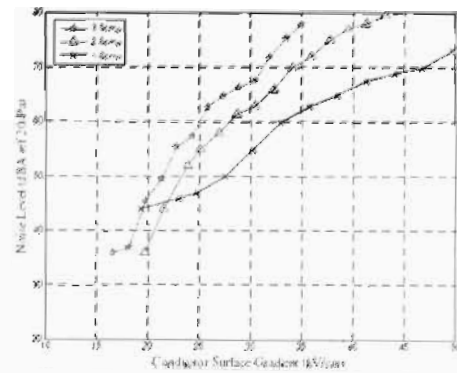


Fig. 5: Effect of conductor size on AN for positive polarity.

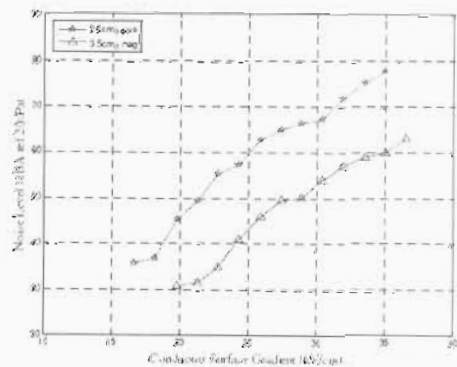


Fig. 6: Effect of polarity on AN.

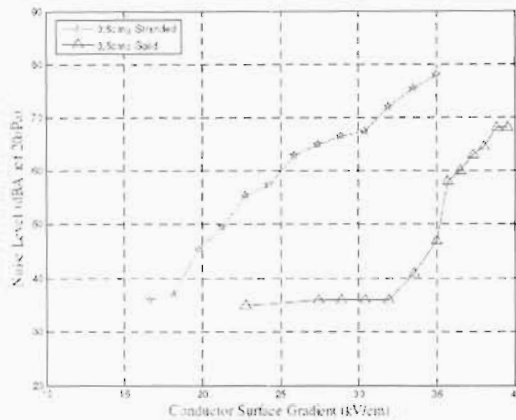


Fig. 7: Effect of conductor surface condition on AN.

Comparison of the corona cage results and the predictions from the EPRI TLW software show that for the positive polarity, the cage results were in good agreement with the EPRI predictions. The negative polarity noise levels were also in good agreement with the EPRI predictions though slightly lower (Figures 8 and 9). Furthermore, the trends of both the cage and predictions are quite similar, as indicated by the curve fitting parameters (Figure 10).

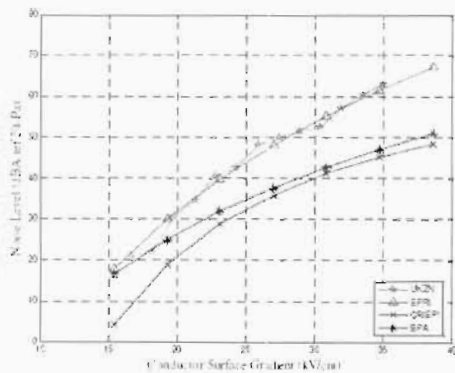


Fig. 8: Comparison of corona cage and prediction results for 2.5 cm diameter stranded conductor (Positive polarity).

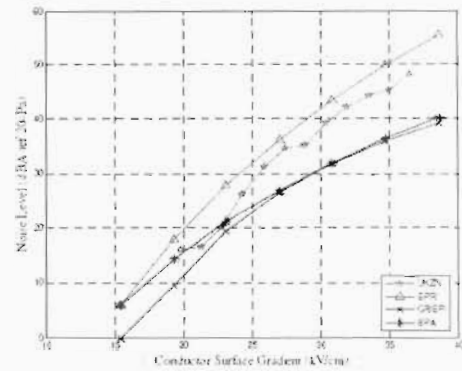


Fig. 9: Comparison of corona cage and prediction results for 3.5 cm diameter stranded conductor (Negative polarity)

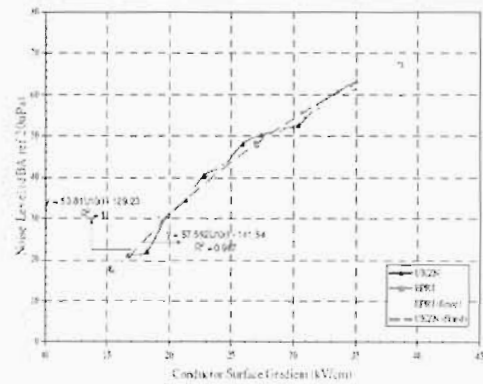


Fig. 10: Comparison of the trends for the cage results and EPRI predictions for positive polarity.

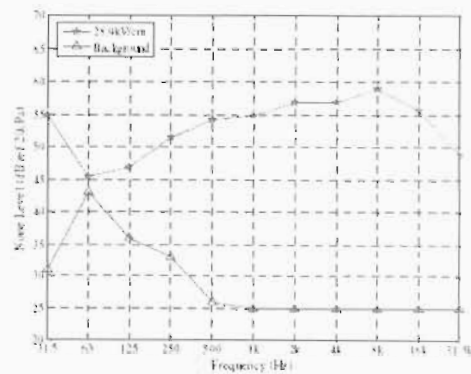


Fig. 11: Positive polarity AN frequency spectrum for 2.8 cm diameter stranded conductor.

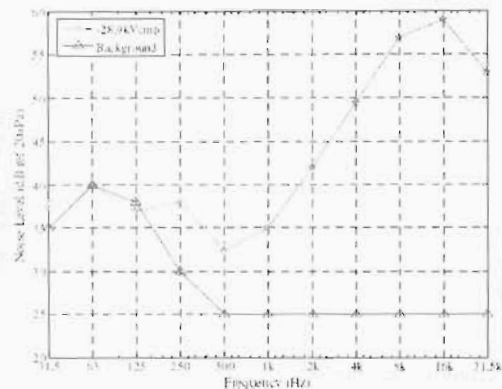


Fig. 12: Negative polarity AN frequency spectrum for 2.8 cm diameter stranded conductor.

The positive polarity frequency spectrum is fairly constant in the range of 0.5kHz to 8kHz. This is agrees with the results obtained from the Dalles DC test line [7]. Under negative polarity the noise level is more frequency dependent. The spectrum is also more affected by the background noise level for frequencies below 0.5 kHz (Figures 11 and 12).

## 5 CONCLUSION

In this paper the effects of various factors on conductor AN have been demonstrated. It has been shown that corona AN is dependent on conductor surface gradient. For both polarities, the noise levels are higher from larger stranded conductors. However, the noise levels are higher for positive polarity. The good agreement between the EPRI predictions and the corona cage results tend to suggest that the predictions can be applied in line design under low altitude conditions. This, however, needs to be verified by further work including test line measurements.

## ACKNOWLEDGMENT

Financial support from ESKOM, THRIP and the University of KwaZulu-Natal is highly appreciated.

## REFERENCES

[1] T. Pillay and S. Boshath (Editors), "The Planning, Design and Construction of Overhead Power Lines," Eskom Power Series Volume 1, 2005  
 [2] P. S. Manryala, Corona Performance of High-Voltage Transmission Lines, Research Studies Press LTD, 2000.

[3] Comber and L. E. Zafanello, "the use of single phase overhead test lines and test cages to evaluate the corona effects of EHV and UHV transmission lines", IEEE Transactions on Power Apparatus and Systems, Vol. PAS-93, Jan./Feb. 1974, pp 81-90  
 [4] G. Gela, J. J. LaForest and L. E. Zafanello, "Corona phenomena on HVDC transmission lines," HVDC Transmission Line Reference Book, EPRI TR-102764, September 1993  
 [5] IEEE Corona and Field Effects Subcommittee Report, "A survey of methods for calculating transmission line conductor surface voltage gradients", IEEE Transactions on Power Apparatus and Systems, Vol. PAS-98, No. 6, Nov./Dec. 1979, pp. 1996-2014  
 [6] L. L. Beranek, *Acoustics*, Acoustical Society of America, Cambridge, 1996.  
 [7] V. L. Chartier and R. D. Stearns, "Formulas for predicting audible noise from overhead high voltage AC and DC lines", IEEE Transactions on Power Apparatus and Systems, Vol. PAS-100, No. 1, January 1981, pp121-129  
 [8] B.Z. Engel and T. Wszolek, "Audible noise of transmission lines caused by the corona effect: analysis, modeling, prediction", ELSEVIER Applied Acoustics, Vol. 47, No. 2, 1996, pp. 149-163  
 [9] "Overall design considerations", Proceedings Power Line Electromagnetic Fields and Corona Technical Seminar, paper 193, Spokane, Washington, 1993  
 [10] H. D. E. Perry, "AN analysis of transmission line audible noise levels based upon field and three-phase test line measurements", IEEE Transactions on Power Delivery, Vol. 91, Jan.-June 1972, pp. 857-865  
 [11] G.B. Johnson, E. V. Larsen, D. J. Lorden, M. Smead, R.H. Lasseter and D.P. Hartmann, "External electrical and audible effects,"HVDC Handbook, 1st Ed., EPRI TR-1041665, 1994  
 [12] V. L. Chartier and J. W. Bankoske, "Waltz Mill 1100kV station conductor selection and laboratory verification", IEEE Transactions on Power Apparatus and Systems, Vol. PAS-88, June 1969, pp. 825-833.  
 [13] C.R.D. Dallaire, P.S. N. Rivest, "HVDC monopolar and bipolar cage studies on the corona performance of conductor bundles", IEEE Transactions on Power Apparatus and System, Vol. PAS-103, No. 1, January 1984, pp. 84-91  
 [14] A. C. Britten, V. L. Chartier, L. E. Zafanello, "Audible Noise", EPRI AC Transmission Line Reference Book - 200kV and Above, Third Edition, December 2005  
 [15] V. L. Chartier, " Empirical Expressions for Calculating High Voltage Transmission Corona Phenomena", A paper presented at the Engineering Seminar of Bonneville Power Administration's Technical Career Program for Professional Engineers, Portland, Oregon, April 7, 1983

## Appendix B-2

## A comparative study of space charge effects on corona current using an indoor corona cage and a monopolar test line

### Abstract

The effect of space charge was investigated through corona current measurements. The tests were carried out in an indoor corona cage with and without aluminium foil cover, and on a monopolar test line with a high speed fan to simulate and assess the effect of wind on the space charge. The results obtained demonstrated that the corona current in the cage and the test line is more dependent on conductor voltage and resistance of the air gap. It has also been shown that the blowing of the wind on a test line conductor and the assisted draining away of charge carriers from the corona cage gap had the effect of reducing corona current.

### 1. INTRODUCTION

Conductor corona has become a very important design factor for both HVAC and HVDC power transmission lines. It has been established, through studies, that conductor surface gradient is one of the design factors which most influences the corona performance of transmission lines [1]. The conductor surface gradient is dependent on line parameters such as conductor geometry, phase or pole disposition, as well as the conductor height above ground [2].

Increased corona activity generates high levels of audible noise, radio noise and corona loss which can be both technically and environmentally unappreciable. A factor that distinguishes d.c. fields from those of a.c. is the space charge. For a.c. lines, space charge generated is confined to a small volume immediately surrounding the conductors and, therefore, has negligible effect on the overall field distribution [3]. However, corona under d.c. fields results in accumulation of positive and negative ions in the vicinity of the conductor depending on the polarity – thus a positive conductor in corona acts as a source of positive ions and vice versa [4,5]. These ions give rise to corona current and are also responsible for electric induction effects produced on objects located in the vicinity of the lines. The distribution of space charge is very much affected by wind. Work carried out at the HVTRC reported in [6] showed that a HVDC line in corona can increase the space charge density downwind and that the small air ions are the predominant charge carriers near the HVDC line whereas aerosols become more predominant as the distance downwind increases.

If space charge is produced in large quantities, it can suppress the corona discharge. The activity resumes after the space charge is removed from the vicinity of the conductor or corona source, through drifting and recombination [7]. A similar observation was made by Sigmond and Goldman, that the space charge in monopolar coronas always tends to reduce the ionisation region field [8]. However, at much higher voltages, the electric field becomes stronger to such an extent that the space charge is unable

to reduce the field sufficiently and pre-breakdown streamers appear [9].

In order to obtain typical conductor surface gradients for corona measurements in a laboratory situation where space constraints play a major role, a corona cage or short test line can be used to replicate actual transmission line conditions. The impact of generated space charge depends on the system configuration and varies for different corona cages, test lines and polarity arrangements, hence, this study was carried out to determine the effects of space charge on different configurations. The basic aim of this study is to understand the effect of corona space charge and its potential impact on HVDC transmission line performance, through measurements in a corona cage and test line.

## II. TEST EQUIPMENT AND PROCEDURE

The tests were carried out in an indoor corona cage in the High Voltage Direct Current (HVDC) Laboratory at the University of KwaZulu-Natal (UKZN), which is situated at sea level. The cylindrical cage with a diameter of 1.50m and a length of 2m is shown in Fig. 1. The two outer sections of the cage are 0.5m in length each, and are connected directly to ground. The central part is 1m long and was grounded through a 500 ohms resistor in series with a digital micro-ammeter. The micro-ammeter was positioned in a specially made measurements cage which was placed adjacent to the corona cage. The cage was later adapted into a short indoor test line. A 500kV, two stage Walton Cockroft HVDC generator whose output is connected to a 1200M $\Omega$  resistive divider was used to supply the required voltages.

Although different stranded and solid aluminum conductors of different diameters were tested, only the results of the 3.5cm diameter conductor will be presented due to its comparatively practical surface gradients. The applied voltage was varied in 10kV/cm increments after corona inception and corona current measurements taken at each increment. The static electric field was calculated from (1) at each applied voltage.

$$E = \frac{V}{r \ln \frac{R}{r}} \text{ kV/cm} \quad (1)$$

The corona current measurements were done for positive and negative polarity DC and for AC voltages. A corona camera (CorCAM) was used to observe the corona activity under different voltage conditions at arbitrarily chosen conductor surface gradients. To assess the effect of the space charge on the measured corona current and observed corona activity, the corona cage was covered on the outside with an aluminum foil. For analysis, the measured corona current was expressed in terms of the cage length and plotted against the conductor surface gradient.

The corona cage was later converted into a test line by removing the cylindrical mesh around the conductor. The effective conductor length increased from 2m to about 2.67m. Corona current measurements were done for a 3.5cm stranded conductor under positive polarity only. A copper plate was used to facilitate current measurements at ground level. The supporting



structure was placed on wooden blocks to isolate it from the metallic plate on the floor. The thickness of the copper plate was 2 cm, its length and width were 205cm and 50cm respectively. It was connected to ground through a 560 $\Omega$  measuring resistor in series with the Fluke 187 digital micro-ammeter. The schematic diagram of the test line is shown in Fig. 2. Current measurements were done with the conductor at a height of 70cm and 37.5cm with respect to the copper plate (ground). The conductor surface gradient was calculated using (2). It can be noted that for the height of 37.5cm, the term 2H equals the radius of the corona cage R = 75cm. As a result (1) and (2) were equivalent for this particular configuration and for the height of 70cm, the air gaps in the cage and the line were almost the same. The results obtained from the test line were compared with those of the cage. Measurements at the height of 37.5cm were repeated with a high power fan directed at the conductor in order to simulate and assess the effect of wind on the generated space charge.

$$E = \frac{V}{r \ln \frac{2H}{r}} \quad (2)$$

### III. RESULTS AND DISCUSSION

Visual observations using the CoroCAM I showed that the corona discharges were less intense when the cage was covered with foil, for both DC polarities and for AC; photos will be presented in the proposed paper. Under both positive and negative polarities, the measured corona current was lower in the case when the cage was covered with foil (Fig. 3 (a) and (b)). It is to be noted that the observed difference was negligible at fields higher than 35kV/cm. This seems to be in agreement with the observation made in [9] that the effect of space charge is negligible at the higher field levels. In the case of AC, the measured current was practically the same with and without the foil (Fig. 3 (c)). This confirms observations in earlier studies about the absence of space charge effects under AC voltages due to the cancellation effect of the polarity reversals.

In the case of the test line measurements, the current was less when the fan was blowing the air away from the conductor. (Fig. 5). A comparison of the cage and test line current measurements (Fig. 4) shows that when the conductor height is almost the same as the corona cage gap, the current was slightly higher for the line. In the case when the conductor height was lower, to produce the same geometric field as in the cage, the measured current was higher for the line.

The observations made in the measurements seem to suggest a number of possibilities with regard to the effect of space charge in the corona cage and the test line. In the case of the test line, the lower current could be due the fact that there are fewer charge carriers due to the blowing away of the air from the vicinity of the conductor. In the case of the cage, the reduced current could either be due to reduced charge carriers in the gap or suppressed field by the space charge. The second possibility implies that the gap current is field dependent. However, the observed cage and test line measurements tend to suggest otherwise. For example, in the case when the geometric field is the same for the cage and the test line, the current was higher for the line.

which had a smaller gap. This tends to suggest that the corona current is dependent more on voltage and resistance of the gap. Therefore, it is possible that the foil cause faster conduction of the charge away from the gap, thus leading to lower current and reduced corona activity as observed. Further work needs to be done in this area to test out the different possibilities. For example covering the cage with an insulating foil as well as observing the time characteristics of the gap current build up.

#### IV. CONCLUSION

In this study an attempt has been made to demonstrate the effect of space charge on corona current in a corona cage and test line. It has been shown that the blowing of the wind on a test line conductor and the assisted draining away of charge carriers from the corona cage gap have the effect of reducing corona current. It has also been demonstrated that the corona activity in the cage and the test line is dependent more on the conductor voltage and the resistance of the air gap. Further work needs to be done to understand the effects of space charge in a corona cage.

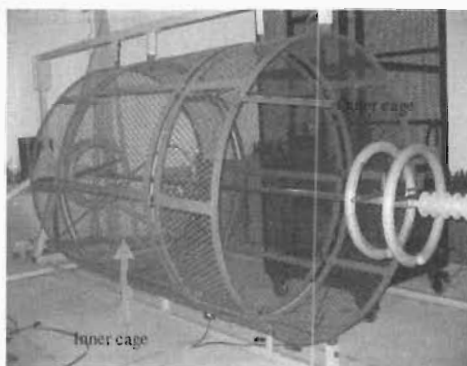


Fig. 1. Indoor corona cage

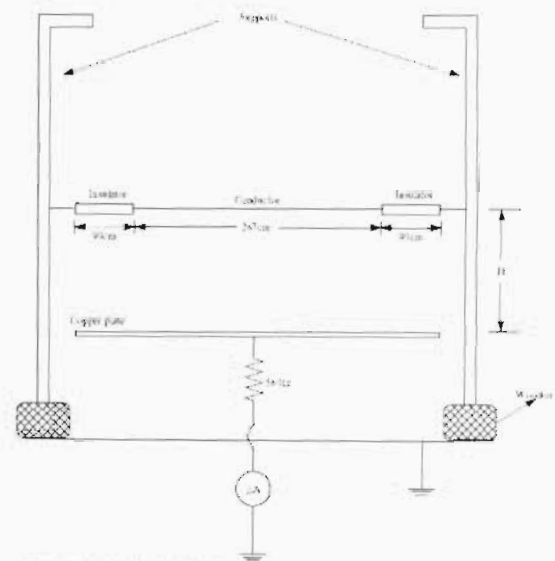


Fig. 2. Indoor test line

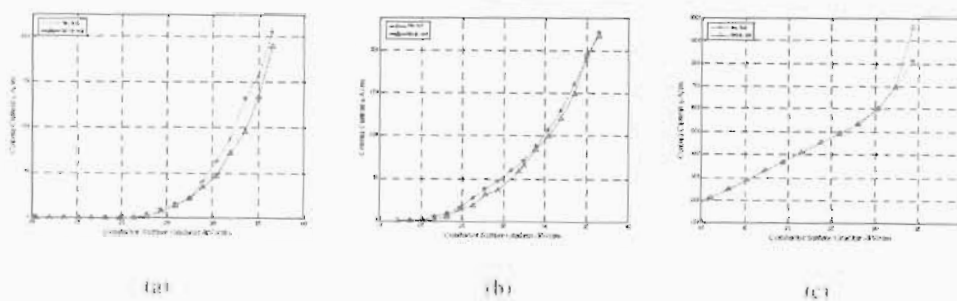


Fig. 3. Space charge effect on cage current measurements. (a) Positive polarity, (b) Negative polarity, (c) AC

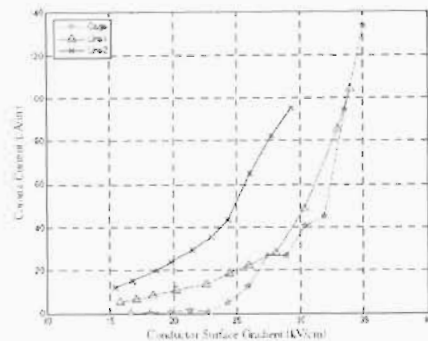


Fig. 4. Test line and cage current measurements.

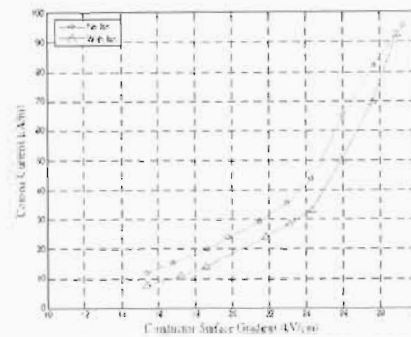
Line 1:  $h=70$ cm, Line 2:  $h=37.5$ cm

Fig. 5. Space charge effect on line current

 $h = 37.5$ cm

## REFERENCES

- [1] IEEE Corona and Field Effects Subcommittee Report, "A survey of methods for calculating transmission line conductor surface voltage gradients", IEEE Transactions on Power Apparatus and Systems, Vol. PAS-98, No. 6, Nov./Dec. 1979, pp. 1996-2014.
- [2] "Overall design considerations", Proceedings Power Line Electromagnetic Fields and Corona Technical Seminar, paper 19J, Spokane, Washington, 1993.
- [3] V. L. Chartier, "Determination of corona generated functions", Proceedings Power Line Electromagnetic Fields and Corona Technical Seminar, Spokane, Washington, 1993.
- [4] P.S. Maruvada, "Corona-generated space charge environment in the vicinity of HVDC transmission lines", IEEE transactions on Electrical Insulation, Vol. EI-17 No. 2, April 1982, pp. 125-130.
- [5] G. B. Johnson, "Degree of corona saturation for HVDC transmission lines", IEEE Transaction on Power Delivery, Vol. 5, No. 2, 1990, pp. 695-701.
- [6] P. L. Carter and G. B. Johnson, "Space charge measurements downwind from a monopolar 500kV HVDC test line", IEEE Transactions on Power Delivery, Vol. 3, No. 4, October 1988, pp. 2056-2063.
- [7] G. Gelfi, J. J. LaForest and L. E. Zaffanella, "Corona phenomena on HVDC transmission lines", HVDC Transmission Line Reference Book, EPRI TR-102764, September 1993.
- [8] L.J. Kundhardt and L. H. Luessen (editors), Electrical breakdown and discharges in gases, Plenum Press, 1982.
- [9] W. Janischewsky, "Characteristics of RI and TVI sources", Publication 76 CH1163-5-PWR pp. 12-19.

## Appendix B-3

## EVALUATION OF PREDICTION METHODS FOR HVDC CORONA GENERATED AUDIBLE NOISE USING AN INDOOR CORONA CAGE

M. J. Lekganyane<sup>1</sup>, N. M. Ijumba<sup>1</sup> and A. C. Britten<sup>2\*</sup>

<sup>1</sup>University of KwaZulu-Natal, HVDC Centre, Westville Campus, Private Bag 554001, Durban, South Africa.

<sup>2</sup>Erikon Resources and Strategy, Consulting, Research and Development, Lower Germiston Road, Eskeriville, South Africa.

**Abstract.** The paper presents a study on HVDC corona audible noise performed with an indoor corona cage at low altitude under fair weather conditions. Aluminium conductors were tested under positive DC, negative DC and AC conditions. Results obtained were analysed and compared with the EPRI, BPA and CRIEPI predictions obtained from the EPRI-TLW software. A good agreement between the UKZN cage results and the prediction method was established.

**Key Words:** audible noise, conductor surface gradient, corona cage, frequency spectrum, HVDC.

### 1. INTRODUCTION

Earlier studies have shown that corona occurrence is related to the conductor surface gradients [1, 2], which in turn, depend on system voltage and conductor geometry. Some of the effects of corona, such as audible noise, radio interference and power losses are important factors to consider in transmission line designs. Now with even much higher transmission voltages being considered for bulk power delivery over long distances, it is imperative that corona effects need to be given more attention. It is not practically possible to design a transmission line to operate with no corona discharges. However, an effort can be made to minimise the operating conductor surface gradients [3].

External environmental factors such as ambient weather conditions can also affect corona discharge characteristics in the following ways:

- temperature, pressure and relative humidity of the ambient air affects the ionisation processes,
- precipitation deposited on the conductor surface distorts the electric field in the vicinity of the conductor [1].

Airborne substances such as dead insects, dust and leaf particles stuck on the surface of the conductors, result in an increase in the conductor surface gradients [3]. Also, altitude has pronounced effects on the generation of corona [4], and it is for this reason that tests have to be carried out at both high and low altitude to determine the related effects.

Corona audible noise (AN) has become an important factor in the design of high voltage (HV) transmission lines. Exposure to high noise levels of any sort can be very annoying and can even harm the human hearing system in case of prolonged exposure. The factor that distinguishes high voltage direct current (HVDC) corona generated AN from the ambient noise, is its broadband nature with significant high frequency content that can extend

Received 15th October 2014

Under alternating current (AC) conditions, conductor surface gradients are mostly below the corona on-set gradient during dry conditions and, therefore, AN levels become a problem only during foul weather [5]. In contrast, the design challenge for HVDC transmission lines is that AN is highest under dry/fair weather conditions [6] which prevail most of the times. It was established that the number of airborne particles stuck on the conductor surface is higher in summer and increases the fair weather corona activity [3].

Negative pole noise levels are normally lower than the positive pole noise levels [1, 6, 7] and are often ignored in the analysis of audible noise measurements.

Work published on AN studies and the prediction methods used are based on measurements done in regions other than Southern Africa. A comparative analysis of some of the prediction methods is presented in [7]. Based on the factors discussed above, the applicability of the currently adopted prediction methods to the local designs needs to be ascertained. The results presented in this paper are part of the study initiated for that purpose. The main objective of the study was to:

- Measure the audible noise generated by conductor corona under HVDC.
- Compare the measured noise levels with the predictions made by the EPRI TLW-software.
- Assess the suitability of the EPRI software prediction methods in the design of transmission lines for local atmospheric conditions.

### 2. TEST EQUIPMENT AND PROCEDURE

AN measurements were carried out at the HVDC laboratory of the University of KwaZulu-Natal. The laboratory is situated in a low altitude coastal area.

A small indoor corona cage was used and only single, solid and stranded conductors of diameter 3.5cm were tested. The detailed design of the corona cage is shown in Figure 1. The DC power was obtained from a two-stage Walton-Cockroft generator whose circuit diagram is shown in Figure 2. The generator is capable of supplying +500kV and -540kV with a rated continuous current of 7.5mA. Both positive and negative polarities were considered in the tests. A digital micro-ammeter was connected between the floating middle section of the cage and ground through a 560Ω resistor as shown in Figure 1.

A Brüel&Kjær sound level meter type 2218 with a 1-inch condenser microphone was positioned

centrally to the cage at the same level as the conductor in a specially designed measurements cage. For all the measurements, the radial distance between the conductor and the microphone was 0.88m. The meter is capable of measuring noise levels from 19dB to 134dB. Supply voltage was varied in steps of 10kV and for every applied voltage, the static conductor surface gradient was calculated from equation (1) and the A-weighted noise recorded. Temperature, pressure, humidity and the background noise level were recorded for every session of the measurements. The results were arranged to demonstrate the effect of system polarity and surface conditions.

$$E = \frac{V}{r \ln \frac{R}{r}} \text{ kV/cm} \quad (1)$$

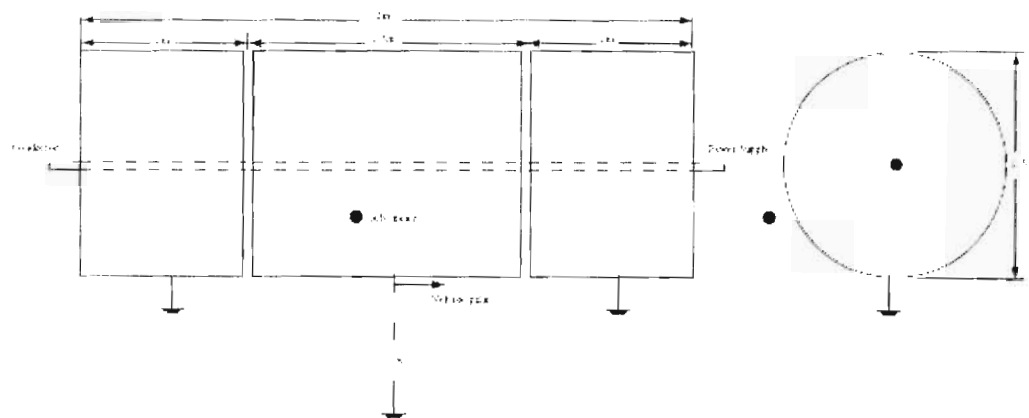


Fig. 1: Indoor corona cage

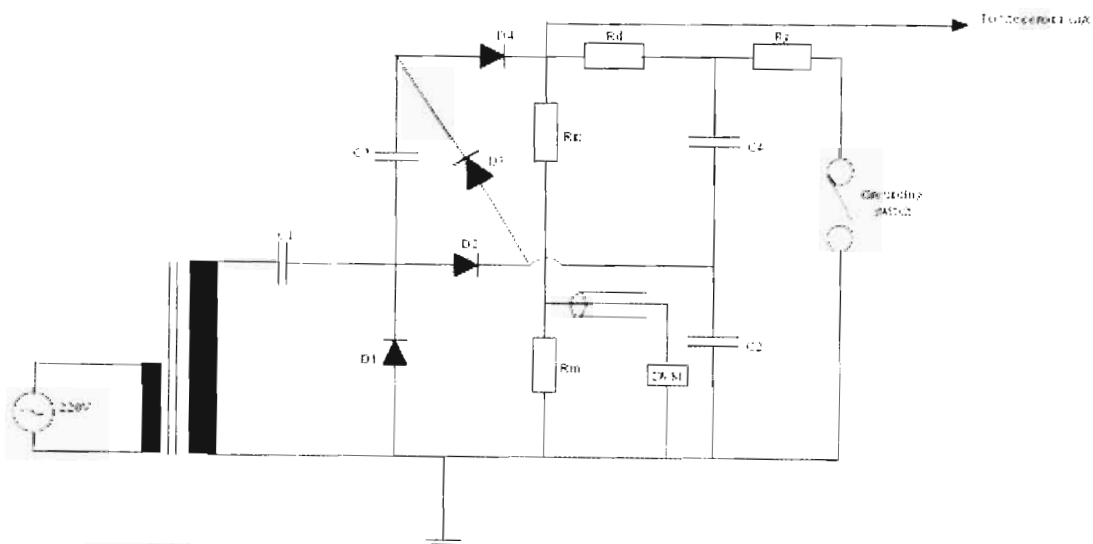


Fig. 2: Two-stage HVDC generator

The EPRI TLW software was used to analyse the results obtained from the corona cage measurements. A single conductor configuration in a typical DC transmission line was assumed for the purpose of comparison. The assumed parameters of the line and the configuration for evaluation of the correction factors are shown in Table 1 and Figure 3. This configuration was used throughout the simulations. The opposite polarity pole was placed 150m away from the energized pole to minimize the field interaction between the two poles. Simulations were run for different voltage levels and the conductor surface gradients plotted against the noise levels. Only the EPRI, BPA and CRIEPI methods were considered.

The radial distance between the microphone and the conductor for the assumed configuration and for the cage configuration are quite different. To bring the two configurations to a comparable level, the correction factors were applied to the cage results. The intensity of noise changes with the proximity to the source producing it. With transmission lines, the noise level changes by approximately 3dB for every doubling of the distance from the line [4, 8]. This implies that the sound pressure level, P is inversely proportional to  $rd$  where  $d$  is the radial distance between the transmission line and the microphone. The correction factor for the height effect was, therefore, obtained from equation (2).

$$\Delta P_r = 10 \log \frac{r}{R} \quad (2)$$

Where  $r$  is the distance to the noise meter from the conductor in the cage and  $R$  is the radial distance to the meter from the line conductor in the assumed configuration. The height correction factor for the measured levels is therefore, -14.76dB. To correct the cage results to an infinitely long line the correction factor as in [1] was adopted and is shown in equation (3).

$$\Delta P_l = 10 \log \left[ \frac{\pi}{2} \tan \left( \frac{l}{2r} \right) \right] \quad (3)$$

Where  $l$  is the length of the cage and  $r$  is the radial distance between the conductor and microphone. The length correction factor for the cage configuration is therefore, -0.71dB. The cage and simulation results were compared through curve fitting.

In order to obtain the frequency spectra of the AN, a Brüel&Kjær octave filter set type 1513 attached to the sound level meter was used. The frequency

spectrum measurements were done for arbitrarily chosen conductor surface gradients for both positive and negative polarities. The filter has centre frequency of  $f_0$  and cut-off frequencies of  $f_0/\sqrt{2}$  and  $\sqrt{2}f_0$ .

AN measurements were also repeated under AC to establish the differences between AC and DC corona AN.

Table 1: Line parameters used for the EPRI TLW software simulations

Parameter	Value
# of conductors	1
Diameter	3.5cm
Height of the conductor	26.3m
sag	16m
Altitude	0m
Microphone height	1.6m
Distance between the line and microphone	10m

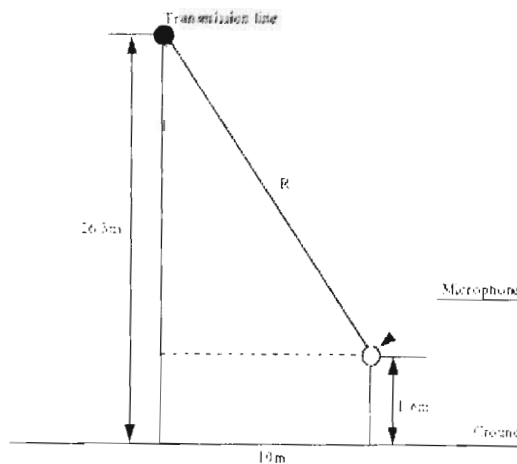


Fig. 3: Line configuration used for evaluation of correction factors.

### 3. RESULTS AND DISCUSSION

Figure 4 shows AN levels results for a solid and a stranded conductor under positive polarity. The ambient noise level was approximately 35dBA. Inception for the smooth and solid conductor is around 32kV/cm, compared to about 18kV/cm for stranded conductor. Consequently, noise levels for the solid conductor are much lower than those generated by a stranded conductor for the same surface gradient. The difference is approximately 25-30dB. This can be attributed to high surface roughness factors associated with smooth conductors. The same characteristic was observed, also under negative polarity.

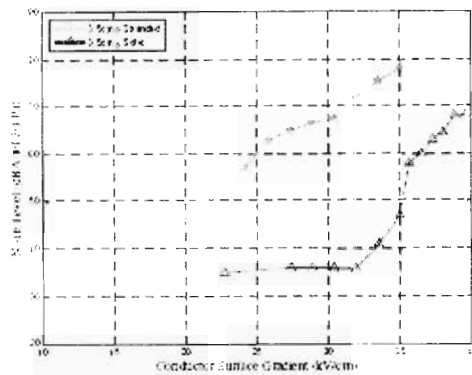


Fig. 4 Effect of conductor surface conditions on AN (positive polarity)

In Figure 5, a comparison of the noise levels generated by a 3.5cm stranded conductor under AC, positive DC and negative DC fields is made. In this case, under dry conditions, the AC and positive DC noise levels appear to have similar magnitudes for the same gradients. These would be expected to be different under foul, wet weather conditions. The negative polarity noise levels are lower than the AC and the positive polarity noise levels. This is in line with the literature that the positive pole of a bipolar produces more audible noise.

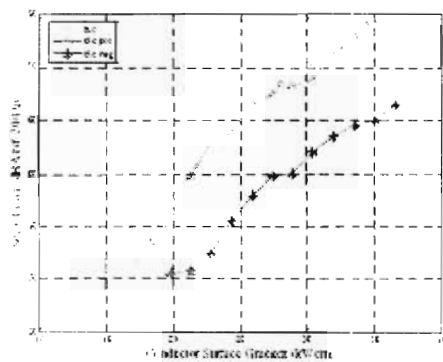


Fig. 5 Comparison of DC positive, negative and AC AN

Results obtained from the UKZN cage measurements were corrected as discussed in section 2 and compared with the software simulations. Figure 6 shows results for positive polarity. All the graphs follow a similar trend. The BPA and the CRIEPI prediction noise levels are much lower than the EPRI and the UKZN results, by about 12dB at high surface gradients. The UKZN cage results agree very well with the EPRI predictions. Comparing their trends, in Figure 7, the two graphs are purely logarithmic in nature and the equations of the fitted curves are of the same order of magnitude.

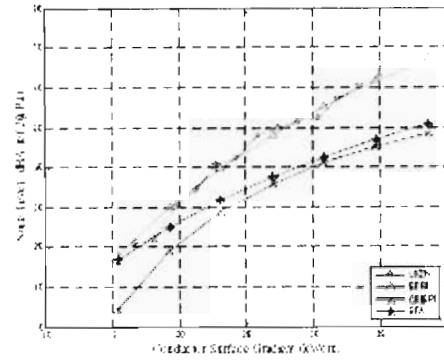


Fig. 6 Comparison of the software simulations with the cage results for positive polarity

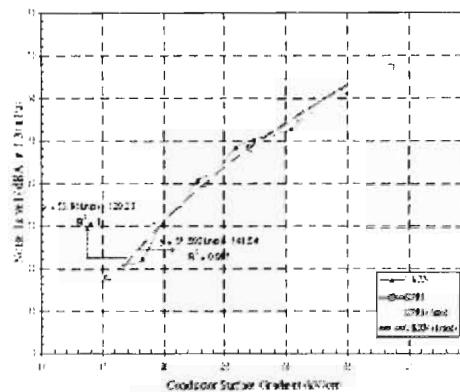


Fig. 7 Comparison between the trends of the EPRI prediction graph and the UKZN cage result- under positive polarity

The UKZN cage results under negative polarity are slightly lower than the EPRI predictions by about 3-5dB. Figure 8. The BPA and CRIEPI predictions coincide for surface gradients above 25kV/cm but both remain noticeably less than the EPRI predictions. Comparison of the trends in Figure 9, shows that the negative polarity AN is also logarithmic in nature and the equations are of the same order of magnitude as was the case with the positive polarity noise levels.

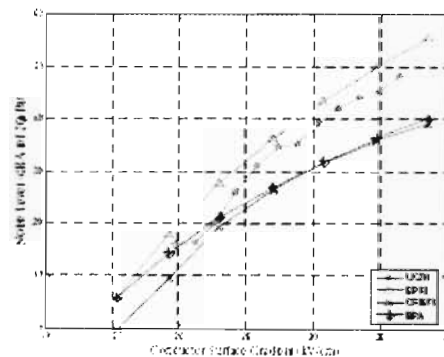


Fig. 8 Comparison of the software simulations with the cage results for negative polarity

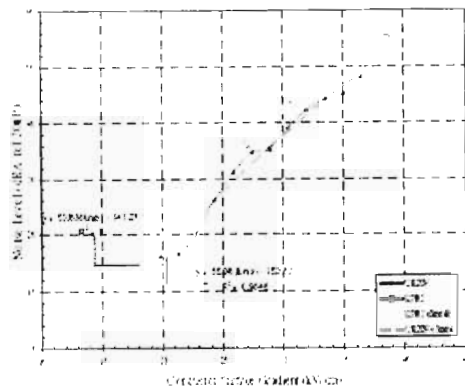


Fig. 9. Comparison between the trends of the EPRI prediction graph and the UKZN cage results under negative polarity.

It was observed from the laboratory measurements that ambient noise contributed to the lower frequencies of up to 500Hz. Positive DC AN frequency spectrum analysis is shown in Figure 10. The noise was mainly broadband and consisted of both mid- and high-frequency components. Hissing and excessive crackling sounds were observed during the tests.

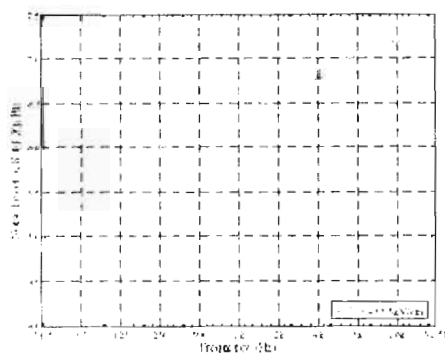


Fig. 10. Broad-band frequency spectrum for positive polarity

Negative polarity noise in Figure 11 was also broadband and mainly consisted of the high-frequency noise which was more of a hissing sound with occasional crackling. During the tests, under AC voltages, the contribution of the hum component to the noise levels was very significant. The noise consisted of the crackling, hissing and bursts of corona from time to time. High noise levels at 125Hz and 240Hz can be noticed in Figure 12, this was due to the hum component at the frequencies of multiples of the supply frequency, 50Hz, AC and positive DC noise level appeared to have a similar annoying effect.

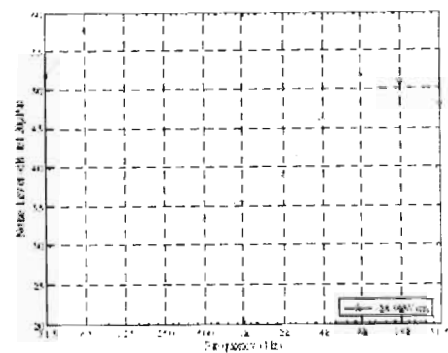


Fig. 11. Octave-band frequency spectrum for negative polarity

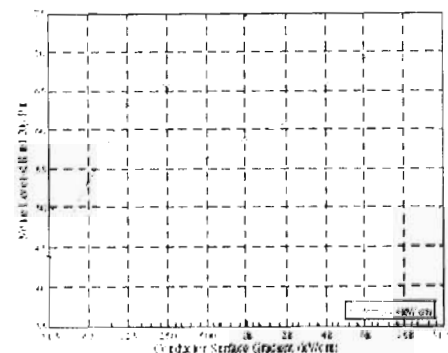


Fig. 12. Octave-band frequency spectrum for AC

#### 4. CONCLUSIONS

Corona measurements were successfully carried out using an indoor corona cage. The presented results confirm a very significant agreement between the EPRI TLW simulations and the cage measurements for dry conditions at low altitude. Solid and smooth conductors cannot represent stranded conductors in the development of prediction methods due to their apparent difference in surface conditions. Positive polarity AN consists of a wide range of frequencies and contribute mostly in DC systems. Under negative polarity, the noise levels are comparatively low and hence, never considered in transmission line design.

#### ACKNOWLEDGEMENTS

The authors would like to acknowledge THRP, Eskom and the UKZN High Voltage Direct Current Centre for their immense support on this research.

#### REFERENCES

- [1] P. S. Maruvada, Corona Performance of High-Voltage Transmission Lines, Research Studies Press LTD, 2000.
- [2] M. G. Comber, L. E. Zafanello, "The Use of Single-Phase Overhead Test Lines and Test Cages to Evaluate the Corona Effects of EHV



- and UHV Transmission Lines", *IEEE Transactions on Power Apparatus and Systems*, Vol. PAS-93, Jan./Feb. 1974.
- [3] G. Gela, J. J. LaForest and L. E. Zaffanella, "Corona phenomena on HVDC transmission lines", EPRI HVDC Transmission Line Reference Book, September 1993.
- [4] V. L. Chartier, "Empirical Expressions for Calculating High Voltage Transmission Corona Phenomena", *A paper presented at the Engineering Seminar of Bonneville Power Administration's Technical Career Program for Professional Engineers*, Portland, Oregon, April 7, 1983.
- [5] D. E. Perry, "An analysis of transmission line audible noise levels based upon field and three phase test line measurements", *IEEE Summer meeting and International Symposium of High Power Testing*, pp857-865, July 18-23, 1971.
- [6] R. D. Dalkaut, P. S. Maruvada, N. Rivest, "HVDC monopolar and bipolar cage studies on the corona performance of conductor bundles", *IEEE Transactions on Power Apparatus and Systems*, Vol. PAS-103, No. 1, January 1984.
- [7] IEEE Corona and Field Effects Subcommittee Report, "A comparison of methods of calculating audible noise of high voltage transmission lines," *IEEE Transactions on Power Apparatus and Systems*, Vol. PAS-101, No. 10, pp. 4090-4099, Oct. 1982.
- [8] A. C. Britten, V. L. Chartier, L. E. Zafanella, "Audible Noise", EPRI AC Transmission Line Reference Book – 200kV and Above, Third Edition, December 2005.

## Appendix B-4

2006 International Conference on Power System Technology

1

# Corona Audible Noise Measurements in a Small Indoor Corona Cage under HVDC Voltages

M. J. Lekganyane, *Student Member, IEEE*, N. M. Jumba, *Member, IEEE*, and A. C. Britten.

**Abstract**—Corona audible noise measurements were carried out in a small indoor corona cage under DC fields and dry conditions. The aim of the experiments was to determine possible audible noise levels under local climatic conditions. The variation between the corona audible noise and the static conductor surface gradient was investigated for stranded aluminium conductors. The results obtained were compared with the EPRI, CRIEPI and BPA predictions generated from the EPRI ACDC Line software. The results demonstrated good agreement with the predictions in terms of trends.

**Index Terms**— Audible noise; conductor surface gradient; corona cage; HVDC; space charge

## I. INTRODUCTION

Extra high voltage systems are applied widely, to ensure efficient transmission of bulk power over long distances. Due to environmental factors, high voltage transmission line design are becoming more and more compact. Also they are characterized by high field levels dependent on the operating voltages. This makes the design of the lines more complex. Selection of some of the line parameters is also dependent on external factors, in addition to engineering constraints. Earlier studies have shown that corona activity is related directly to the high levels of conductor surface gradients [1]. Apart from the conductor surface gradients, corona depends on atmospheric conditions, such as, temperature, pressure, humidity, snow, rain, fog, dust and movement of the air [2].

Corona audible noise (AN) results from acoustic pulses generated during electron collisions and other ionization processes occurring on the surface of the conductors or at the end fittings. It has a very high annoyance factor during dry conditions under DC voltages, and has become a very important design factor for high system voltages, particularly at high altitudes [3]. Therefore, it is of utmost importance to consider design parameters that will reduce corona intensity, to eliminate anticipated problems and regulatory penalties

thereof.

Different corona AN prediction methods have been developed for both ac and dc systems as presented in [4]. Details of the AN prediction methods for dc systems, based on long-term AN measurements on outdoor test lines are described in [1] and [5]. None of these methods were developed based on measurements obtained from Southern Africa or elsewhere on the continent.

In order, to obtain typical conductor surface gradients in a laboratory situation where space constraints play a major role, a corona cage was used. The corona cage does not necessarily replicate a practical transmission line. So, correction factors for the length and the height have to be applied to cage results. AN measurements obtained from an outdoor corona cage are discussed in [6].

A factor that distinguishes dc fields from those of ac is the space charge generation. In AC systems, it is swept away each time the polarity reverses. However, in DC systems, it keeps on moving to ground or opposite polarity pole [7]. The space charge is known to distort the main gap field as well as reduce conductor surface gradient [8].

The basic aim of this study is to:

- Measure the audible noise and corona current generated by conductor corona under HVDC.
- Compare the measured noise levels with the predictions made by the EPRI TLW-software
- Assess the suitability of the EPRI software prediction methods in the design of transmission lines under the South African atmospheric conditions.

## II. TEST EQUIPMENT

The tests were carried out in the corona cage of the High Voltage Direct Current (HVDC) laboratory at the University of KwaZulu-Natal (UKZN), which is situated at sea level. A 500kV, two stage Walton Cockroft HVDC generator was used to supply the required voltages.

The corona cage used for the tests is shown in Fig. 1. It is cylindrical with a diameter of 1.50m and a length of 2m. The

This work was fully supported by ERMDC, the National Research Foundation through the THRIP program and the University KwaZulu-Natal.

M. J. Lekganyane is with HVDC Centre, University of KwaZulu-Natal, Durban, South Africa (e-mail: lekiganyame@ukzn.ac.za).

N. M. Jumba is with the HVDC Centre, University of KwaZulu-Natal, Durban, South Africa (e-mail: jumban@ukzn.ac.za).

A. C. Britten is with Resources and strategy department, Eskom, Johannesburg, South Africa (e-mail: Tony.Britten@eskom.co.za).

1-4244-0111-9-06-010-00 ©2006 IEEE.

A study of HVDC transmission line audible noise and corona loss in an indoor corona cage

two outer sections of the cage are 0.5m in length each, and are connected directly to ground. The central part is 1m long, grounded through a 560 ohms resistor in series with a micro-ammeter. To assess the effect of the space charge on the measured noise and corona current, the corona cage was covered on the outside, with an aluminium foil and is shown in Fig. 2. A Sony Corocam™ was used to verify the corona inception levels.

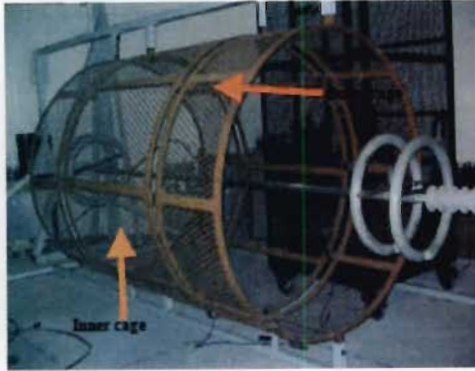


Fig. 1. Indoor corona cage.



Fig. 2. Cage covered with the foil for space charge effect assessment.

Only single aluminium stranded conductors were used for the tests. Two corona rings, each with a diameter of 50cm, were fitted at both ends of the test conductor to eliminate corona activity at the end-fittings. Fig. 3 shows a close-up view of the corona rings.

The sound intensity (A-weighted) and the corona loss currents were measured by a Rohde & Schwarz sound level meter (ELT3) and a digital micro-ammeter respectively. Both the instruments were placed in a measurements cage positioned adjacent to the corona cage (Fig. 4).

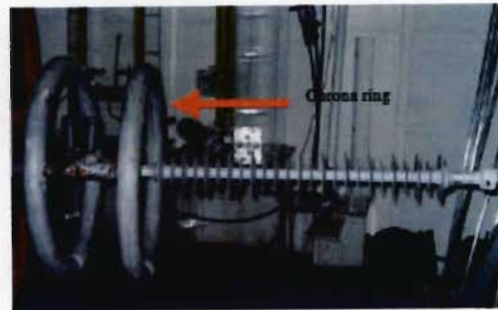


Fig. 3. Corona rings fitted at the end of the test conductor.

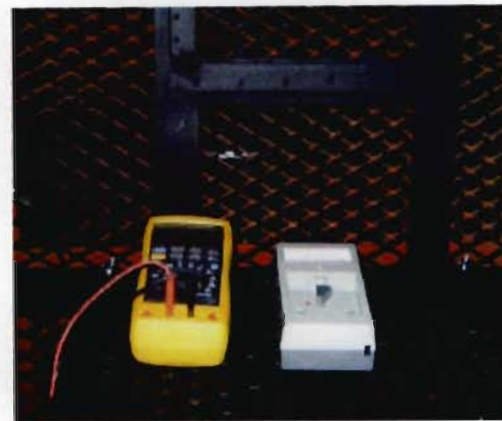


Fig. 4. Measuring instruments in the measurements cage.

### III. TESTS PROCEDURE

Stranded conductors of 1.6cm, 2.85cm and 3.5cm diameters were tested under both negative and positive polarity dc voltages. The results for 2.85cm and 3.5cm stranded conductors are presented in this paper. For each conductor, the static electric field was calculated from (1) at each applied voltage.

$$E = \frac{V}{r \ln \frac{R}{r}} \text{ kV/cm} \quad (1)$$

The current and the sound pressure level measurements were taken from the measurements cage at 0.88m from the centre of the conductor and at the same level. The corona current and the sound pressure level values were plotted against the calculated fields to obtain the trends.

The EPRI TL Workstation software was used to predict sound pressure levels for EPRI, BPA and CRIEPI empirical methods. The data shown in Table I was used as the input for

software. The voltage was varied to obtain a range of conductor surface gradients while all the other line parameters were fixed. Both the negative and the positive poles were considered in the simulations. In each case the opposite polarity pole was placed further from the pole under consideration, to effectively simulate a monopolar configuration. The 3.5cm stranded conductor results obtained at the UKZN were then compared with the EPRI TLW results. For comparison, the noise level results were corrected for the length and height of the conductor. The respective correction factors were calculated using the following expressions:

$$\Delta P_h = 10 \log \frac{r}{R} \quad (2)$$

Where  $r$  is the distance to the noise meter from the conductor in the cage and  $R$  is the radial distance to the meter from the line conductor.

$$\Delta P_l = 10 \log \left( \frac{\pi}{2} \tan^{-1} \left( \frac{l}{2r} \right) \right) \quad (3)$$

Where  $l$  is the length of the cage [6].

Curve fitting was performed for the purpose of comparing the trends in the measured and predicted values.

TABLE I  
VALUES OF THE LINE PARAMETERS USED FOR THE EPRI TLW SOFTWARE

Parameter	Value
# of conductors	1
Diameter	3.5cm
Height of the conductor	26.3m
sag	16m
Alnode	0m
Microphone height	1.6m
Distance between the line and microphone	10m

Temperature, pressure, humidity and the background sound pressure level were recorded for each set of measurements and the relative air density  $\delta$  calculated. In order to demonstrate the effect of the space charge, the corona cage was covered with aluminum foil and the corona current measured for the 3.5cm diameter conductor for both positive and negative polarity. The corocam was used to observe corona inception. The calculated corona inception field was then used to estimate the conductor surface roughness using Peek's formulae (4) and (5).

$$E_{c+} = 33.7m\delta \left( 1 + \frac{0.24}{\sqrt{r\delta}} \right) kV/cm \quad (4)$$

$$E_{c-} = 30m\delta \left( 1 + \frac{0.30}{\sqrt{r\delta}} \right) kV/cm \quad (5)$$

#### IV. RESULTS AND DISCUSSION

The results of the measured sound pressure levels are shown in Fig. 5. The background noise was in the region of 35-38dBA. It can be seen that the larger diameter conductor generates high audible noise than the smaller conductor for the same field. In terms of polarity, the positive polarity resulted in more noise for both conductors. This may be as a result of the intense discharge activity around the positive conductor due to the presence of electrons in the high field region [1]. The observed effect is in agreement with earlier reports that the main source of the audible noise is the positive pole [5] and [9]. As the noise level increases with the conductor surface gradient, for fields beyond 45kV/cm there seems to be some saturation in the noise levels.

Fig. 6 shows the corona currents measured under both positive and negative polarities. In both cases the larger diameter conductor generated more corona current for a given surface gradient as with the audible noise. Analyzing the negative and the positive polarity currents, inception is delayed for positive as opposed to negative.

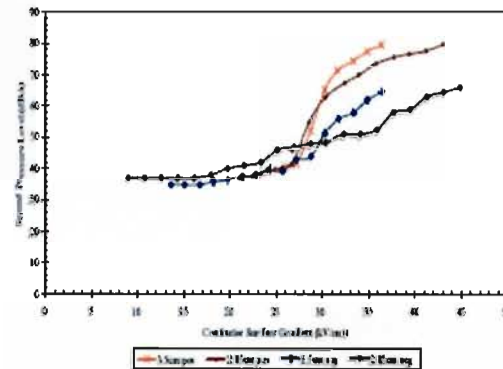


Fig. 5. Variation of the sound pressure levels with the conductor surface gradients for both positive and negative polarity.

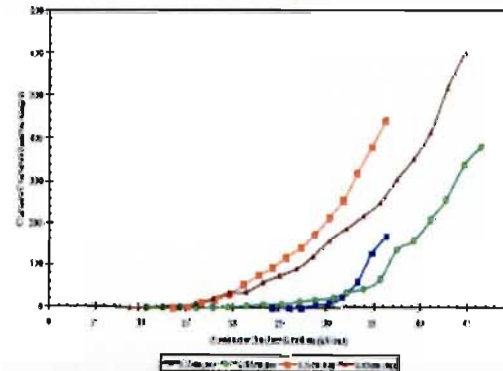


Fig. 6. Measured corona currents for both positive and negative polarity.

The observed differences in the currents and intensity of



corona discharge under negative and positive polarity can be attributed to space charge effects. The reduced currents levels under positive polarity are due to the suppression effect of the space charge.

In Fig. 7 and Fig. 8, a comparison is made of the experimental results and simulations obtained with the EPRI TLW software for positive and negative polarity respectively. There appears to be good agreement between the experimental results and the predictions. The curve fitting equations show that the predicted curves and the experimental results are of a logarithmic trend.  $R^2$  shows how close the fitted graph is to the actual graph. Its value lies between 0 and 1, with 0 being the worst fit and 1 being the perfect fit. The experimental results are higher but closer to the EPRI prediction curve compared to the BPA and the CRIEPI curves.

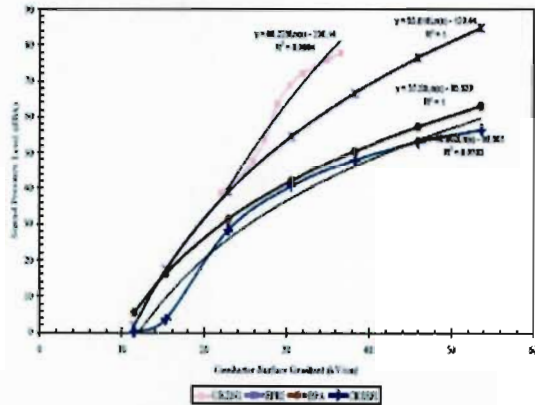


Fig. 7. Comparison of the UKZN audible noise results with the software simulations for positive polarity.

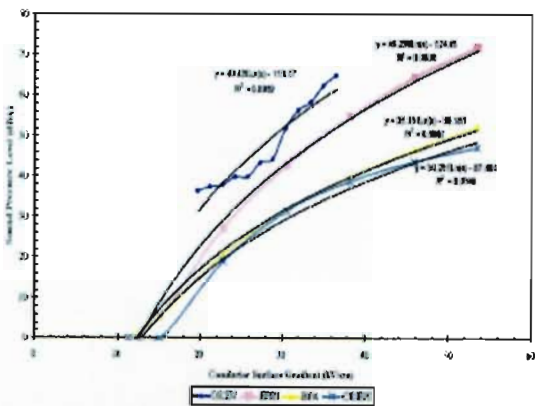


Fig. 8. Comparison of the UKZN audible noise results with the software simulations for negative polarity.

When the cage was covered with foil, there was no change with the measure noise levels. However, there were slight

differences with the measured corona current. Under positive polarity, (Fig 9) the currents were slightly lower at low fields when the cage was uncovered. As the surface gradient increased the two graphs tend to merge. This could be that the space charge under positive polarity is so high that covering the cage with foil does not have a noticeable impact. The corona discharge pictures shown Fig. 10-11, captured at 200kV corresponding to a field of 30.4kV/cm, show that the corona activity was more intense when the cage was not covered.

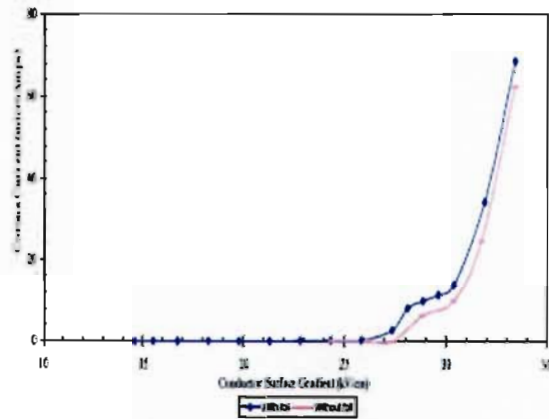


Fig. 9. Space charge assessment under positive polarity.



Fig. 10. Corona activity observed under positive polarity when the cage was covered with foil.



Fig. 11. Corona activity observed under positive polarity when the cage was not covered with the foil.

The use of the foil seemed to be successfully trapping the space charge under negative polarity for surface gradients of

up to 35kV/cm beyond which the two graphs merge. This is shown in Fig. 12. With the cage covered, the currents were slightly lower compared to the case where it was not covered. Comparing Fig. 9 and Fig. 12, the corona current is generally high for negative polarity.

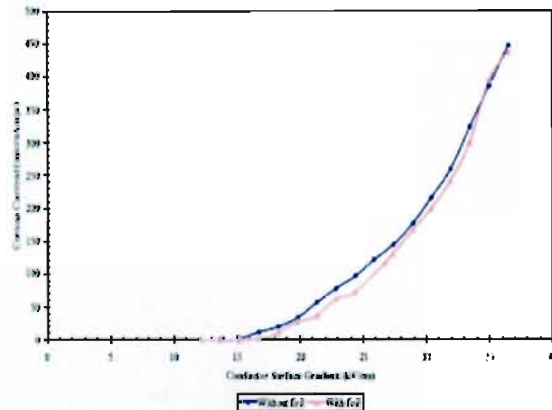


Fig. 12. Space charge assessment under negative polarity.

The inception voltages observed with a Corocam™ and the corresponding surface gradients for both the conductors, under positive and negative polarity are shown in Table II. As it was seen from the current graphs above, the inception field is lower for positive polarity. The calculated surface roughness factors ( $m$ ) show that the two conductors were of a roughness of about 0.6, which is low.

TABLE II  
CALCULATED VALUES OF THE CONDUCTOR SURFACE ROUGHNESS

Polarity	$d$ (cm)	$U_i$ (kV)	$E_i$ (kV/cm)	$\delta$	$m$
Pos	3.5	140	21.3	0.96	0.56
Pos	2.85	125	22.1	0.97	0.57
Neg	3.5	125	19.0	0.95	0.54
Neg	2.85	120	21.3	0.95	0.59

## V. CONCLUSION

Throughout the study, the corona audible noise and corona current increased with conductor surface gradient under both positive and negative polarity. Under positive polarity, the corona discharge activity was more intense but measured currents low. The effect of the space charge appeared to be more effective in suppressing the field under negative polarity. The results obtained also show that for the audible noise, there was good agreement between the corona cage measurements and the predictions based on the test line data especially the EPRI ones. The higher noise levels obtained can be attributed to the conductor roughness and comparatively high field levels in the cage.

## VI. REFERENCES

- [1] P S Maruvada, Corona Performance of High-Voltage Transmission Lines, Research Studies Press LTD, 2000.
- [2] R Arora and W Mosch, High Voltage Insulation Engineering, Wiley Eastern Limited, 1995. E. H. Miller, "A note on reflector arrays," *IEEE Trans. Antennas Propagat.*, to be published.
- [3] T Pilley and S Bisnath (Editors), "The Planning, Design and Construction of Overhead Power Lines," Eskom Power Series Volume 1, 2005.
- [4] IEEE Corona and Field Effects Subcommittee Report, A comparison of methods of calculating audible noise of high voltage transmission lines," *IEEE Transactions on Power Apparatus and Systems*, Vol. PAS-101, No. 10, Oct. 1982, pp. 4090-4099.
- [5] G. Gela, J. J. LaForest and L. E. Zaffanello, "Corona phenomena on HVDC transmission lines," HVDC Transmission Line Reference Book, EPRI TR-102764, September 1993.
- [6] Y Nakano and Y Sunaga, "Availability of Corona Cage for predicting Audible Noise generated from HVDC Transmission Line," *IEEE Transactions in Power Delivery*, Vol. 4, No. 2, April 1989, pp. 1422-1431.
- [7] P. S. Maruvada, "Methods of calculating corona loss," Notes from IEEE PES special course on corona effects of AC and DC High Voltage transmission lines, presented July 14-20, 1981 at Portland.
- [8] V. Jaiswal and M. J Thomas, "Finite element modeling of ionized field quantities around a monopolar HVDC transmission line," *Journal of Physics D: Applied Physics* 36, 2003, pp. 3039-3094.
- [9] G.B. Johnson, E. V. Larsen, D. J. Lorden, M. Smead, R.H. Lasseter and D.P. Hartmann, "External electrical and audible effects," HVDC Handbook, 1<sup>st</sup> Ed., EPRI TR-1041665, 1994.



Mokwape J. Lekganyane graduated with a BSc degree in Electrical Engineering from the University of KwaZulu-Natal where she is currently completing her MSc degree at the HVDC Centre. She is a registered candidate engineer with the Engineering Council of South Africa (ECSA) and a student member of the IEEE and the SAIEE. She is also a member of the Golden Key International Honour Society. Her research interests are in the areas of high voltage.



Nelson M. Ijumba graduated from the University of Dar es Salaam, Tanzania, with first class honours degree in Electrical Engineering. He obtained his masters and doctorate degrees in Electrical Engineering from the universities of Salford and Strathclyde, in the UK, respectively. Currently he is the Dean of Engineering at the University of KwaZulu-Natal and also the Coordinator of the High Voltage Direct Current (HVDC) Centre. Professor Ijumba is a member of the IEE, IEEE, and a registered professional engineer in UK, South Africa, Kenya and Tanzania. His research interests are in HVDC, high voltage insulation and power systems technologies.



Anthony C. Britten is Eskom's Corporate Consultant in High Voltage Engineering. He is a registered Professional Engineer in SA, and is a Fellow of the S.A. Institute of Electrical Engineers. He is active in the disciplines of EMC, power systems, external insulation, insulation co-ordination and corona effects on AC and DC overhead power lines. He recently co-authored a chapter on Audible Noise in the Revised EPRI Red Book. He also served as co-editor and co-author for two books in the Eskom Power Series titled "The Planning, Design and Construction of Overhead Power Lines" and "The Fundamentals and Practice of Overhead Line Maintenance".



## The Effect of Conductor Surface Gradient on Corona Generated Audible Noise Under HVDC

M J Lekganyane, N M Ijumba and A C Britten\*

HVDC Centre

University of KwaZulu-Natal

\*Eskom (Resources and Strategy)

Email: [lekganyanem@ukzn.ac.za](mailto:lekganyanem@ukzn.ac.za)

**Abstract.** The relationship between corona audible noise generated by HVDC conductor surface gradients, was investigated under local climatic conditions at sea level. The measurements were done under dry conditions in a small cylindrical corona cage. The sound pressure levels were measured as a function of the calculated conductor surface gradient. Both solid and stranded conductors were considered. The results obtained are compared with the BPA, CRIEPI and EPRI predictions, which were derived from test line data. The experimental results have demonstrated good agreement with the predictions.

**Key Words:** Corona audible noise, conductor surface gradient, corona cage, HVDC

### 1. INTRODUCTION

Corona is the partial breakdown or ionisation of the air in vicinity of the conductors and fittings energized at high AC and DC voltages. It occurs in non-uniform electric fields. Practical transmission line configurations always constitute non-uniform fields and are, therefore, prone to corona. The processes that characterise corona activity are electron collisions, attachment, detachment and recombination [1].

Earlier studies have shown that corona activity is related directly to the high levels of conductor surface gradients [2]. Corona audible noise (AN) results from acoustic pulses generated during electron collisions and other ionization processes occurring on the surface of the conductors or at the end fittings. It has a very high annoyance factor during dry conditions under DC voltages, and has become a very important design factor for system voltages of 400kV and above, particularly at altitudes exceeding 1000m [1]. For example, in South Africa, the 765kV AC lines are

considered equivalent to 1000kV lines from the corona point of view [3].

Conductor corona tests for practical transmission line fields at low voltages, are mainly carried out in a corona cage. Details of the laboratory model of a corona cage are shown in Figure 1.

Corona produces space charge which, in AC systems, is swept away each time the polarity reverses. However, in DC systems, it keeps on moving to ground or opposite polarity pole [2]. The space charge is known to distort the main gap field as well as reduce conductor surface gradient [4].

Apart from the conductor surface gradients, corona also depends on weather conditions, such as, temperature, pressure, humidity, snow, rain, fog, dust and movement of the air [5].

There has not been many reported corona problems with regards to the currently operating DC lines. However, with much higher transmission voltages now being considered, extra care needs

to be taken, in the design stage, when selecting line parameters.

Extensive corona AN tests have been carried out in other regions, and from these, empirical equations for predicting audible noise have been developed. Most of the tests were done on outdoor test lines. Details of the different methods of predicting AN are described in [2], [4] and [3]. The results based on cage measurements done at CRIEPI are discussed in [6].

The basic aim of this study is to:

- Measure the audible noise and corona losses generated by conductor corona under HVDC.
- Compare the measured noise levels with the predictions made by the EPRI TLW-software.
- Assess the suitability of the EPRI prediction methods in the design of transmission lines under the South African atmospheric conditions.

## 2. TEST FACILITIES

The tests were carried out in the corona cage of the High Voltage Direct Current laboratory at the University of KwaZulu-Natal (UKZN), which is situated at sea level. A 500kV, two stage Walton Cockroft HVDC generator was used to supply the required voltage.

The test set-up is as shown in Figure 1. The cage is cylindrical with a diameter of 1.50m. It has two grounded outer sections of 0.5m length on each side of the central part which is 1.5m long. The central part is grounded through a 560 ohms resistor in series with a microammeter. The total length of the cage is 2m.

Two corona rings were fitted at each end of the test conductor to ensure that only the noise from the conductor was measured. Each ring has a diameter of 50cm. Figure 2 shows a close-up view of

the corona rings. Only single conductors were used for the tests, and they were either smooth solid aluminium or stranded.

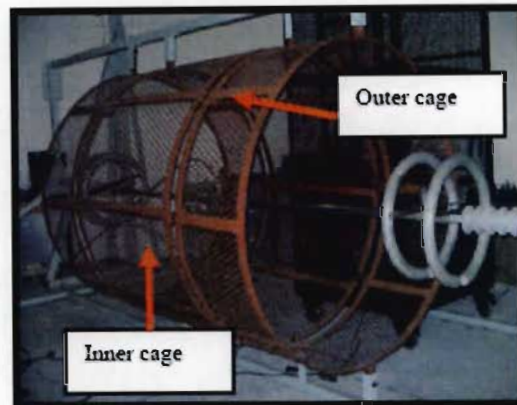


Figure 1: The test set-up

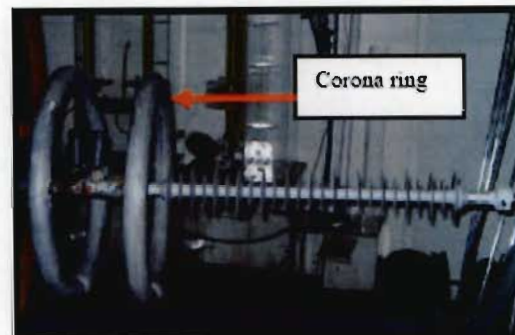


Figure 2: Corona rings fitted at the end of the test conductor

To assess the effect of the space charge on the measured noise and corona current, the corona cage was covered with an aluminium foil as shown in Figure 3. For this study, only the 3.5cm smooth solid conductor was considered. Similar tests for a stranded conductor will be carried out and the results reported in the subsequent publications.



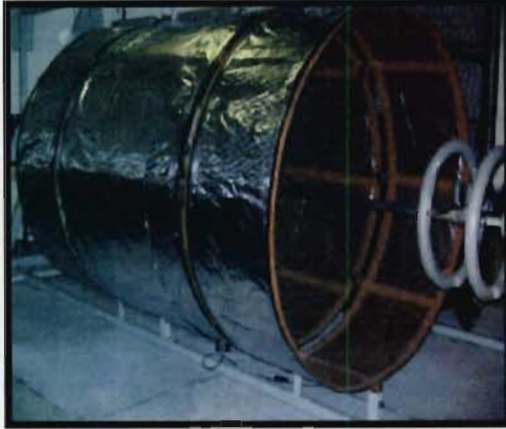


Figure 3: The cage covered with foil for space charge assessment.

The sound intensity (A-weighted) and the corona loss currents were measured by a Rohde & Schwarz sound level meter (ELT3) and a digital microammeter respectively. Both the instruments were placed in a measurements cage placed adjacent to the corona cage (Figure 4).

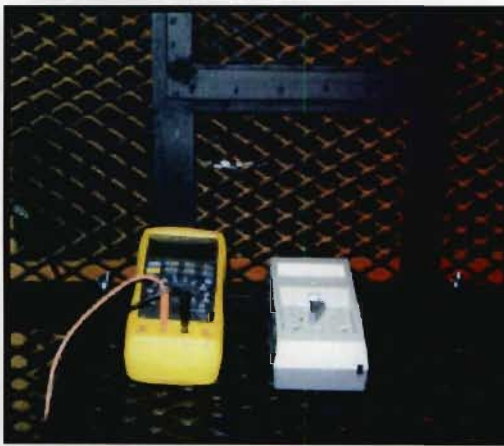


Figure 4: The measuring instruments in the measurements cage.

### 3. EXPERIMENTAL PROCEDURE

Smooth solid conductors of 1.6cm, 2.8cm and 3.5cm diameters as well as stranded conductors of diameters 1.4cm and 2.8cm were considered for the tests.

Both positive and negative polarity DC voltages were used. For each conductor, the static electric field was calculated at each applied voltage using the equation:

$$E = \frac{V}{r \ln \frac{R}{r}} \text{ kV/cm} \quad (1)$$

Using Peek's formula (2) and (3) for positive and negative conductor corona respectively, the corona inception fields for the conductors were estimated as indicated in Table 1. The inception gradient was calculated using the roughness factor  $m$  of 0.9 for solid conductors and 0.7 for stranded conductors. Temperature, pressure, humidity and the background sound pressure level were recorded for each set of measurements and the relative air density  $\delta$  calculated.

$$E_{c+} = 33.7m\delta \left( 1 + \frac{0.24}{\sqrt{r\delta}} \right) \text{ kV/cm} \quad (2)$$

$$E_{c-} = 31.0m\delta \left( 1 + \frac{0.308}{\sqrt{r\delta}} \right) \text{ kV/cm} \quad (3)$$

Table 1: Estimated corona inception gradient for smooth conductors

Conductor Diameter (cm)	Inception Gradient (kV/cm)	Inception Gradient (kV/cm)
	Positive	Negative
1.6	37.4	36.5
2.8	35.4	34.2
3.5	34.8	33.4

Table 2: Estimated corona inception gradient for stranded conductors

Conductor Diameter (cm)	Inception Gradient (kV/cm)	Inception Gradient (kV/cm)
	Positive	Negative
1.4	29.5	28.9
2.8	27.5	26.6

The current and the sound pressure level measurements were taken from the measurements cage at 0.88m from the centre of the conductor and at the same level.

The EPRI TL Workstation software was used to predict sound pressure levels for EPRI, BPA and CRIEPI empirical methods. The Cahora Bassa line configuration data was used as the input except for a single 2.8cm conductor was used. Both the negative and the positive poles were considered. In each case the opposite polarity pole was placed further from the pole under consideration. The measuring point was set at a distance of 10m and a height of 1.6m. The 2.8cm stranded conductor results obtained at the UKZN were compared with the EPRI TLW results

#### 4. RESULTS AND DISCUSSION

Figure 4 shows a comparison between the sound pressure levels measured for the stranded and smooth conductors under positive polarity. The graphs for the smooth conductors have very steep slopes and show corona inception and saturation levels clearly. The characteristics for the stranded conductors show a gradual increase of sound pressure level with electric field and there are no signs of saturation. Through curve-

fitting it is shown that the trends of the stranded conductor graphs are logarithmic.

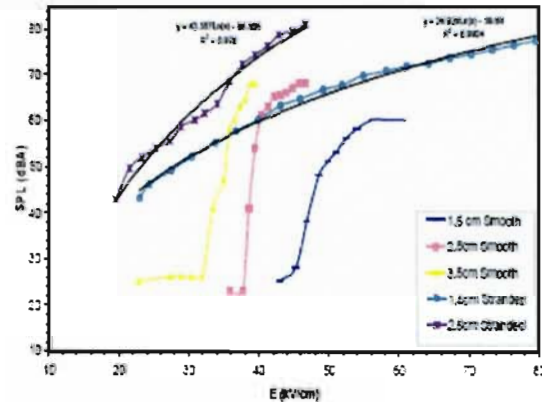


Figure 4: Variation of the measured sound pressure levels (SPL) with the surface gradient (E) for smooth and stranded conductors (positive polarity).

The measured sound pressure levels for stranded conductors match the predicted levels very closely compared to the smooth conductors. This was observed for both positive polarity and negative polarity. In both cases, the curve fitting parameters are of the same order of magnitude (Figures 5 and 6).

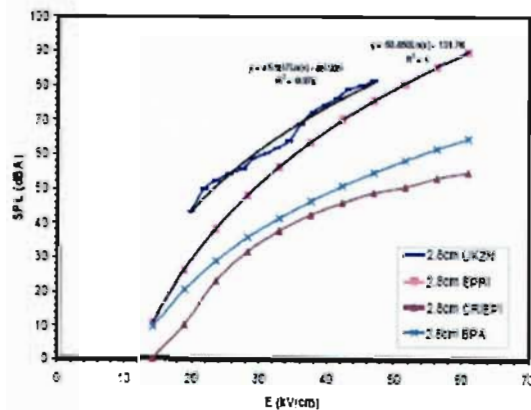


Figure 5: Comparison of the measured sound pressure levels (SPL) and the EPRI TLW predictions (positive polarity).

The measured noise levels were higher for positive polarity. There was good agreement



between the trends of the EPRI prediction curve and the experimental results.

In Figure 6, a comparison is made of the experimental results and simulations obtained with the EPRI TLW software for negative polarity. Again, there appears to be good agreement between the experimental results and the predictions. The graphs obtained at the UKZN (both clean and unclean conductor) are closer to the predicted EPRI graph. As expected, the clean conductor produced less noise compared to the unclean one. The measured noise levels at negative polarity were lower than at positive polarity.

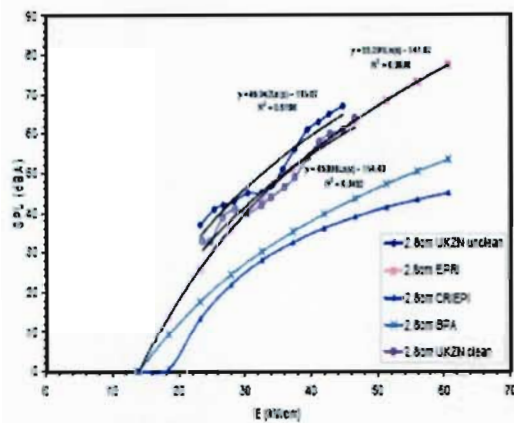


Figure 6: Measured sound pressure levels (SPL) and the EPRI TLW predictions (negative polarity).

Under both positive and negative polarity conditions, stranded conductors produced more corona current than the smooth conductors. It was also observed that, for a given conductor surface gradient the larger diameter conductors produce more corona current than the smaller ones. The reason could be that a larger conductor provides more surface area for generation of longer streamers. Figure 7 shows the results obtained with positive polarity. Unlike with the sound pressure levels, the corona current follows the same pattern for both the smooth and stranded conductors.

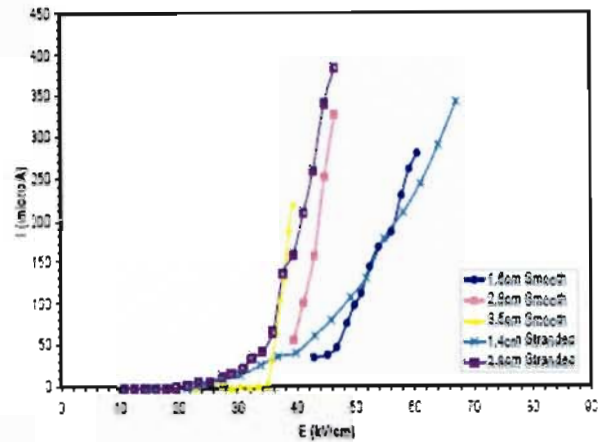


Figure 7: Corona current for smooth and stranded conductors obtained from the UKZN measurements (positive polarity).

When the corona cage was covered with aluminium foil, sound pressure levels did not appear to be affected much by the space charge presence. This was the case for both positive and negative polarity. However, the space charge appears to have an impact on the corona current levels. From Figures 8 and 9, it can be seen that the space charge trapped within the cage by the aluminium foil was effective in reducing the corona current through "field choking".

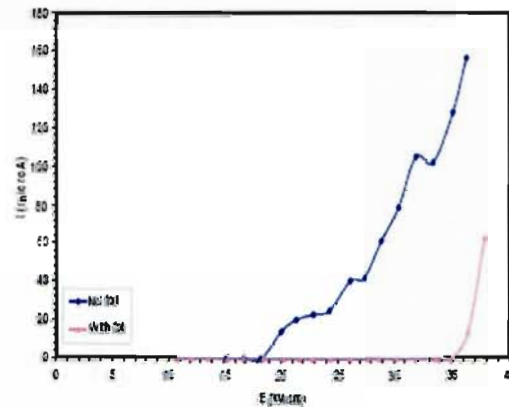


Figure 8: Space charge effect for 3.5cm diameter smooth conductor (positive polarity).

The suppression of the field, and hence reduction in current, was more pronounced under positive polarity (Figure 8). This can

be attributed to the fact that the space charge field under positive polarity is higher, and hence more effective in suppressing the field as compared to the case of negative polarity. This could also be a possible explanation for the observed large corona current measured under negative polarity (Figure 9)

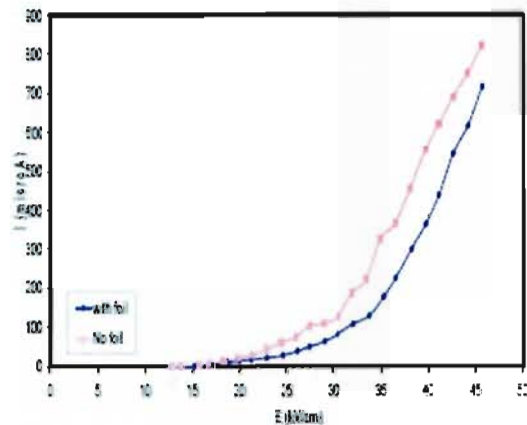


Figure 9: Space charge effect for 3.5cm diameter smooth conductor (negative polarity).

## 5. CONCLUSIONS

Throughout the study, the corona audible noise and corona current increased with conductor surface gradient for all the conditions. The biggest challenge is to minimise the operational conductor surface gradients during the design stage of the transmission lines. The results obtained so far for the audible noise, show encouraging agreement between the cage predictions and the predictions based on the test line data. Cage tests under HVDC appear to be valid, at least for audible noise.

## ACKNOWLEDGEMENT

The authors would like to acknowledge THRIP and Eskom for funding this research and the UKZN High Voltage Direct Current Centre, for the test facilities.

## REFERENCES

- [1] T Pillay and S Bisnath (Editors), "The Planning, Design and Construction of Overhead Power Lines", Eskom Power Series Volume 1, 2005.
- [2] P S Maruvada, Corona Performance of High-Voltage Transmission Lines, Research Studies Press LTD, 2000.
- [3] EPRI AC Transmission Line Reference Book-200kV and above, 3<sup>rd</sup> Edition, 2005.
- [4] HVDC Transmission Line Reference Book, EPRI TR-102764, September 1993.
- [5] R Arora and W Mosch, High Voltage Insulation Engineering, Wiley Eastern Limited, 1995.
- [6] Y Nakano and Y Sunaga, 'Availability of Corona Cage for predicting Audible Noise generated from HVDC Transmission Line', IEEE Transactions in Power Delivery, Vol. 4, No. 2, pp. 1422-1431, April 1989.

## Appendix B-6

SAUPEC 2006

## THE DEPENDENCE OF CORONA AUDIBLE NOISE ON CONDUCTOR SURFACE GRADIENT

M J Lekganyane\*, N M Ijumba\* and A C Britten\*\*

\*University of KwaZulu-Natal, HVDC Centre, Wazville Campus.

\*\*ESKOM, CR&D, Rocherville

**Abstract.** The relationship between the corona audible noise and the conductor surface gradient is investigated under local climatic conditions. The measurements were done under HVDC conditions using a small cylindrical corona cage. The conductor surface gradients were computed and the sound pressure levels were measured for different voltage levels. The results are discussed and compared with the BPA, CRIEPI and EPRI predictions. Corresponding values obtained from the corona cage were generally higher, mainly due to the comparatively high field levels at which they were obtained. However the dependence of sound pressure levels on the electric field was similar to the results reported earlier.

**Key Words.** Corona audible noise, conductor surface gradient, corona cage

### 1. INTRODUCTION

Corona is the partial breakdown or ionisation of the air in the vicinity of the conductors and fittings when energized at high voltages, both AC and DC. It occurs in non-uniform electric fields. Practical transmission line configurations always constitute non-uniform fields and are therefore prone to corona. The processes that characterise corona activity are collisions, attachment, detachment and recombination. It can be in a positive or a negative mode [1].

Conductor corona is responsible for audible noise from the transmission lines, the radiated and conducted radio noise, ozone generation, and additional system power losses. Audible noise (AN) results from acoustic pulses generated during collisions and other ionization processes occurring on the surface of the conductors or end fittings. It has become a very important design factor for voltages of 400kV and above. It is important for the utilities to set and achieve standards for corona AN limits depending on the country's regulations. AN has a very high annoyance factor during dry conditions for DC voltages.

The conductor surface gradient depends on the applied voltage, the geometry of the system and the presence of space charge. The corona cage is designed with a grounded wire mesh surrounding the conductor's under tests. This enables the practical fields of transmission lines to be achievable with the use of lower voltage supplies. In ac systems, the space charge is swept away each time the polarity reverses. In DC systems the space charge keeps on moving to the ground or conductors of opposite polarity [1]. It distorts the gap field thus affecting the measured values.

Corona AN tests have been carried out in other regions and equations for predicting the corona

noise sound pressure levels have also been developed. Details of the different methods of predicting AN are described in [1], [2] and [3]. The generation of AN depends on factors such as the applied voltage, conductor surface gradient, bundle radius, conductor surface conditions, local climatic conditions and altitude. Altitudes above 1000m are significant for AN line design [4]. It is also stated in [5] that the radio noise and audible noise from HVDC lines decrease with increasing relative air density.

The ultimate aim of this study is to find the audible noise prediction methods, which are applicable to the local climate conditions. These methods will then be used to predict possible AN levels in the design of new transmission lines.

### 2. TEST FACILITIES

The test set-up is shown in Figure 1. A small laboratory corona cage was used for the tests. The cage is cylindrical with a diameter of 1.50m. It has two outer sections of 0.5m on each side and the centre part of 1.5m. The center part is grounded and is used for measurements through a series resistor of 56 ohms. The total length of the cage is 2m. Two corona rings were fitted at each end of the conductor to ensure that only the noise from the conductor was measured. For the initial studies, single and smooth aluminium conductors were used.

To assess the effect of the space charge on the measured values, a high output fan was used to sweep the space charge away.





Figure 1. The test set-up

The noise and the current meters were placed in a measurement cage adjacent to the corona cage. The instrument used to measure the sound pressure level is the Rohde & Schwarz sound level meter. The meter measures A-weighted sound pressure level. The corona current was measured using a digital multimeter. The positioning of the meters is illustrated in Figure 2.

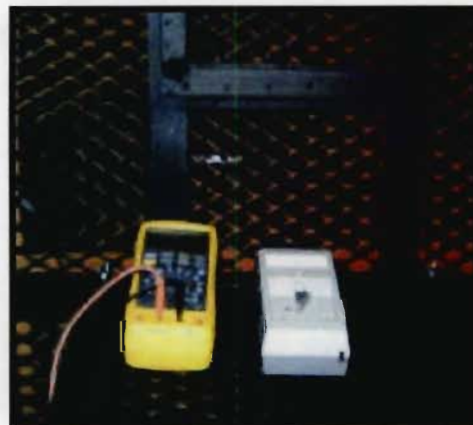


Figure 2. The measuring instrument.

A two stage Walton Cockcroft HVDC supply was used. Its output is connected to 1200Mega-ohms resistive divider. The cage is connected to the output of the generator through a 400Mega-ohms series resistor.

### 3. EXPERIMENTAL PROCEDURE

Conductors of 1.6cm and 2.8cm diameters were considered for the tests. For each conductor the static electric field was calculated at every applied voltage using the equation:

$$E = \frac{U}{r \ln \frac{R}{r}} \text{ kV/cm} \quad (1)$$

Using Peek's formula (2) for positive conductor corona, the corona inception fields for the conductors were estimated as indicated in Table 1. The inception gradient was calculated using the roughness factor,  $m$  of 0.9 and the relative air density  $\delta$  of 1.

$$E_c = 33.7m\delta \left( 1 + \frac{0.24}{\sqrt{r\delta}} \right) \text{ kV/cm} \quad (2)$$

Only positive polarity DC was considered since most corona is produced from the positive pole. The results of the tests under negative polarity DC and AC conditions will be presented in the future.

Table 1: Estimated corona inception field:

Conductor Diameter (cm)	Inception Gradient (kV/cm)
1.6	38.47
2.8	36.48

The current and the sound pressure level measurements were taken at 0.88m from the conductor and directly in the centre of the conductor.

Temperature, pressure, humidity and the background sound pressure level were recorded for every session of measurements.

The sound power denoted as  $A$  was computed from the sound pressure level measurements obtained from the cage. Equation 3 was used to derive  $A$ .

$$P = \sqrt{\frac{\delta c A}{4r}} \quad (3)$$

Substituting the values, Equation 3 resulted in Equation 4 which was used throughout the study to compute noise power values for the cage.

$$A = P - 54.85 \text{ dBA} \quad (4)$$

The sound power in equation 4 is expressed in dBA at a reference of  $1 \mu\text{W/m}$ .

The EPRI TLW software was used to generate sound pressure levels for EPRI, BPA and CRIEPI predictions. The Cahora Bassa line configuration data was used as the input. The negative pole was placed much further from the positive pole, to obtain the noise contribution from the positive pole only. The 1.6cm diameter conductor was considered and an average transmission line height of 14.8m was used for the simulations. The measuring point was set at a distance of 10m and a height of 1.8m.

#### 4. RESULTS

Figure 3 shows the results obtained from the UKZN cage and the CRIEPI test facility. At CRIEPI corona cages of different diameters and length were used with  $4 \times 2.85\text{cm}$  conductor bundle [3]. The graphs obtained using the EPRI TLW software are shown together with the UKZN cage results in Figure 4. The measurements obtained from the cage were corrected to an equivalent transmission line, taking into account the length of the conductor.

Figure 5 shows the relationship between the sound power (A) and the conductor surface gradient obtained from the UKZN cage and the EPRI and CRIEPI predictions. The CRIEPI and the EPRI curves were derived from reference [3] and the EPRI TLW software respectively. Figure 6 shows the relation between the corona current and the conductor surface gradient for the UKZN cage measurements and the CRIEPI results described in reference [3].

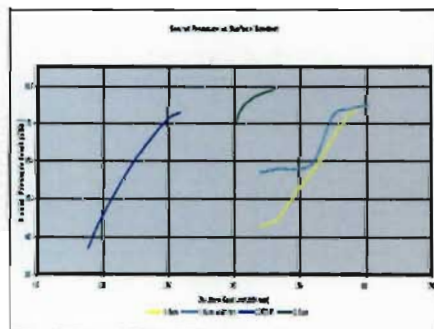


Figure 3: The relationship between the sound pressure level and the conductor surface gradient.

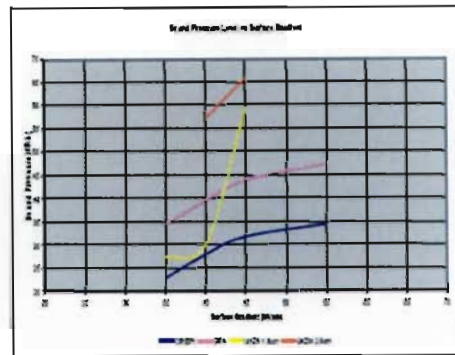


Figure 4: The relationship between the sound pressure level and the conductor surface gradient obtained from the EPRI software

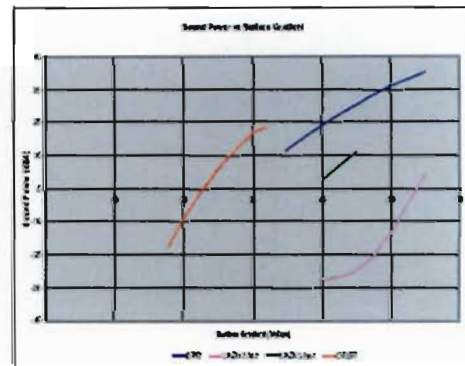


Figure 5: The relationship between the sound power and the conductor surface gradient.

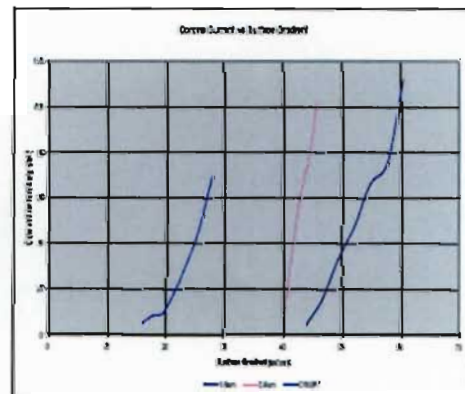


Figure 6 The relationship between the corona current and the conductor surface gradient

## 5. DISCUSSION OF RESULTS

The AN and corona current measurements obtained using the UKZN test facility are generally higher compared to the BPA, EPRI and the CRIEPI results. The CRIEPI results were obtained at lower field levels due to the conductor bundles used in the tests. The BPA and the EPRI results are based on test line measurements at practical field levels. However, both the CRIEPI and the UKZN show similar relationship between the sound pressure level and the conductor surface gradient. The slopes for the CRIEPI, 1.6cm diameter conductor and 2.8cm diameter conductor sound pressure level curves are 2.4dBA/kV/cm, 2.54dBA/kV/cm and 2dBA/kV/cm respectively (Figure 3).

For the tests done at CRIEPI, an attempt was made to quantify the space charge effect. At UKZN, a fan was used to assess the space charge effect. The results obtained show only a minimal effect.

The 2.8cm conductor required very high voltages to attain conductor corona. In which case the end-fittings go into corona prior to conductor corona and contributed to the overall noise measured. A modification of the test set-up is being done to eliminate the corona at the end fittings.

In Figure 4, the BPA and the CRIEPI results obtained from the software are in good agreement with the 2.8cm diameter conductor UKZN cage results in terms of slopes. However, the slope of the 1.6cm diameter conductor is completely different. There is not enough information to explain the observed variation at this stage. The cage measurements were still higher even after the corrections for conductor height and length were made. This could be due to the high fields under which the measurements were taken.

In Figure 5, there are similar trends for the CRIEPI and the 1.6cm diameter conductor noise power results. Similarly, the slopes of the EPRI and the 2.8cm diameter conductor curves are also in good agreement. It was difficult to compare all the results within the same surface gradient ranges due to differences in the experimental set-ups. However the similarities in the trends confirm that the dependence of sound power

on surface gradient was almost the same in the three cases (EPRI, CRIEPI and UKZN)

In Figure 6, there is a good agreement between the UKZN and CRIEPI results. In both cases the measurements were done in a corona cage. The measured current is an indication of the corona activity on the conductor. High current measurements were obtained for the conductor with the larger diameter compared to the smaller diameter conductor. The levels at the UKZN cage are lower for a given field level due to the comparatively smaller conductors used.

## 6. CONCLUSIONS

In this paper, it has been demonstrated that results obtained from the UKZN corona cage are in good agreement with the available prediction methods in terms of the trends. This validates the tests procedure. The variations in the measured values are due to the differences in the use of conductor sizes used, the test configurations and climatic conditions. Future measurements will be conducted in the cage using bigger diameter conductors to achieve practical field levels. This will facilitate a better comparison with test line measurements obtained elsewhere. The work done at CRIEPI shows that it is possible to relate corona cage measurements with test line results.

## ACKNOWLEDGEMENT

The authors would like to acknowledge THREP and Eskom for providing the funds for this research and the UKZN High Voltage Direct Current Centre, for the test facility.

## REFERENCES

- [1] P Sarma Muruvada, *Corona Performance of High-Voltage Transmission Lines*, Research Studies Press LTD, 2000.
- [2] HVDC Transmission Line Reference Book, EPRI, 1993.
- [3] Yukio Nakano and Yoshitaka Sunaga, "Availability of Corona Cage for predicting Audible Noise generated from HVDC Transmission Line", *IEEE Transactions in Power Delivery*, Vol. 4, No. 2, pp. 1422-1431, April 1989.
- [4] T Pillay and S Esmatji (Editors), "The Planning, Design and Construction of Overhead Power Lines", Eskom Power Series, Volume 1, 2005.



SAUPEC 2006

- [5] Vernon L. Chartier and Richard D. Stearns, "examination of grizzly mountain data base to determine effects of relative air density and conductor temperature on HVDC corona phenomena", *IEEE Transactions on Power Delivery*, Vol. 5, No. 3, pp. 1575-1582, July 1990.